POWERED WHEELS IN THE TURNED MODE

OPERATING ON YIELDING SOILS

By

GARY NEIL DURHAM

Bachelor of Science in Civil Engineering
University of Alabama
University, Alabama
1967

Master of Science
Mississippi State University
Mississippi State, Mississippi
1971

Submitted to the Faculty of the Graduate College
of the Oklahoma State University
in partial fulfillment of the requirements
for the Degree of
DOCTOR OF PHILOSOPHY
July, 1976

POWERED WHEELS IN THE TURNED MODE

OPERATING ON YIELDING SOILS

Thesis Approved:

_____
Thesis Adviser

_____

_____

_____

_____

964137

ii

ACKNOWLEDGEMENTS

TABLE OF CONTENTS

LIST OF TABLES

LIST OF FIGURES

CHAPTER I

INTRODUCTION

General

In off-road untracked vehicles the tire is the link between the
ground and the vehicle. Engineering construction equipment, agricultural
and forest management machinery, and cross-country vehicles having
pneumatic tired tractive devices will achieve the best results in off-
road operations only when the interaction between tire and soft soil is
understood and quantitatively defined in engineering terms.

A portion of recent U. S. Army mobility research was the develop-
ment of a comprehensive analytical model of ground vehicle systems. In
1971 the existing research and engineering knowledge of terrain-vehicle-
operator interactions was collected, appraised, and assimilated into a
simulation model for the prediction of ground vehicle mobility (Rula and
Nuttall, 1971; U. S. Army Tank-Automotive Command, 1973). The second
generation of this model was released Army-wide in 1975 as the Army
Mobility Model (AMM-75) (Jurket, et al, 1975).

Basically the AMM-75 consists of computer modules that allow for
simulating the entire vehicle as it interacts with soil, vegetation,
slopes, ditches, obstacles, and other features of any geographical area.
The basic output of the model consists of a map which specifies the
maximum feasible straight-line speed which the vehicle under considera-
tion might achieve at any point in the terrain.

1

In assessing the current program and identifying future research and development needs for the U. S. Army, the Office of the Director of Defense Research and Engineering (1974) identified as needed methodology development those areas associated with mobility, agility, and survivability of combat and combat support vehicles. Potential need was identified for reliable engineering bases to predict vehicle performance limits while maneuvering in off-road terrain. The current computational modules incorporated in AMC-71 and AMM-75 that address vehicle maneuvering consist of simple empirical relations which do not address the problems in fundamental engineering terms.

One important consideration to vehicle maneuvering capability in off-road terrain derives from the steering forces which the vehicle's running gear can generate in soils. These forces influence not only the stability of the vehicle, but also its power requirements and ability to develop net traction for slope negotiation.

Purpose and Scope

The principal objectives of this study were:

1) Investigate the performance of single, pneumatic tired, powered wheels when operating in the turn mode one fine- or coarse-grained soils.

2) Formulation of relations to predict total side force developed by a tire during a cornering maneuver in soft soil. The forces generated result from the tire slip angle determined by the forward velocity, turn radius, and wheel steer angle in combination with wheel load, pertinent tire parameters, and characterization of the soil medium.

3) The results of 1) and 2) will be translated into prediction equations suitable for incorporation into a digital program to calculate

the response of a four-wheeled vehicle executing steady-state flat turns in soft soil terrain.

Controlled laboratory tests were conducted with a single powered wheel equipped with a 6.00-9 pneumatic tire and at turn angles ranging from 0 to 20 degrees. Wheel loads and tire deflections were varied. Tests were conducted on a near saturated fine-grained plastic clay of one consistency and on a predominantly coarse-grained air-dried sand at two consistencies. Tests were conducted with the single-wheel dynamometer carriage of the Army Mobility Systems Division, Waterways Experiment Station (WES). The single wheel dynamometer permits pneumatic-tired wheels to be tested dynamically at various controlled speeds and loads and under a variety of consistent and known soil conditions. The mechanical arrangement of the system yields measurements of tire load, tire deflection, wheel sinkage, wheel slip, torque input, and net longitudinal and lateral forces.

Current off-road mobility modeling does not predict or evaluate a vehicle's responses during the path following sequences or complex maneuvering. The path following model should use as much of existing straight-line travel routines from the AMM Mobility Model as practical. One course of action might consist of an iterative computation process of a vehicle moving from point A to B over a specified terrain. The first computation predicts path performance as though there was no curvature (current procedure), and with successive interactions introduce curvature, rate of change in heading and the feasible steering response, and the required acceleration and deceleration for obtaining successive adjustments to speeds along the actual path. A beginning toward achieving the complete path-following model is to develop initial

relations between independent variables of tire, load, and soil
strength and dependent performance parameters that adequately describe
the tire/soil interactive forces generated while a wheeled vehicle
undergoes steady-state turning.

CHAPTER II

BACKGROUND

General Aspects of Cornering Performance of

Pneumatic Tires in Yielding Soils

General Aspects of Tractive Performance

The vehicle applies forces to the wheel at the axle while the soil medium applies forces at the soil-tire interface. To study these forces the wheel can be considered as a free body, disconnected from both the vehicle and the soil, and restored to equilibrium by forces and moments applied to the axle and at the interface area. Figure 2.1 (after Schuring, 1966) illustrates the possible combination of torque and horizontal pull. Vertical force W , horizontal pull P , and torque M are applied to the axle, all of which are counteracted by soil force F . These occurrances can be illustrated graphically by imagining a wheel with a constant vertical load W being applied while it is being propelled in a horizontal direction. For this discussion the input torque is constantly undergoing change beginning with input torques that are opposed to wheel rotation (braked condition) to positive values of input torque (powered wheel). If these input torques are known, and the corresponding values of pull and wheel slip are measured, a relation of torque and pull versus wheel slip will appear as qualitatively shown in Figure 2.2. The various regions (1-5) defined in

5

		TORQUE M		
		DRIVING	O	BRAKING
AXLE PULL P	TOWING	③	④	⑤
	O	②	AT REST	
	DRIVING	①		
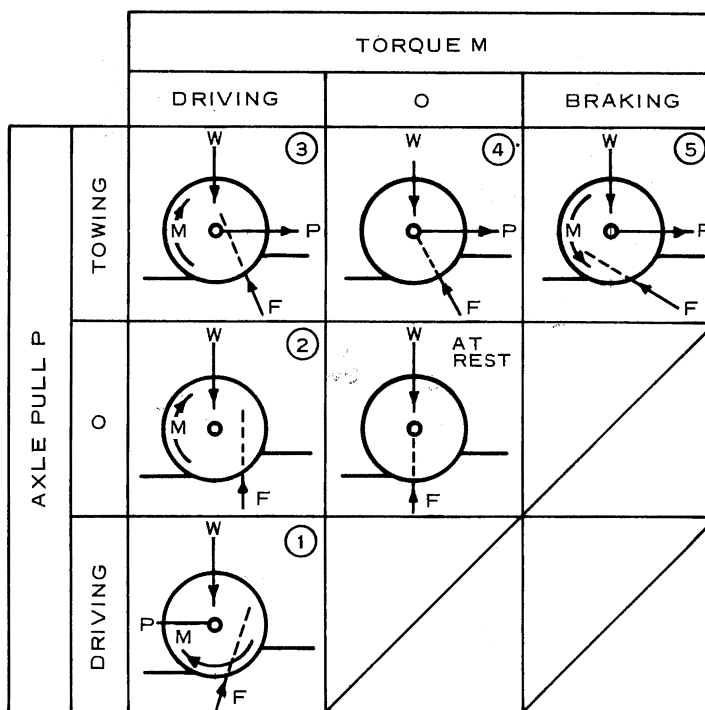
Figure 2.1.   Combination of Torque M and
              Horizontal Axle Pull P of a
              Free-Bodied Wheel (after
              Schuring, 1966).
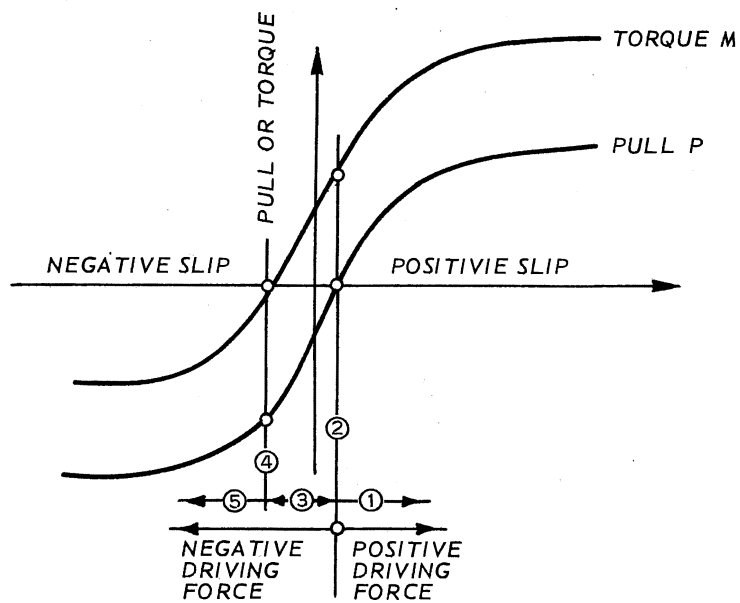
① DRIVEN-PULLING
② DRIVEN-FREE ROLLING-SELF PROPELLED POINT
③ DRIVEN-PULLED
④ PULLED FREE ROLLING-TOWED POINT
⑤ BRAKED-PULLED

Figure 2.2. Conditions of a Wheel on Yielding Soil.

Figure 2.2 as a wheel operates on yielding soils have been keyed to the illustrations on Figure 2.1.

The first quadrant of the axes shown in Figure 2.2 represent the operating status where the wheel is providing a drawing force and hence is a tractive device. Evaluating traction performance begins by establishing performance criteria and determining the interdependency of the critical parameters by making simultaneous measurements in various states of dynamic equilibrium. Pull, torque, weight carried by the wheel, rate of angular rotation, forward speed, and wheel slip are basic measurements that describe the state of dynamic equilibrium.

Tire Slip Angle

The lateral forces acting on pneumatic tires operating on a hard or semi-rigid roadway have been frequently investigated and reported. The early studies in the mid-1920's and early 1930's concerning the mechanics of cornering were made in France and Germany. In the United States during this era automobiles had solid front axles and the center of gravity located considerably aft of the midpoint which produced oversteer and instability at higher speeds (Sigel, 1966). This characteristic of American automobiles plus an end of technical exchange with Germany just prior to World War II produced an influx of investigations in this country during the 1930's concerned with the dynamics of the rolling tire and relating this mechanical behavior to the directional properties of automobiles.

A wheel which is fitted with a pneumatic tire and which is constrained to a specific plane to which no perpendicular forces are applied, will roll in a direction coinciding with the vertical plane.

If, however, a force is applied obliquely to the wheel's axis then as the wheel rolls it will move along a path making an angle with the plane of the wheel. Broulhiet (1925) is credited with illustrating the importance of this angle in analysis of vehicle handling. Fiala (1954) used an analytical model to show the importance of the slip angle concept in generating lateral forces. Segal (1956) combined side slip with wheel camber angle and the self-aligning torque concept to appraise tire forces generated during cornering.

The angle formed between the plane of the wheel and the instantaneous velocity vector is generally designated "slip angle." The magnitude of the slip angle depends on many factors. The most important of which are the magnitude of the force applied obliquely to the plane of the wheel, the vertical wheel load, the inflation pressure, and the construction and elastic properties of the tire itself. Steeds (1960) states that the speed at which a vehicle rolls on hard surfaces has little effect on the value of the slip angle.

As previously implied, an external force must be applied for a vehicle to deviate from a straight line. When a tire is steered across the path of motion a deformation and displacement of the contact path occurs which gives rise to a side force (also designated in the literature as the cornering or steering force) and a moment that attempts to realign the wheel in the rolling direction. The side force does not act in the vertical plane containing the axis of the wheel, but in a parallel plane lying slightly behind the wheel axis, as illustrated in Figure 2.3. The resulting SF·C acts on the wheel and tends to turn so its plane coincides with the direction of motion; this is resisted by an equal and opposite couple applied by steering system and suspension
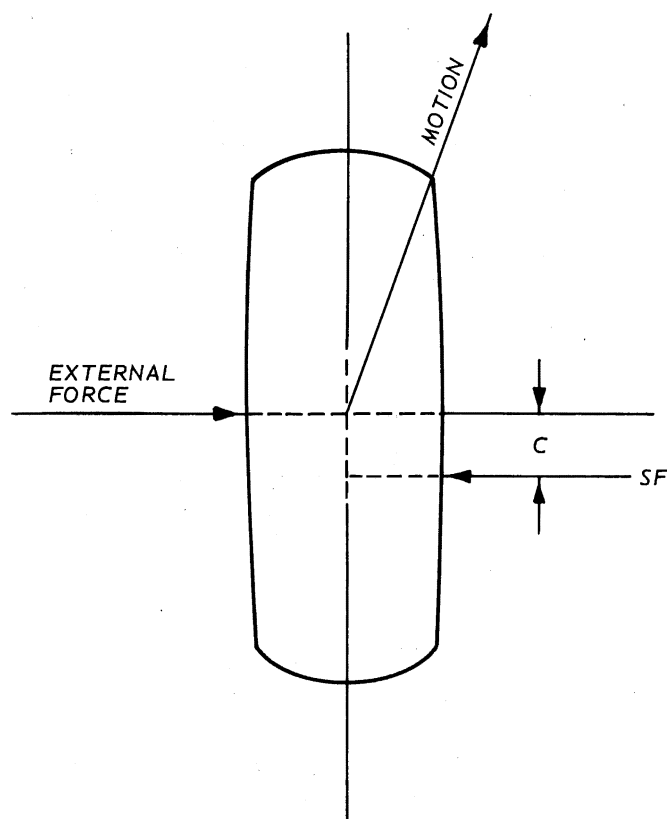
Figure 2.3. Development of Trail Moment
SF·C from an Externally
Applied Force.

of the vehicle. The distance C is called the pneumatic trail and couple SF·C referred to as the trail moment or self-aligning torque. Self-aligning torque is of secondary interest in describing the handling behavior of a fixed control vehicle, but is important which the loads within the steering mechanics are required. Kirch (1973) states that the self-aligning torque as a function of slip angle is of little consequence to the driving behavior of a vehicle in soft soils because of the low speed encountered with off-road operations.

Driving or braking a wheel will considerably reduce the lateral force obtained at any given side slip angle (Ellis, 1969). This occurs because the additional traction applied in the wheel utilizes more of the available local friction which in turn reduces the amount available in a lateral direction.

Related Research at WES

WES Numeric Prediction System

Tire and soil modeling is a fundamental part of the simulation of cross country operation of off-road vehicles. A system was developed at WES from the examination of a large number of carefully controlled laboratory single-tire tests conducted on a saturated plastic clay and on two air-dried sands. The WES system allows the prediction of certain performance parameters (dependent variables) by combining the independent variables through dimensional reasoning (Freitag, 1965).

In the dimensional analysis, the following independent variables were condsidered to influence the tire-soil system behavior significantly:

Soil:	Friction angle	(ϕ)
	Cohesion	(c)
	Unit weight	(γ)
	Spissitude	(a measure of viscosity)

Tire:	Dimensions	(diameter, section width and height)
	Deflection	(δ) as measured on a rigid surface

System:	Load
	Translational velocity
	Slip
	Soil-tire friction
	Gravitational constant

Freitag made use of the Pi Theorem to establish that 14 different Pi terms were necessary to describe the tire-soil system (Bridgman, 1931; Duncan, 1953; and Langaar, 1951). The actual relations that exist among Pi terms cannot be established analytically. Experiments must be conducted with the Pi terms as controlled variables. The problem was somewhat simplified by adopting then established conventional terms for some of the Pi terms and by inspection (from an extensive background of judgment and experience), which lead to 10 Pi terms being written immediately. The remaining four Pi terms were developed by matrix manipulation. In evaluating the Pi terms the time dependent parameters (spissitude, velocity) were disregarded and only purely frictional (c = 0), or purely cohesive (ϕ= 0) soils were considered and used in the tests that established performance relations for use in each particular soil type. With the type of the soil limited to either purely cohesive or purely frictional, the soil is modeled by cone penetration values, as follows:

Frictional soils: cone penetration resistance gradient (rate of increase of cone index)

Cohesive soils: cone penetration resistance

The independent variables were combined by dimensional analysis into so-called mobility numbers of the two soil types tested:

1) Clay mobility number N_c :

$$N_c{}^1 = \frac{Cbd}{W} \left(\frac{\delta}{h}\right)^{1/2} \frac{1}{1 + \frac{b}{2d}} \qquad (2.1)$$

and

2) Sand mobility number N_s :

$$N_s = \frac{G(bd)^{3/2}}{W} \cdot \frac{\delta}{h} \qquad (2.2)$$

where

C = Average cone penetration resistance of the 0- to 15-centimetre soil layer as measured with WES standard cone penetrometer.

G = Average cone penetration resistance gradient of the 0- to 15-centimetre soil layer as measured with the WES standard cone penetrometer.

b = Unloaded tire section width.

d = Unloaded tire diameter.

W = Vertical load applied to the tire through the axle.

δ = Difference between unloaded and loaded tire section heights.

h = Unloaded tire section height.

Relations were established between each of the following performance parameters and the sand and clay mobility numbers, respectively: pull coefficient P/W , torque coefficient M/Wr_a , and sinkage

_____

[1] The dimensional term $\dfrac{1}{1 + \dfrac{b}{2d}}$ did not appear in Freitag's work but was added later by Turnage (1972) to enable the total collapse of additional laboratory data obtained with tires having large b/d ratios (e.g. terra tires whose width b may be equal to the diameter d).

coefficient z/d , all at 20 percent wheel slip, and towed force

coefficient P_T/W

where

P = Net pull.

M = Torque input to the axle.

r_a = Effective tire radius in the soil.

z = Sinkage.

These relations (Figure 2.4 for clay and Figure 2.5 for sand) describe the performance at the towed point and at 20 percent slip. The pull generated at 20 percent slip is generally referred to as the "maximum pull." Actually higher pull values may occur at other slip values but greater amounts of input power are required and the trade-off between pull and required torque has been shown to be optimized at a wheel slip of 20 percent (Freitag, 1965).

More recent developments include expanding the dimensionless single tire relations to permit prediction of tire performance over a broader slip range. Smith (1976) performed a thorough reanalysis of the basic laboratory data obtained during the 1960's and developed relations describing critical performance parameters over the pull slip range for single tires operating in clay. Smith began by altering the clay numeric so that rigid wheels could be considered (i.e. $\frac{\delta}{h} = 0$ for rigid wheels and Equation 2.1 and 2.2 would be equal to zero) within the same framework as pneumatic tires. Smith suggested that the clay mobility number (herein designated as N'_c) take the form:

$$N'_c = \frac{Cbd}{W \left(1 - \frac{\delta}{h}\right)^{3/2} \left(1 + \frac{b}{d}\right)^{3/4}} \qquad (2.3)$$
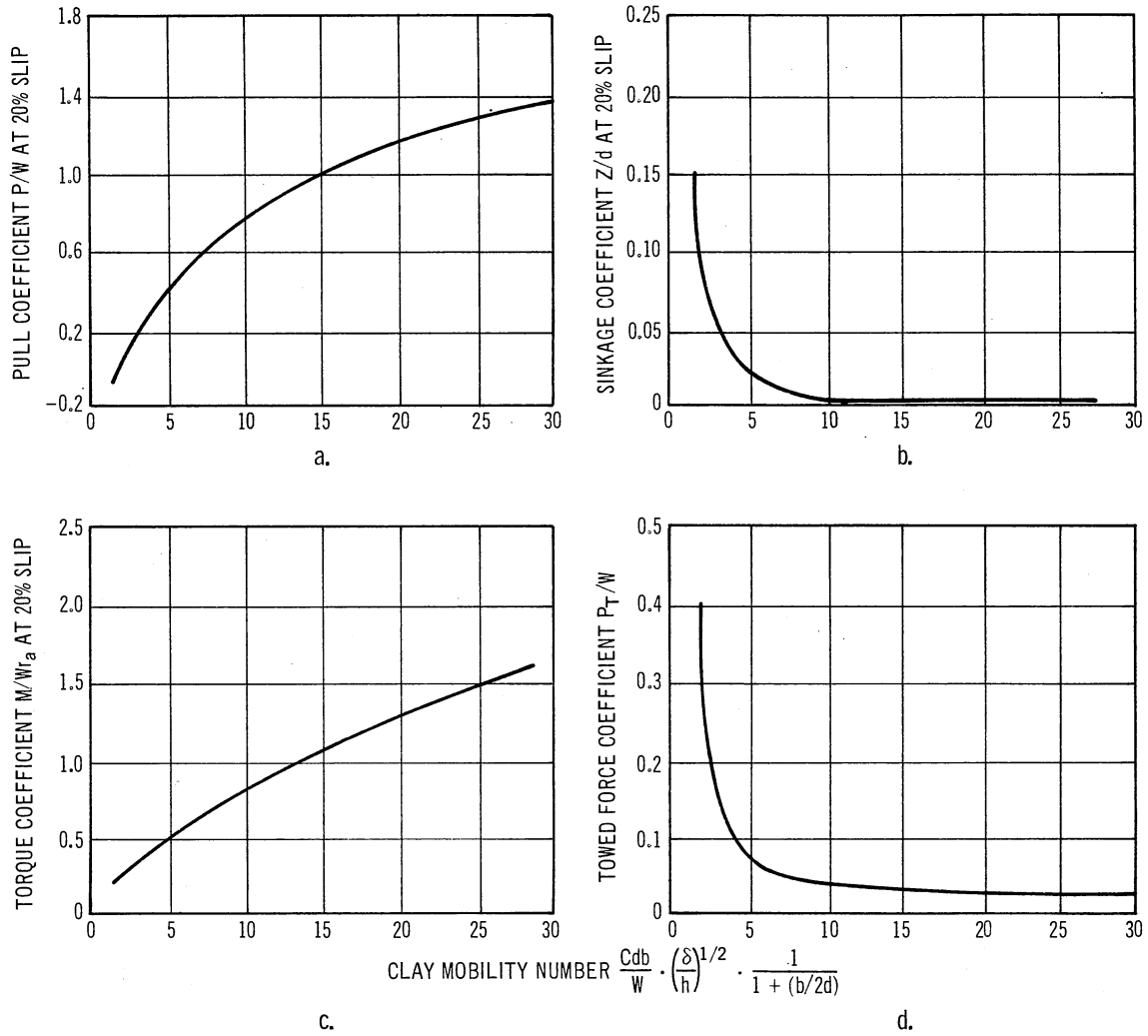
Figure 2.4.   Relation of Performance Coefficients to Clay Mobility
Number (after Turnage, 1972, Figure 4).
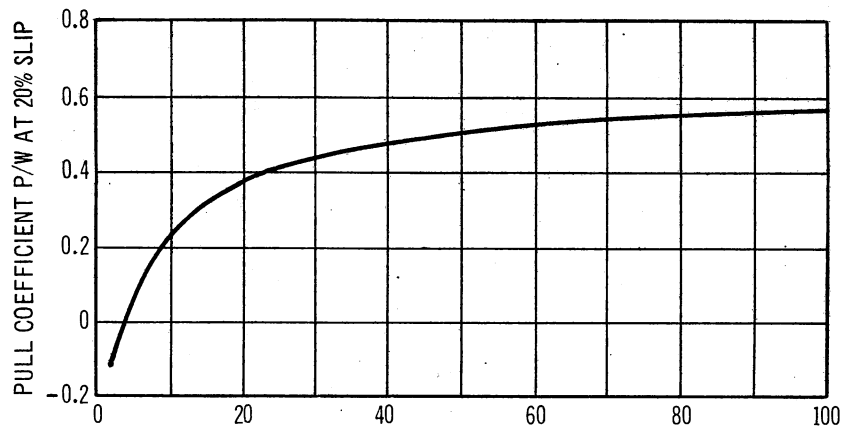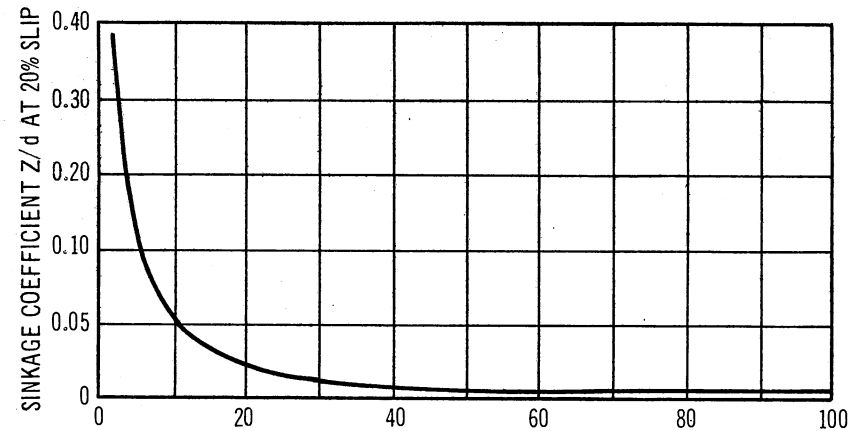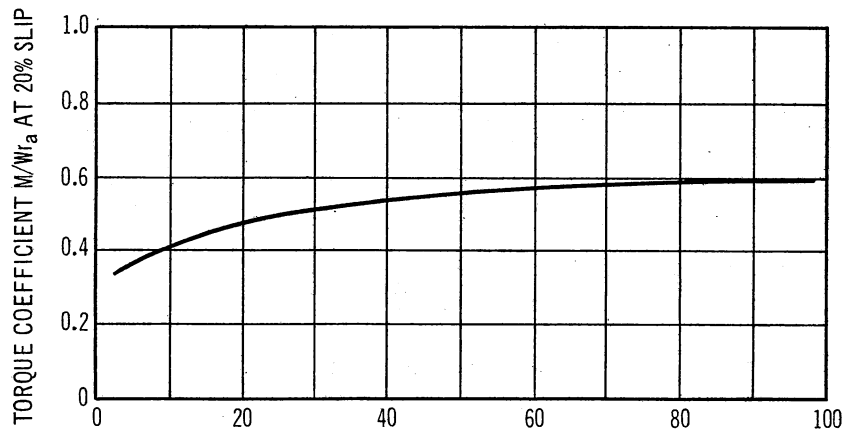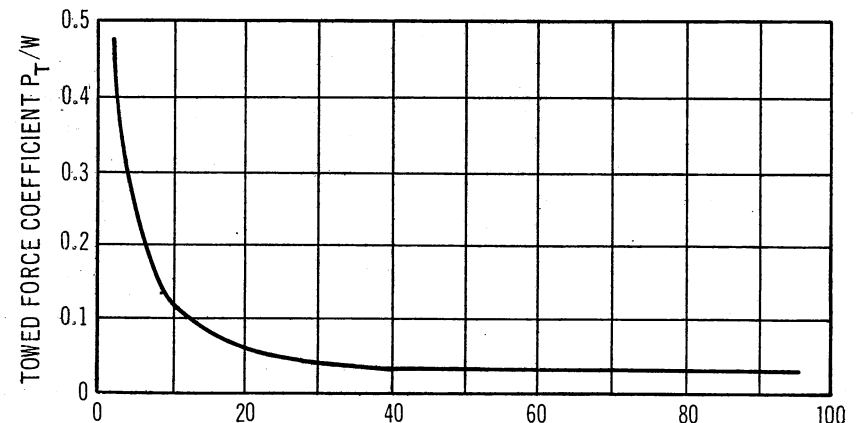
Figure 2.5. Relation of Performance Coefficients to Sand Mobility Number (after Turnage, 1972, Figure 3).

Smith found for powered wheels with constant test conditions (i.e. N_c' a constant value) a linear relation existed between the pull coefficient and the input torque coefficient (Figure 2.6a). $\frac{M_{sp}}{Wr_a}$ is defined as the input torque at the self-propelled point (i.e. $\frac{P}{W} = 0$) corresponding to the slip at self-propelled, S_{sp} as shown in Figure 2.6b. By inspection of Figure 2.6a the relation between $\frac{P}{W}$ and $\frac{M}{Wr_a}$ is seen to be

$$\frac{P}{W} = \frac{M - M_{sp}}{Wr_a} \cdot K_T \qquad (2.4)$$

where

$$K_T = \frac{1}{\left(1 + \frac{b}{d}\right)^{1/4}}$$

For most conventional pneumatic tires K_T varies from about .88 to .97. A relation was found to exist between the slip at the self-propelled point, S_{sp} and the clay numeric N_c'

$$S_{sp} = \frac{21}{\left(N_c'\right)^{5/2}} + 0.005 \qquad (2.5)$$

As N_c' becomes very large S_{sp} approaches 0.005. For example if C became infinitely large (rigid pavement) the self-propelled point would be approximately 0.5 percent slip. If S_{sp} is related to N_c', it would not seem unreasonable from noting Figure 2.6b that $\frac{M_{sp}}{Wr_a}$ is likewise related to N_c' as

$$\frac{M_{sp}}{Wr_a} = \frac{12}{\left(N_c'\right)^2} + 0.007 \qquad (2.6)$$

$N_1 > N_2 > N_3$
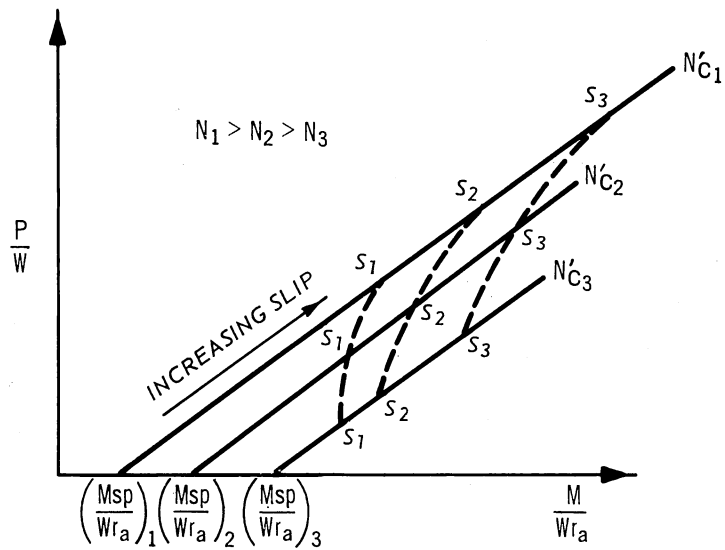
a. TIRE DEPENDENT
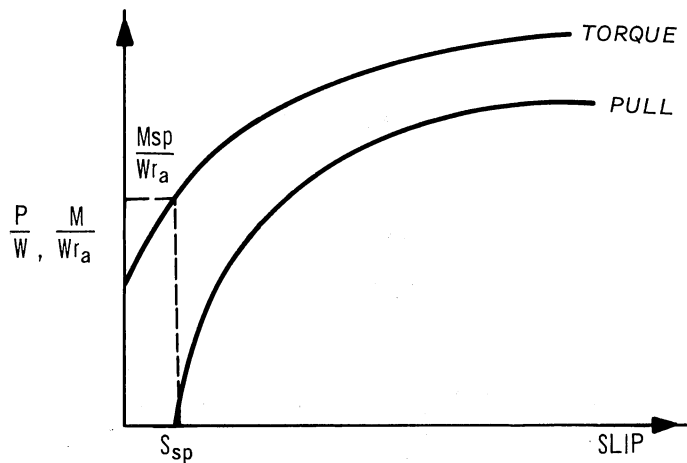
b. N_C' CONSTANT

Figure 2.6.   Qualitative Interdependency of
Pull, Torque, and Wheel Slip.

Figure 2.6a also suggestes that the loci of equal slips exists as various test conditions (i.e. changes in $N_c^!$) occur. Smith found the following relation to best fit the existing laboratory data.

$$\frac{P}{W} = \frac{M - M_{sp}}{Wr_a\left(1 + \frac{b}{d}\right)^{1/4}} = 0.5 \log \frac{S}{S_{sp}} \qquad (2.7)$$

Equation 2.4 through 2.7 permit $\frac{P}{W}$ to be computed from given test conditions $N_c^!$ (and likewise the required torque input) for a given slip.

The relation between the revised clay numeric and the towed coefficient $\frac{P_T}{W}$ was found to be

$$\frac{P_T}{W} = \frac{12}{\left(N_c^!\right)^2} = 0.007 \qquad (2.8)$$

which is incidentally numerically equal to $\frac{M_{sp}}{Wr_a}$, however, the physical relation between the two dependent variables is not apparent.

Melzer (1973) developed a prediction system for the pull and the power required of a single wheel operating in sand of various densities. The primary results of earlier studies was a system for predicting maximum pull (system output), torque (system input) necessary to develop the maximum pull, and towed force (zero torque) for pneumatic tires operating on soil. Melzer's relations are limited because: 1) only a representative portion of the sand data was selected for inclusion in the development; and 2) the slip range was limited from the slip at the towed point to that of 20 percent. Only a portion of the available sand data was reanalyzed because the new data had to be compiled for values of pull and torque at intermediate values of slip

between the self-propelled point and 20 percent slip – a time consuming and expensive task because most of the information had to be "hand-read" from oscillographs.

Melzer's summary relations consisted of a nomograph plot of power coefficient[2] as a function of the pull coefficient, slip, sand mobility number, and slope angle of the soil surface that the wheel must negotiate (Figure 2.7). Using the basic data used to develop Figure 2.7 more fundamental plots of the output pull coefficient (Figure 2.8a) and input torque coefficient (Figure 2.8b) were constructed.

Using modified Honeywell (1971) computer library routines for curve fitting the following relations were formulated from the curves illustrated in Figure 28. For the pull coefficient:

$$\frac{P}{W} = A_P - \frac{A_P \, B_P}{N_S - C_P + B_P} \qquad (2.9)$$

where

$$A_P = 0.69 - \frac{0.01}{s}$$

$$B_P = 10.8$$

$$C_P = \frac{2.23}{s^{1/3}}$$

and the input torque coefficient

$$\frac{M}{Wr_a} = A_M - \frac{A_M \, B_M}{N_S - C_M + B_M} \qquad (2.10)$$

where

$$A_M = 0.66$$

---

[2]Power coefficient $PN = \dfrac{M}{Wr_a} \cdot \dfrac{1}{1 - s}$.
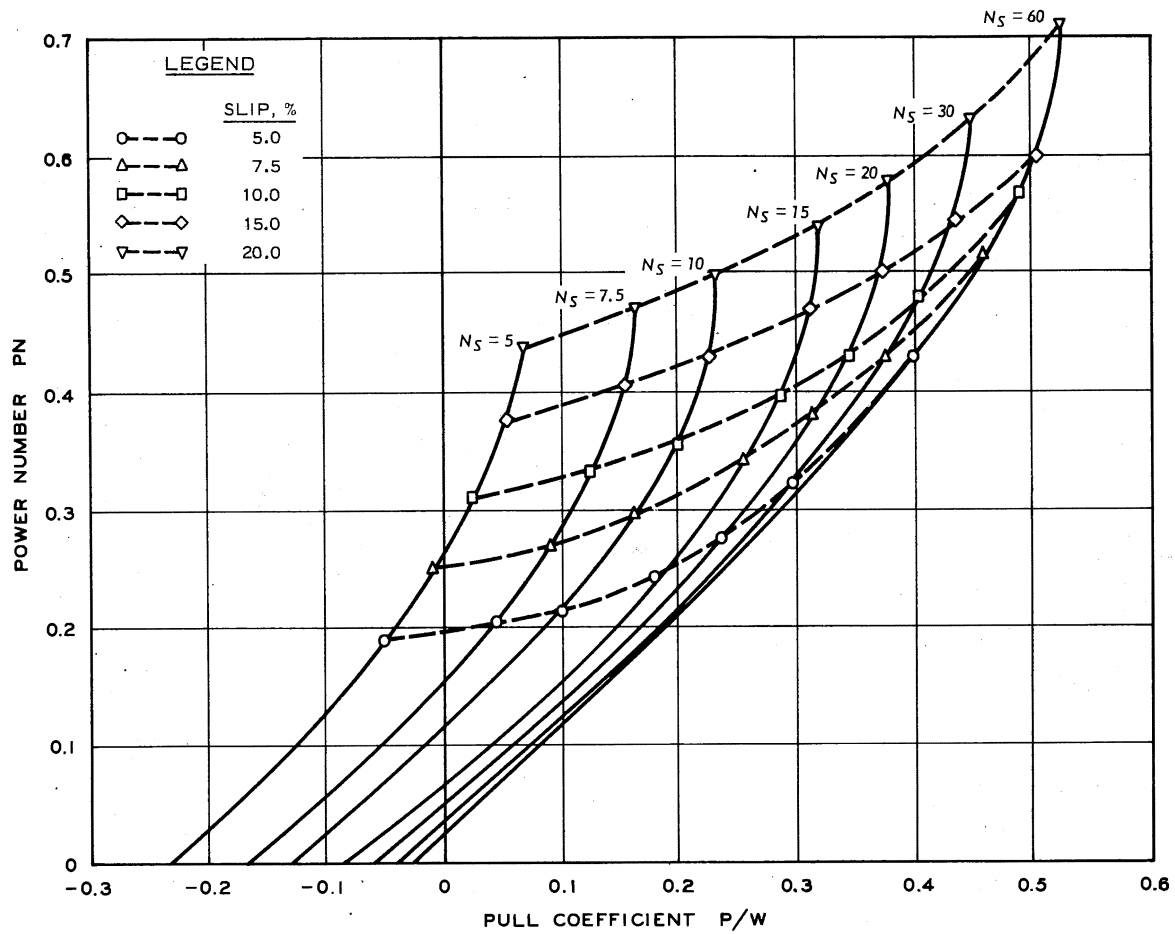
Figure 2.7.   Power Number as Function of Pull Coefficient, Slip, and
Sand Mobility Number (from Melzer, 1973).
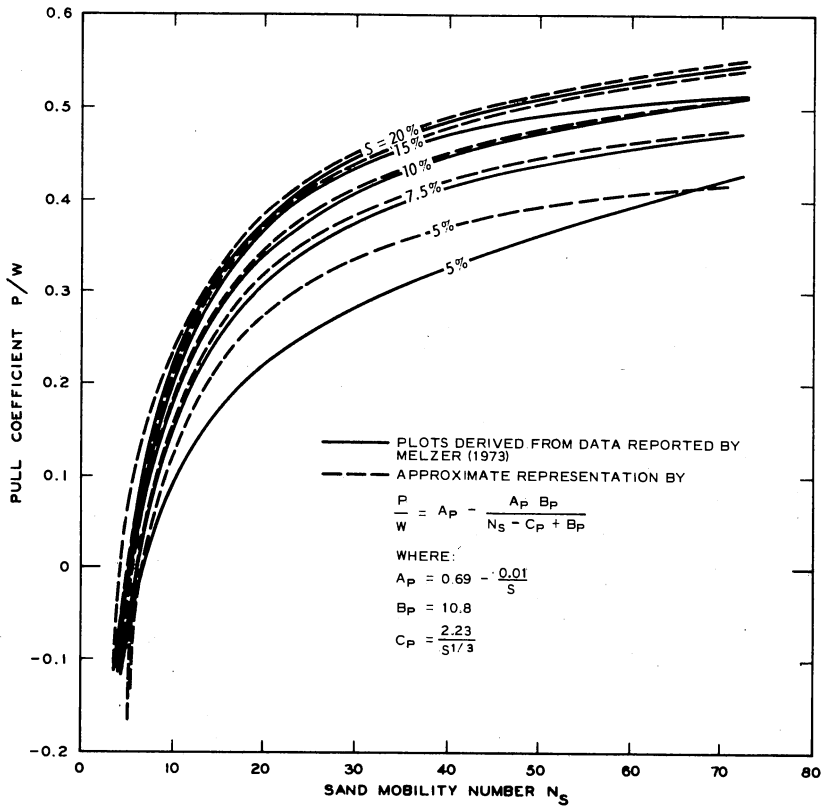
a. PULL
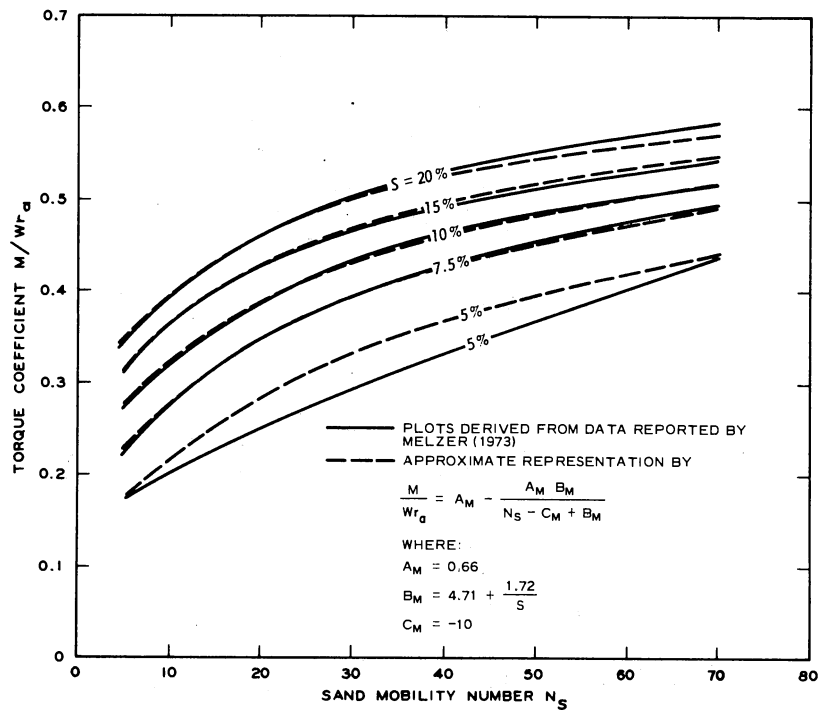
b. TORQUE

Figure 2.8. Pull and Torque Coefficients Versus
Sand Mobility Number for Wheel
Slips Less Than 20 Percent (after
Melzer, 1973).

$$B_m = 4.71 + \frac{1.72}{s}$$

$$C_M = -10$$

WES Towned Turn Tire Test Programs

Green (1971) reported the results of a series of towed tests conducted with a Lunar Roving Vehicle (LRV) wheel operating on a lunar soil simulant of crushed basalt. The turn angle of the wheel was varied obliquely to the direction of travel from -5 to +90 degrees; in the latter case, the plane of the wheel was perpendicular to the travel direction. The applied wheel loads were extremely light and the forward velocity was varied from 1.07 to 3.05 metres per second.

Side-force coefficient S/W increased with increasing turn angle α to a value of about 1.2 at $\alpha = 90$ degrees. Speed had an effect on side force with slightly higher values of S/W generally corresponding to the higher wheel speed.

Unpowered single wheel tests were conducted at the WES in 1973 to define relations between side force and turn angle for two pneumatic tires common to the landing gear structure of military transport aircraft capable of operating on unprepared soil runways (Krick, 1975). Tests were conducted on mortar sand and Vicksburg buckshot clay of various soil strength. Melzer (1976) agumented those tests by incorporating a third tire of differing dimensions, expanded test conditions, and a third soil, Yuma sand. All together Melzer reported on 99 one-pass unpowered single wheel tests conducted in the laboratory on the one clay and the two sands with 8.50-10, 7.00-6, and 6.00-9 tires; turn angles were 0, 5, 10, 15, and 20 degrees. Wheel loads were varied from about 1000 to 7000 N; tire deflections were 0.15, 0.25, 0.35, 0.40 of the

undeflected tire section heights. Clay cone penetration resistance ranged between 255 and 540 kPa. The air-dry sands had cone penetration resistance gradients ranging from 0.7 to 4.6 MPa/m.

In generalities Melzer found that the side-force coefficient S/W for clay and sand increased as the mobility number became larger for a given turn angle α ; conversely, S/W increased with α when the mobility number was held constant. Also for both clay and sand tests the towed force coefficient P_T/W did not show a well defined dependency on the turn angle α . With consideration of these observations Melzer's tabulated data was used to formulate relations (between forces acting on the wheel and turn angle for varied soil types and consistencies) consistent with the wheeled vehicle modeling needs to be discussed in Chapter V.

Figure 2.9 presents the towed force coefficient clay data obtained by Melzer as a function of the clay mobility number N_c' [3] and the turn angle α . The towed force P_T is that force acting in the plane of the wheel. The curve shown on each plot is a pictorial of Equation 2.8,

$$\frac{P_T}{W} = \frac{12}{\left(N_c'\right)^2} + 0.007 \tag{2.8}$$

which is the equation for predicting the towed force coefficient for a towed wheel following a straight path. Figure 2.9 indicates that Equation 2.8 amply predicts the performance parameter P_T/W independent of turn angle α .

Since P_T/W is independent of the turn angle α , it can be used

---

[3]Melzer reported N_c values as determined from test conditions by Equation 2.1; however his test conditions were reported which permitted N_c' values to be calculated from Equation 2.3.
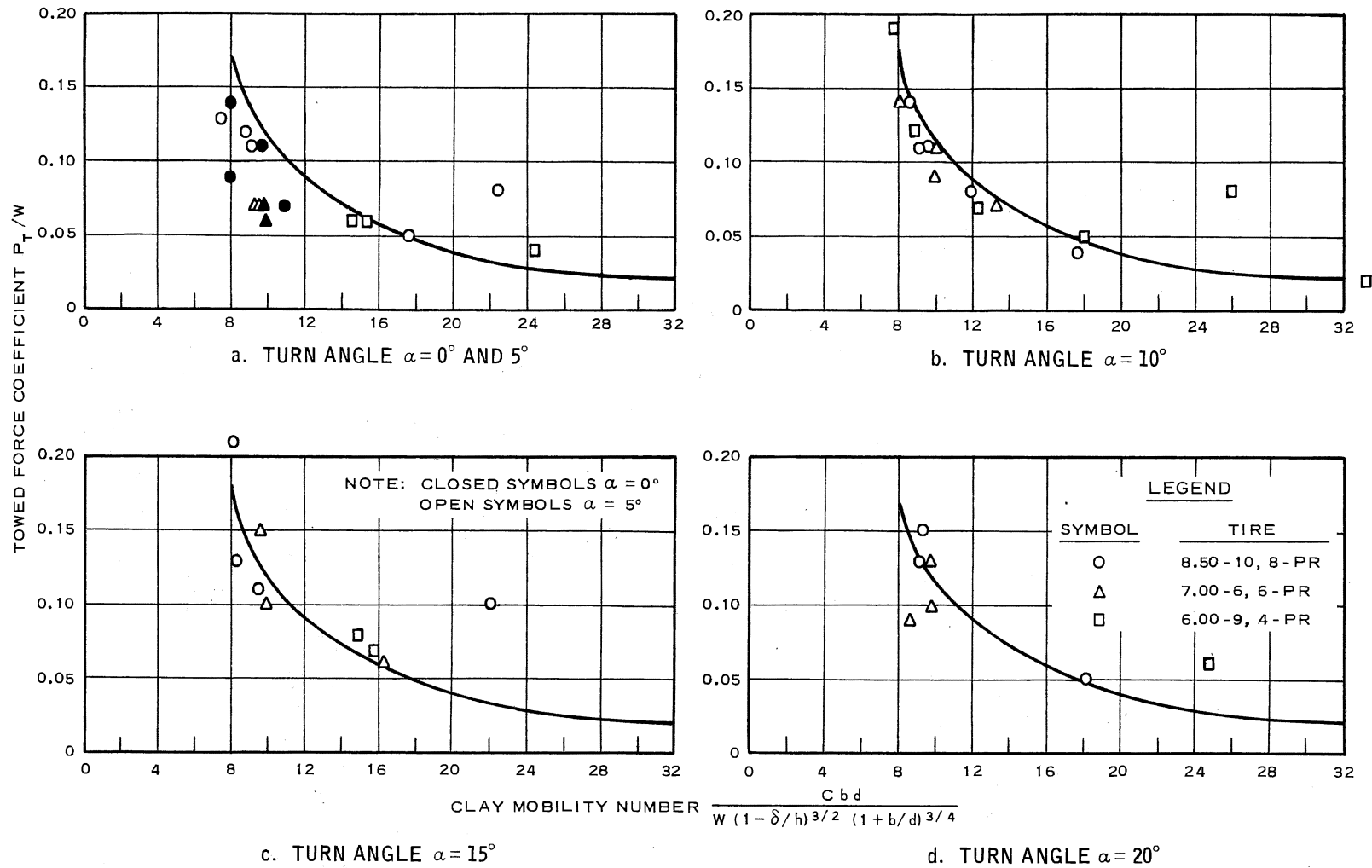
Figure 2.9. Towed Force Coefficient as a Function of Clay Mobility Number and Wheel Turn Angle (Data from Melzer, 1976).

to normalize S/W so that the effect of the independent variables, namely those variables comprising the clay mobility number N_c' and the wheel turn angle α, can be inspected. Figure 2.10 illustrates the relation between the side force/towed force coefficient and the clay mobility number and the wheel turn angle. For the specific wheel turn angles and test condition used in this study the side force of the towed wheel increased nonlinearily with increases of the wheel turn angle and the clay mobility number. These data cannot be effectively extrapolated significantly beyond the testing limits. If all variables were held constant and the soil strength progressively increased (with subsequent increases in the clay mobility number) then for a given turn angle the side force would reach some maximum value and then decrease to a near constant value as the soil approaches a rigid mass. The maximum value would occur, for a given turn angle, when an optimized condition of the two interrelated process developed. Resistance develops from the volume of soil undergoing displacement by passive action of the turned wheel partially embedded in and pushing against the soil. Increased soil volumes are involved as the wheel sinks deeper into the soil medium which occurs with decreasing values of soil shear strength or under larger wheel loads. Conversely, as shear strength increases sinkage decreases but the passive force developed by the wheel required to over-come the resisting side force increases per unit volume of soil displaced because of the higher shearing resistance offered by the soil mass.

Curves were fitted to the plotted values of S/P_T versus N_c' for the various turn angles as shown on Figure 2.10a through 2.10d. These curves are summarized and shown as solid lines in Figure 2.10e. The
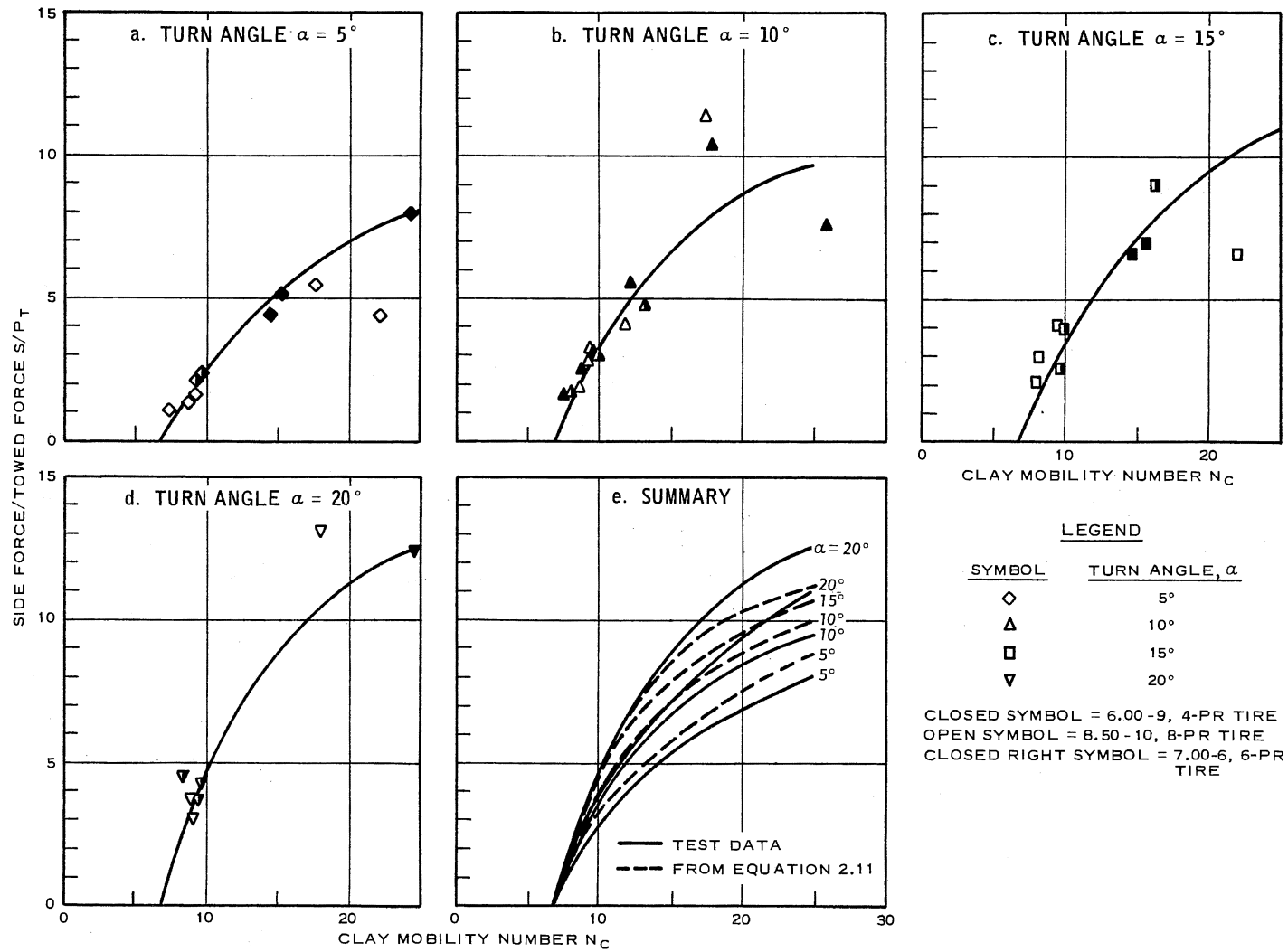
Figure 2.10. Ratio of Side Force/Towed Force as a Function of Clay Mobility Number and Wheel Turn Angle (Data from Melzer, 1976).

following equation was selected to analytically represent these graphical relations:

$$\frac{S}{P_T} = 15.4 - \frac{15.4\ B}{N_c' - 7 + B} \tag{2.11}$$

where

$$B = \frac{4}{\alpha^{1/2}}$$

The dashed lines shown on Figure 2.10e are the corresponding graphical representation of Equation 2.11 for the various turn angles shown. Stability problems will occur for Equation 2.11 for very small values of turn angle α . In the absence of towned data for turn angles less than 5 degrees it would be recommended that Equation 2.11 be linearly interpolated by the ratio of the turn angle in question to a turn angle of 5 degrees and with coefficient B equal 13.5, corresponding to a α of 5 degrees.

Prediction of the forces acting on an unpowered turn wheel being towed in soft clay can be made by using Equation 2.8 for determining the clay mobility number, Equations 2.9 and 2.10 for determining the tow and developed wheel torque, respectively, and Equation 2.11 for the side force.

Figure 2.11 presents the towed force coefficient sand data reported by Melzer as a function of the sand mobility number N_s and the wheel turn angle α . The continuous curve shown on each plot was derived from the equation

$$\frac{P_T}{W} = 0.015 + \frac{0.83}{N_s - .2} \tag{2.12}$$

This equation was first reported by Turnage (1972) and developed from a large data base of single wheels equipped with various pneumatic tires
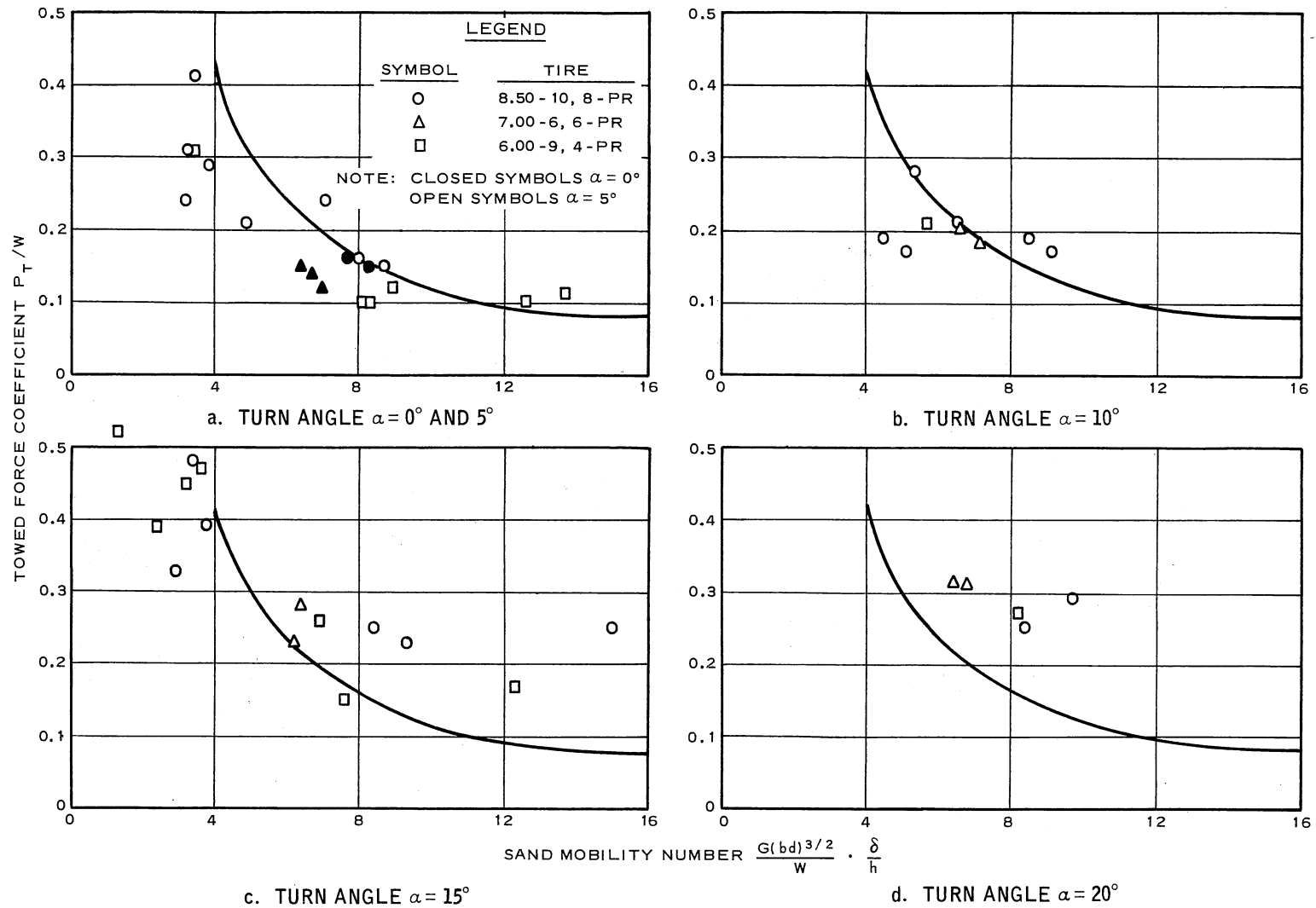
Figure 2.11. Towed Force Coefficient as a Function of Sand Mobility Number and Wheel Turn Angle (Data from Melzer, 1976).

and towed through two sands at a zero wheel turn angle. Although there is somewhat more scatter in the data of Figure 2.11 as compared to the similar presentation of the clay data, Equation 2.12 can be effectively used to predict the force in the plane of the hub for a turned wheel being towed through sand.

The scatter of P_T/W for the towed tests in sand prevented the use of that dependent variable for normalizing S/W as was done for the clay data. Instead the relation between side force coefficient S/W and the sand mobility number N_s were compared and graphically presented in Figure 2.12. Over the range of N_s reported by Melzer (1976), S/W increases with increasing turn angle α. For a specific turn angle, S/W increases with increasing N_s; however, in comparison with the corresponding relation obtained for clay (Figure 2.10), this increase with N_s is not as pronounced.

A fundamental equation having the form of a rectangular hyperbola was selected to represent the S/W versus N_s illustrated in Figure 2.12. The derived rectangular hyperbola is moved vertically within the plot depending upon the value of the turn angle. The basic relation

$$\frac{S}{W} = A + 0.83 - \frac{46}{N_s + 55.4} \qquad (2.13)$$

where

$$A = 1.275 \ \alpha^{1.23}$$

is shown for each of the four values of α with broken lines on Figure 2.12. Although Equation 2.13 adequately describes the experimental data for relating S/W versus N_s, values of S/W will result for $\alpha = 0$ thus predicting a physical anomaly. In the absence of towed
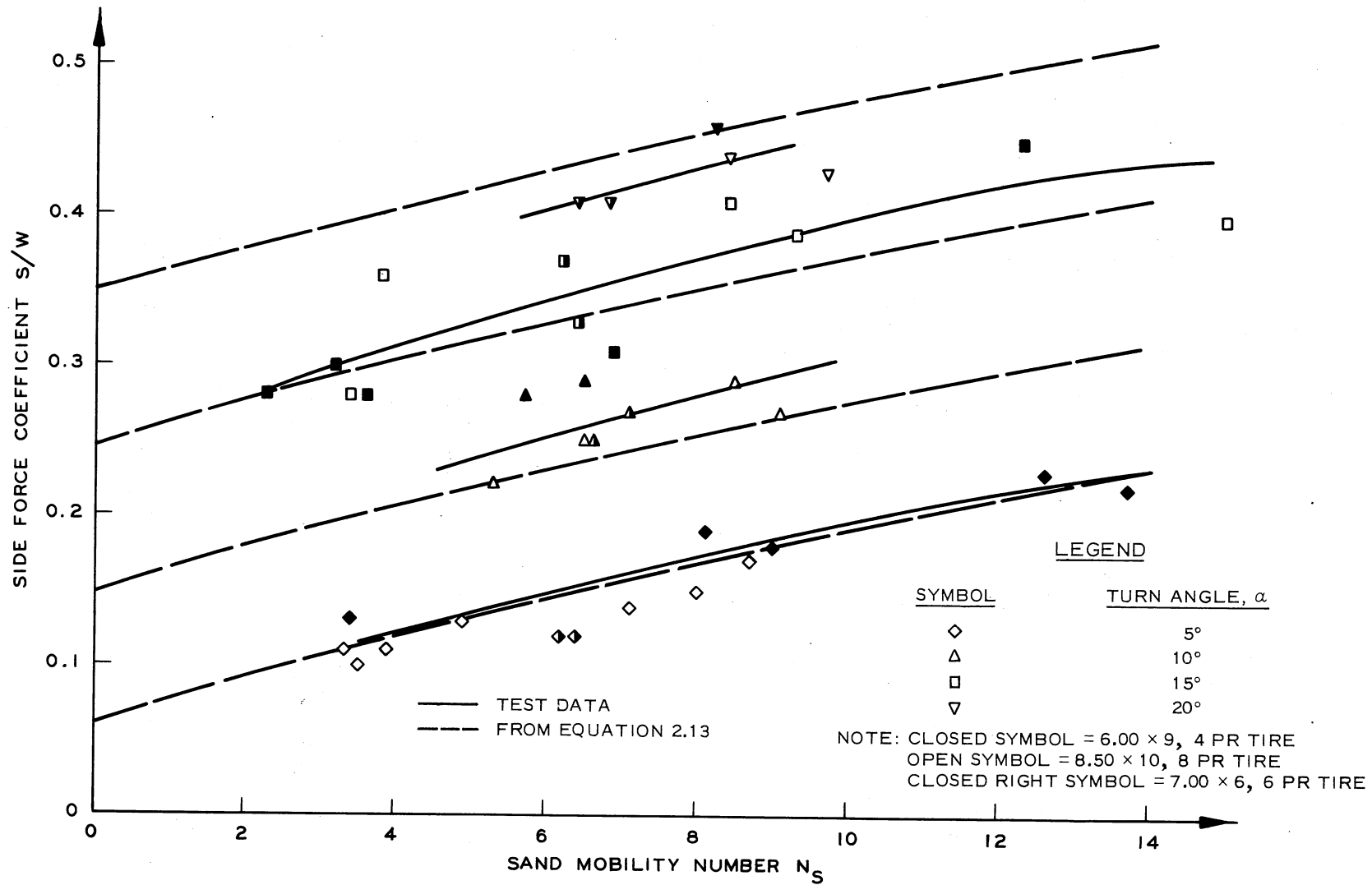
Figure 2.12. Side-Force Coefficient as a Function of Sand Mobility Number and Wheel Turn Angle (Data from Melzer, 1976).

data for turn angles less than 5 degrees it would be recommended that Equation 2.13 be linearly interpolated by the ratio of the turn angle in question to a turn angle of 5 degrees, thus coefficient A equals 0.06.

Other Pertinent Studies

Schwanghart (1968) reported on the results of tests conducted with towed single wheels equipped with agricultural machinery tires and front tires of tractors of various sizes. Measurements of towing force, lateral force, sinkage, and wheel slip were determined for each test condition. The single soil used for this study was reported as a sandy clay processed in a fixed test bin to a moisture content of 14.5 percent with the angle of internal friction ϕ varying from 30 to 36 degrees and cohesion of near zero. Figure 2.13 exemplifies Schwanghart's finding by illustrating the results from one test tire inflated to 1 atmosphere pressure and tested at various turn angles up to 28 degrees and wheel loads between 1000 and 4000 N[4]. Schwanghart noted that the towing force in the plane of the wheel is nearly independent of the wheel turn angle α (Figure 2.13a) when tested at a particular wheel load and up to a turn angle of about 20 degrees. The side force (Figure 2.13b) in the plane of the wheel and wheel sinkage (Figure 2.13c) increased with wheel turn angle at a certain load. Schwanghart results are completely compatible with the program on towed tires in the turned mode reported by Melzer (1976) and discussed earlier.

Taylor and Birtwistle (1966) investigated the most effective wheel

---

[4]Figure 2.13 is reproduced almost directly from Schwanghart (1968) and force units are designated as kp where 1 kp ≈ 1 kg and 1 kg is equal to 9.81 N.
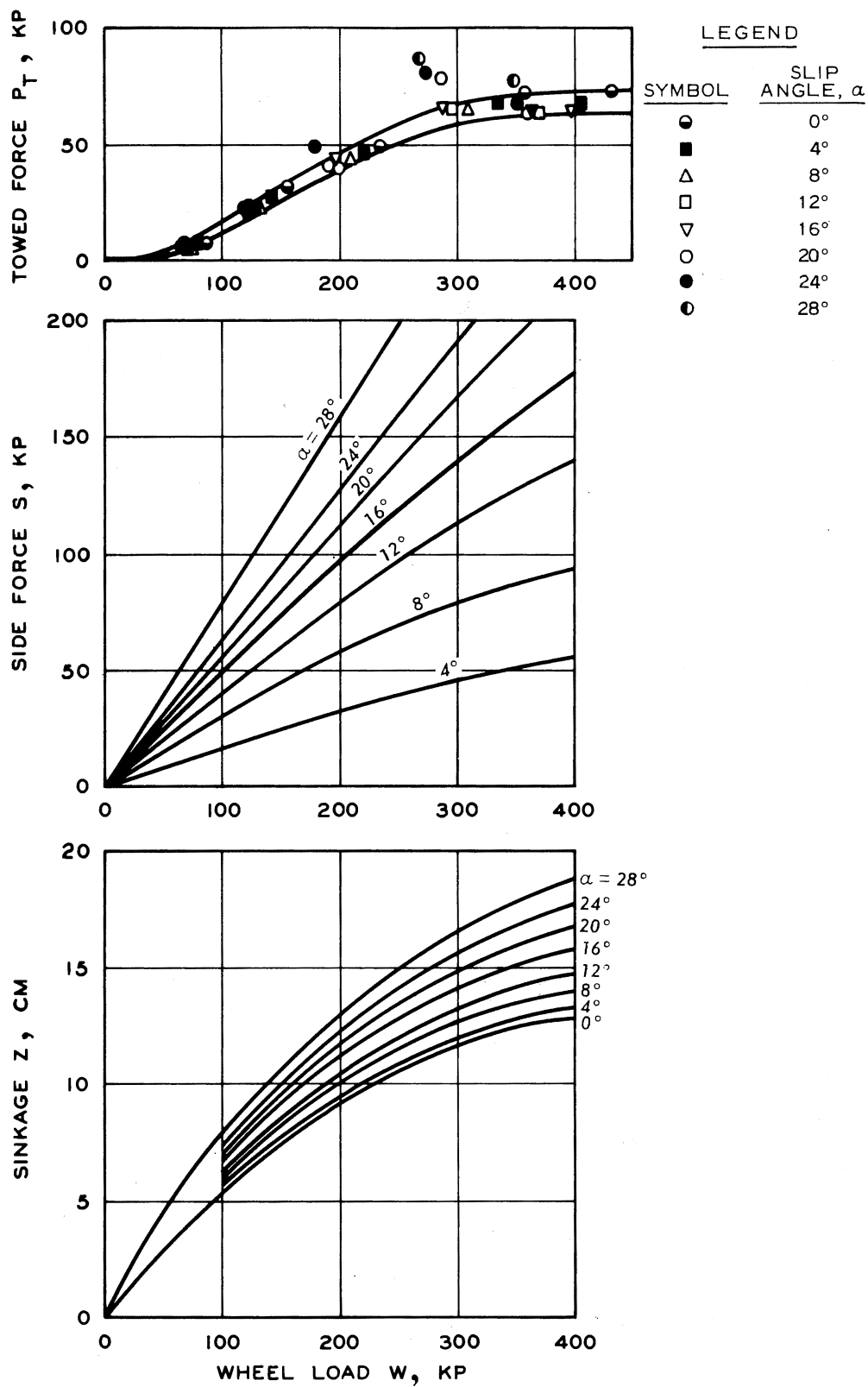
Figure 2.13. Towed Force, Side Force, and Sinkage of a 5.50-16
Tire at 1 atm as a Function of Wheel Load for
Various Wheel Turn Angles (from Schwanghart,
1968).

angular setting of the disc plough supporting wheels which would provide

for a maximum ratio of lateral force to drawbar force (i.e., side force

to counteract side forces generated by the plough discs with minimum

amount of forward motion resistance). The reported coordinate system

placed the drawbar force parallel to the direction of forward motion and

side force perpendicular to the direction of forward motion. Towed

tests were performed with a wheel equipped with 7.50-16, 6-ply tire of

three tread configuration and with inflation pressures either 40 or

70 psi. Two loads of 1000 or 1500-pounds were selected for variation of

the vertical wheel load. Two soils were selected for testing. One was

a sandy clay of very low plasticity (LL = 21, PI = 8) and having an

averaged in-place moisture content of 19 percent. The other soil was a

moderately plastic clay (LL = 46, PI = 20) and with an average placement

moisture content of 33 percent. For most test conditions the test

soils were processed to two general conditions, a loose and slightly

compacted consistency so as to simulate the wheels of a multi-disc

plough which generally have two wheels run the furrows (loose soil condi-

tion) and the other(s) on the unploughed ground (compacted soil).

Taylor and Birtwistle found that for the agricultural tires towed

through the two soils that wheel camber and tire tread pattern had very

little effect on the drawbar pull. In terms of measured side forces

perpendicular to the direction of travel, Taylor and Birtwistle results

showed that the side force increased with increases in wheel turn angle

(all other variables being held constant) up to an angle of about

12 degrees and then decreased slightly with further increases of the

wheel turn angle. The effect of wheel camber (0 to 15 degrees) was

somewhat linear for a given wheel loading and at a specific wheel turn

angle the side force was increased by 8 to 10 percent for each five degree increment of wheel camber. Magnitude of side forces was found to separate according to tire tread pattern for tests conducted on the sandy clay soil; however, this separation was not apparent for tests performed with the lean clay test soil.

Krick (1973) reported the results of tests conducted with single wheels equipped with agricultural tractor and cross country vehicle tires mounted within a six-degree-of-freedom dynamometer system. The results reported were conducted within a soil bin containing a sandy loam soil moderately compacted to resemble tractor traffic during cultivation and at a moisture content of 14.5 percent; reference to a measure of soil strength or its physical properties was not provided.

Performance was expressed in terms of side forces acting perpendicular to the plane of the wheel and tractive forces in the plane of the wheel. From the experimental data Krick developed relations between tractive and side forces as a function of side slip angle and wheel slip. Example plots shown in Figure 2.14 are typical of Krick results developed with a 7.50-18 tire at a pressure of 1 atmosphere with a wheel load of 530 kp. These results indicated that for the given test conditions (to include wheel turn angle) the side force decreases and the tractive force increases with increasing wheel slip (Figure 2.14a and 2.14b). Krick depicted the relations between tractive force, side force, wheel turn angle (designated as side slip angle by Krick), and wheel slip with "characteristics graphs" of the type shown in Figure 2.14c. In order to insure linear equation of steady state motion, Krick linearized the characteristics curves (Figure 2.15b)

a. SIDE FORCE VERSUS SLIP ANGLE

b. TRACTIVE FORCE VERSUS SLIP ANGLE

c. SIDE FORCE VERSUS TRACTIVE FORCE AND RELATION TO WHEEL SLIP AND SLIP ANGLE
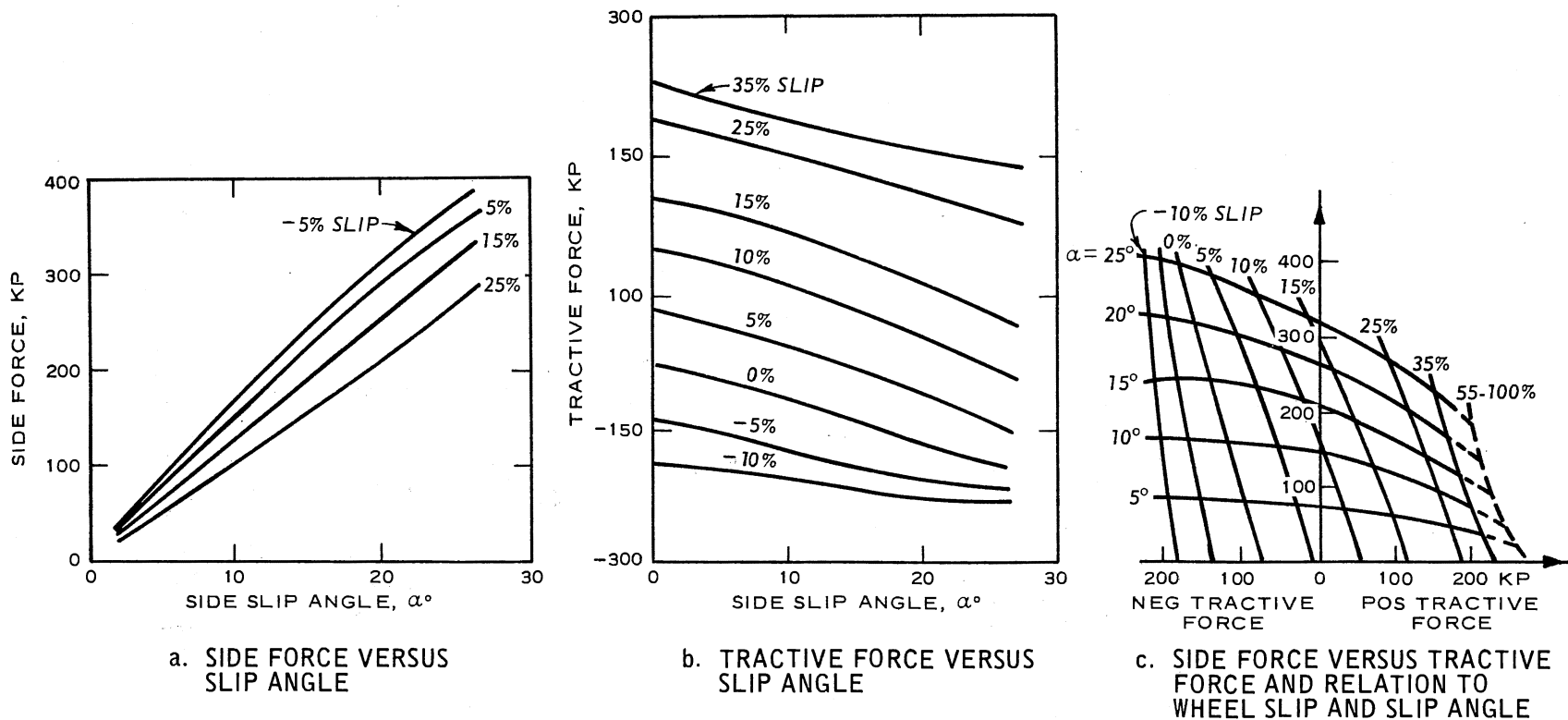
Figure 2.14. Side Force and Tractive Force in Relation to Side Slip Angle at Various Wheel Slips. Wheel Load = 530 kips. 7.50-18 AS Tire with 1 atm (98 kPa). Sandy Loam Soil, Water Content = 14 percent (after Krick, 1973).
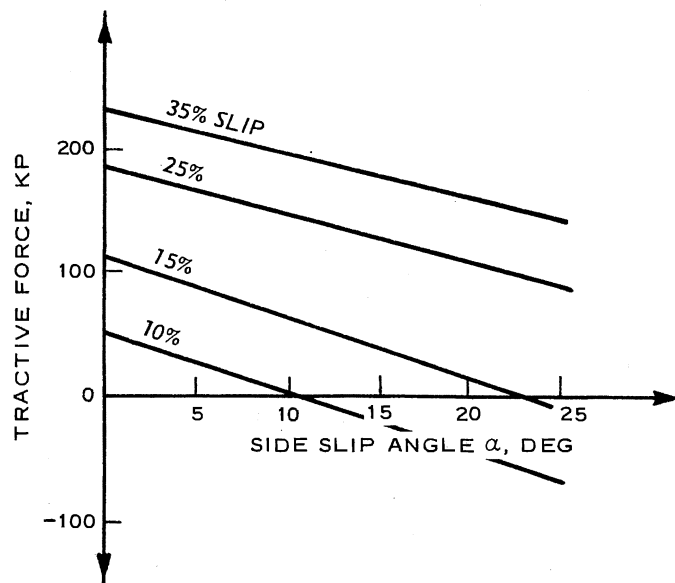
a. LINEARIZED TRACTIVE FORCE VERSUS SLIP ANGLE
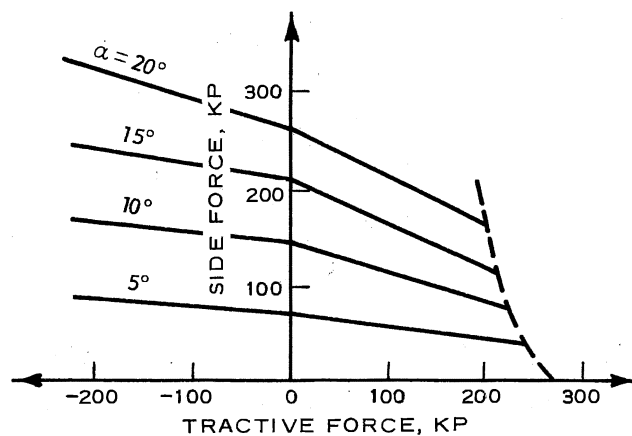
b. LINEARIZED SIDE FORCE VERSUS TRACTIVE FORCE RELATIONS

Figure 2.15. Linearized Turn Tire Test Results. Wheel Load = 530 kips. Tire - 7.50-18 AS Tire with 1 atm (98 kPa). Soil = Sandy Loam at 14 Percent Moisture Content. (After Krick, 1973).

and assumed a linear dependence tractive force and side slip angle

for given value of wheel slips (Figure 2.15a).

CHAPTER III

LABORATORY EQUIPMENT, TEST PROCEDURES,

AND TESTING PROGRAM

Introduction

This chapter describes the soils, equipment, and procedures used
to carry out the research on powered pneumatic tires operating in soft
soils in a turned mode. Pertinent engineering properties of the two
soils are presented and discussed. The section on equipment describes
the pneumatic tire, dynamometer, cone penetrometer, and related instru-
mentation used to measure the forces and important physical parameters
while conducting turned tire tests. Preparation of soil cars and
testing procedures is also described.

Materials

The entire research program was carried out on two soils that
represent the limits of the soil-type spectrum: a near saturated
purely cohesive soil ($\phi = 0$) and an air-dried cohesionless sand ($c = 0$).

Clay

One of the two soils tested was a cohesive, alluvial clay obtained
from floodplain deposits of the Mississippi River near Vicksburg,
Mississippi and is locally referred to as Vicksburg buckshot. This
material is classified as plastic clay (CH) according to the Unified

Soil Classification System. The consistency data, together with the particle size distribution curve are recorded in Figure 3.1. Compaction characteristics for Vicksburg buckshot are shown in Figure 3.2. The compaction test was performed using standard compaction effort according to procedures given in ASTM Standard D-698-70, method A (ASTM, 1975). As indicated, the particular buckshot tested has an optimum moisture content of 21.4 percent corresponding in a maximum density of 99.1 pounds per cubic foot.

Sand

The sand used in the laboratory tests was taken from an active dune area near Yuma, Arizona. Figure 3.3 shows the gradation and index properties of this soil, which is uniformly graded, subangular, and classified as SP-SM in accordance with the Unified Soil Classification System.

Preparation

The soils were prepared in movable soil bins (Figure 3.4) that are 0.8 metres deep, 1.6 metres wide, and long enough to accommodate test lanes 16 metres long. The procedures used to prepare clay and sand test bins with the desired consistencies and relative density, respectively, are briefly described in subsequent paragraphs with detailed narrative having been previously made by McRae et.al. (1965).

Soil Bin Preparation. Soil preparation began by drying the soil to a uniform low water content of about nine percent. Lumps within the dried soil were then reduced by mechanical crushing to a maximum 1/4-inch size. The soil was next blended with the desired amount of water
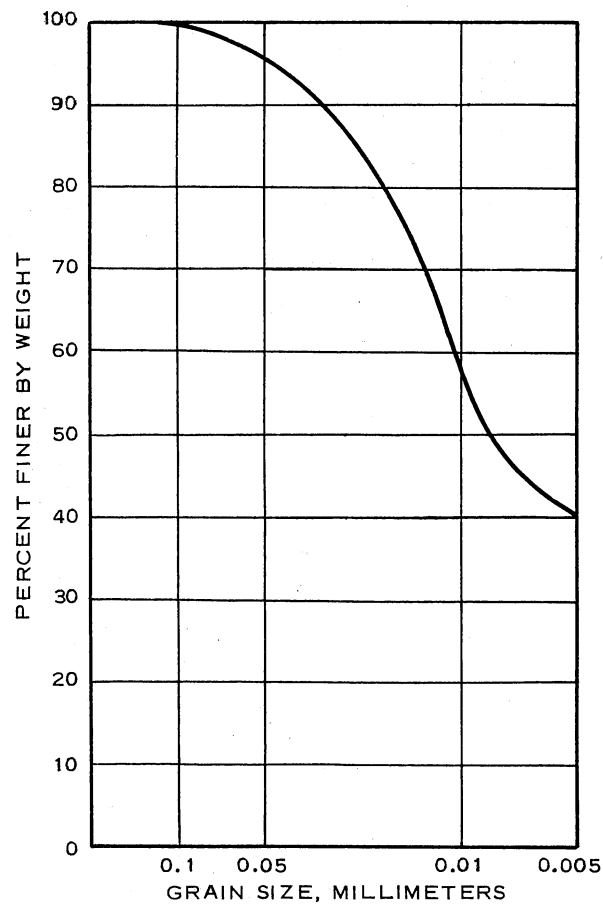
Figure 3.1. Particle-Size Distribution and
Classification Data for
Vicksburg Buckshot Clay.
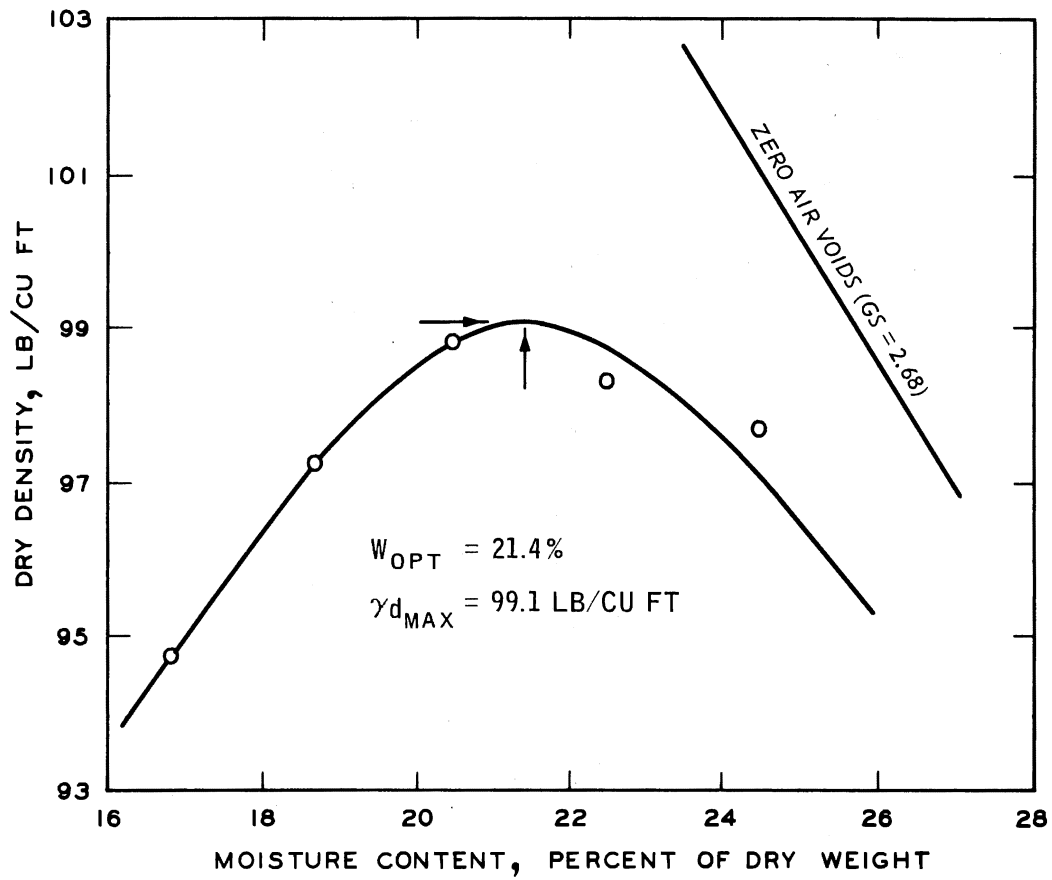
Figure 3.2. Standard Compaction Test on Vicksburg Buckshot.
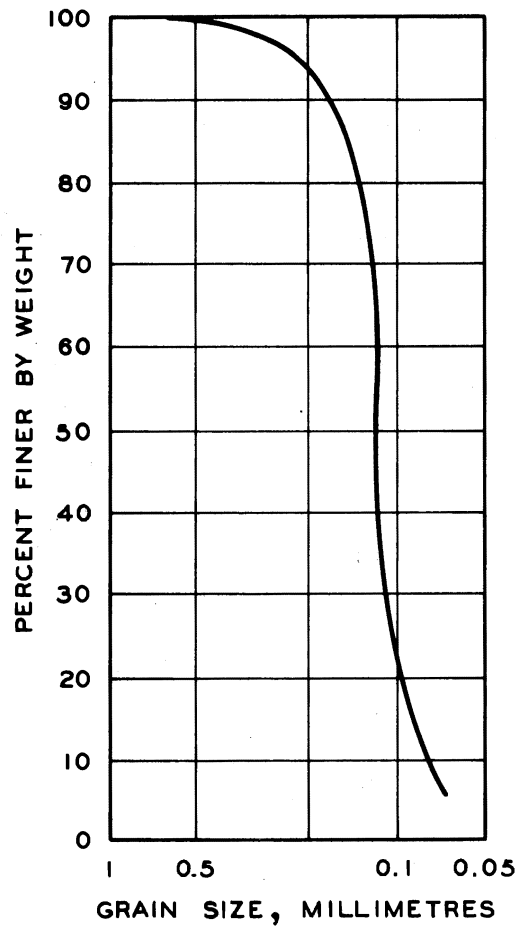
INDEX PROPERTIES OF YUMA SOIL

PROPERTY	VALUE
SPECIFIC GRAVITY OF SOLIDS	2.65
COEFFICIENT OF UNIFORMITY $CU = D_{60}/D_{10}$	1.50
CURVATURE COEFFICIENT $CC = (D_{30})^2 (D_{10} \times D_{60})$	1.26
D_{10}	0.08 MM
MAXIMUM DENSITY DRY UNIT WEIGHT VOID RATIO	104.3 LB/ CU FT 0.587
MINIMUM DENSITY DRY UNIT WEIGHT VOID RATIO	87.4 LB/ CU FT 0.893

Figure 3.3. Grain Size Distribution and Index Values of Yuma Sand.

in a pugmill (Figure 3.5) of the type used in brickmaking plants. Different degrees of soil strength can be achieved by preparing the soil at different moisture contents. The prepared soil issues continuously from the end of the pugmill into the soil bins, which are propelled slowly back and forth by a forklift truck. When sufficient soil has been deposited into the bin to produce an approximately six inch compacted layer, a lumberyard straddle truck equipped with a heavy pneumatic tired roller (Figure 3.6) provides the compacting effort. For this test program sufficient compaction was applied to achieve a desired compacted dry density of 88.6 pounds per cubic foot corresponding to a 33.0 percent moisture content and a degree of saturation of 99 percent. Additional layers were then added and compacted until the soil bin was filled. Finally the surface was leveled by using a grader blade attached to the straddle truck. After construction was completed, measurements were made to determine whether the desired soil conditions had been achieved.

Previous experience has found that the clay test bins can be reconstituted several times after being subjected to tire tests by filling the ruts left by the test tire and recompacting with a pneumatic tired roller. Before each test five cone penetrations were made along the traverse of the test cars to ensure an acceptable and uniform consistency had been achieved.

Sand Car Preparation. Uniform deposits of air-dried sand is achieved by allowing the soil to fall through a 1/4-inch mesh screen in uniform layers until the test bins were filled. The procedure is illustrated in Figure 3.7. The desired test density is achieved with the use of a small vibrating skid unit able to deliver a dynamic force of
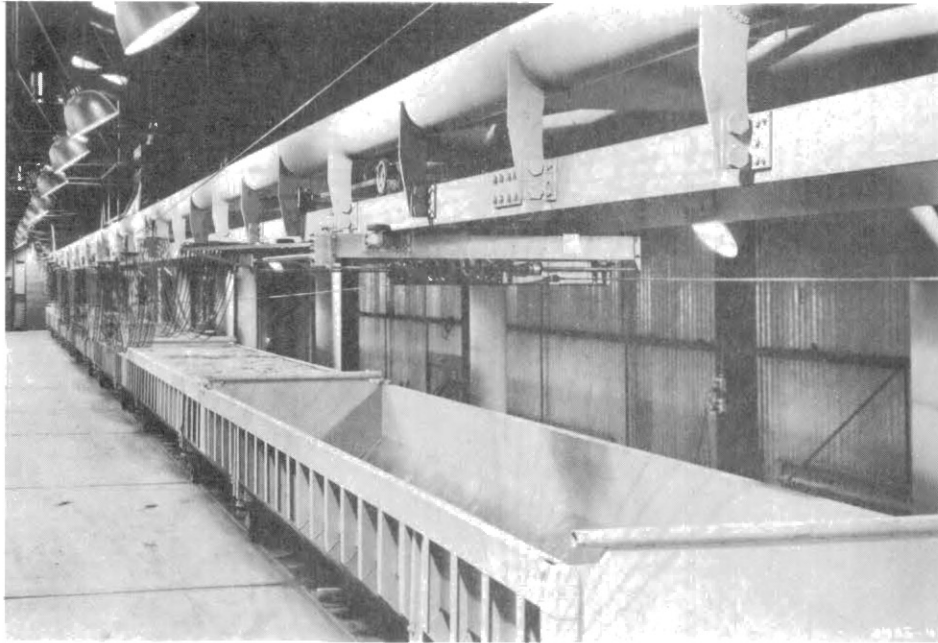
Figure 3.4.   Soil Bin in Position Beneath Overhead Rail System.
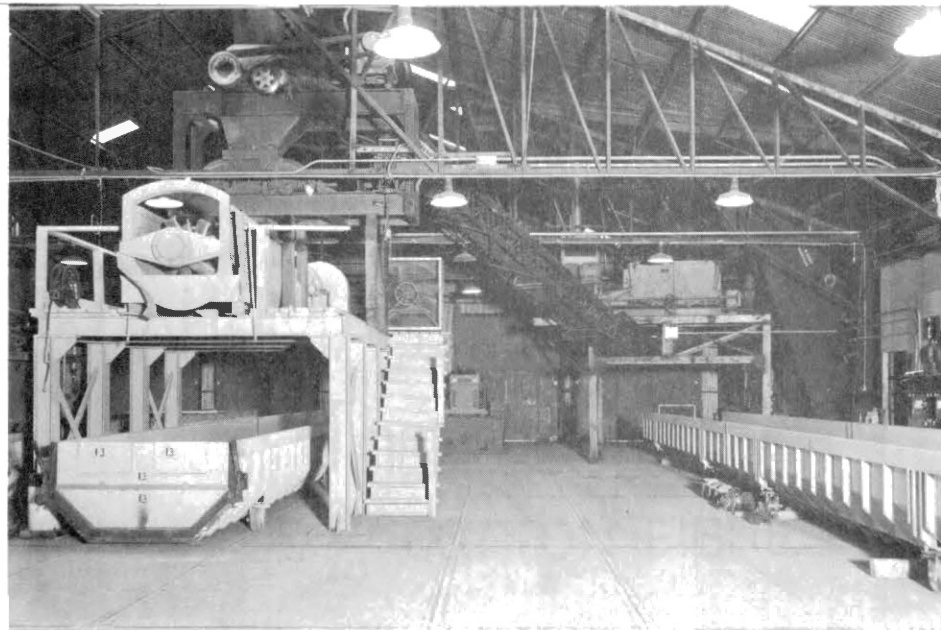
Figure 3.5.   Fine-grained Soil Processing Plant.
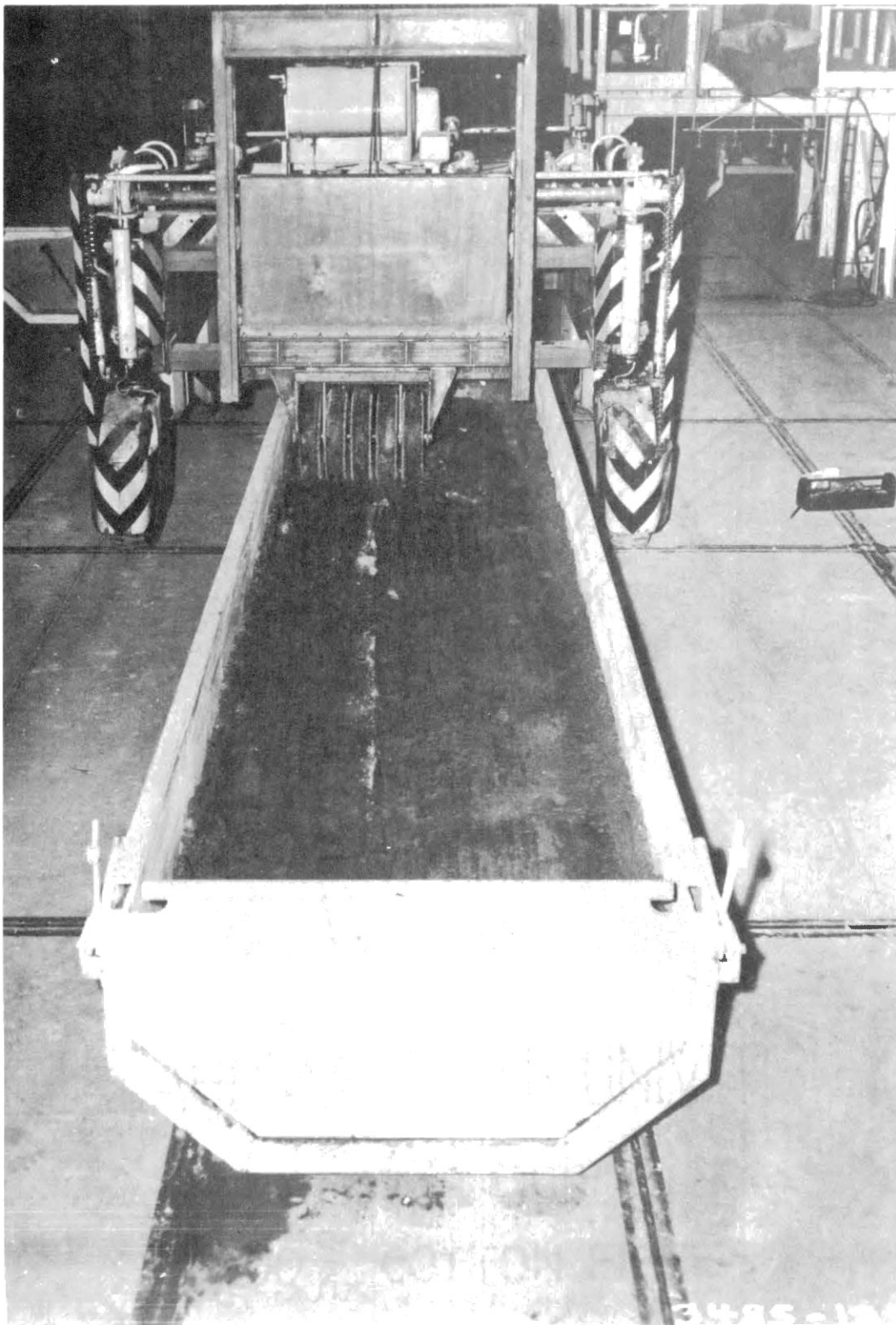
Figure 3.6. Straddle Truck Equipped with Pneumatic Tired Compactor.

Figure 3.7. Front-end Loader Spreading Sand on Screen During Filling of Soil Bins.

1800 pounds at a rate of 3600 blows per minute. The specific density
was achieved by controlling the speed of travel and the number of stops
of the vibrator over the sand surface.

The objective of soil processing of a test bin is to prepare uni-
form test sections in which the increase in strength (as determined
with a cone penetrometer) with depth is approximately linear to a depth
at least as great as the width of the test tire. Generally five cone
penetration determinations were made along the test cars traverse prior
to a tire test. After a tire test was performed the test section was
rehabilitated by scarifying (Figure 3.8) to a depth of 150 millimetres
and revibrating until the desired consistency was achieved.

Test Equipment

Tire

A 6.00, 4-PR trailer tire buffed free of tread was used during
the testing program. Pertinent tire data are listed in Table I. The
selection of this tire was somewhat dictated by the dimensions of the
modified carriage system used with the existing dynamometer system
that will be described in the following paragraphs.

Dynamometer System

The dynamometer system, or test carriage, used in this study is
part of the basic testing equipment available at the WES to investigate
running gears in single configuration (McRae, 1965). The carriage is
supported by solid rubber-tired rollers on a pair of overhead rails
aligned over the soil bins. These rails are suspended from cantilever
columns and cross arms (Figure 3.9). The carriage is towed along the
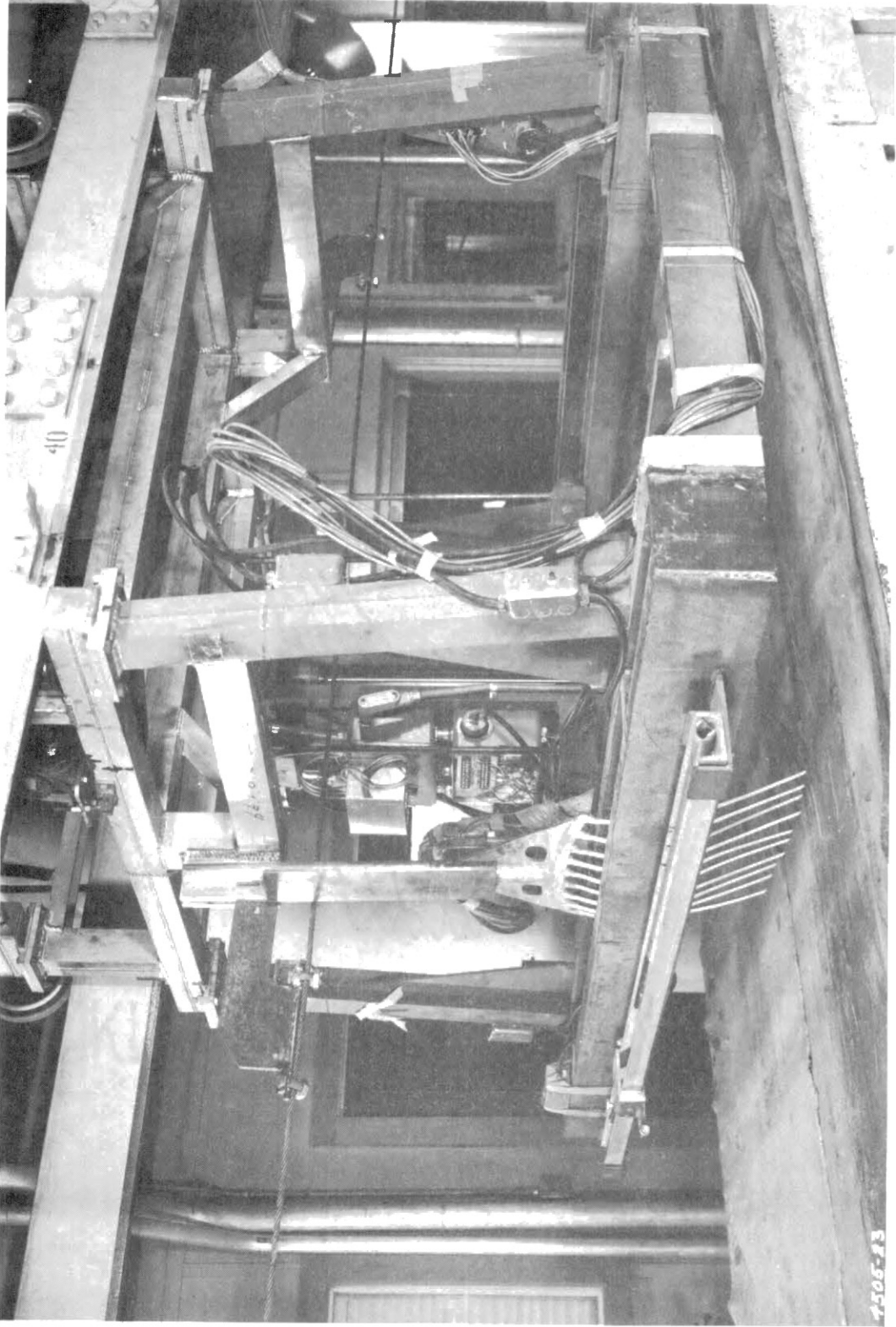
Figure 3.8. Hay Rake Used in Scarifying Sand.

Figure 3.9. Test Carriage in Position on Soil Bins.

rails by an electrically driven endless cable that is fastened fore and
aft to the carriage passing over pulleys at the end of the track
system. The speed of the towing cable, and thus the speed of the
carriage, can be varied up to velocities of about nine metres per
second. The test carriage and the cable can be shifted transversely
across the width of the soil bin.

TABLE I

DATA FOR 6.00-9, 4-PR GOODYEAR TIRE
(BUFFED SMOOTH)

Deflec-tion %	Load N	Unloaded Section Height h, m	Unloaded Carcass Diameter d, m	Unloaded Section Width b, m	Unloaded Inflation Pressure kPa
15	1000	0.128	0.516	0.159	52.7
15	2000	0.128	0.516	0.160	133.5
15	3000	0.128	0.516	0.160	191.5
15	4000	0.128	0.516	0.163	281.0
25	1000	0.128	0.516	0.159	14.5
25	2000	0.128	0.516	0.159	57.2
25	3000	0.128	0.516	0.159	100.0
25	4000	0.128	0.516	0.160	144.5
35	1000	0.128	0.516	0.159	5.0
35	2000	0.128	0.516	0.159	28.9
35	3000	0.128	0.516	0.159	56.5

The carriage consists of a main structure (Figure 3.10), which con-
tains the pneumatic load system, and a lower frame assembly to which,
under normal circumstances (tests exclusively in straight paths), the
test wheel is mounted in such a manner that it can be loaded and powered
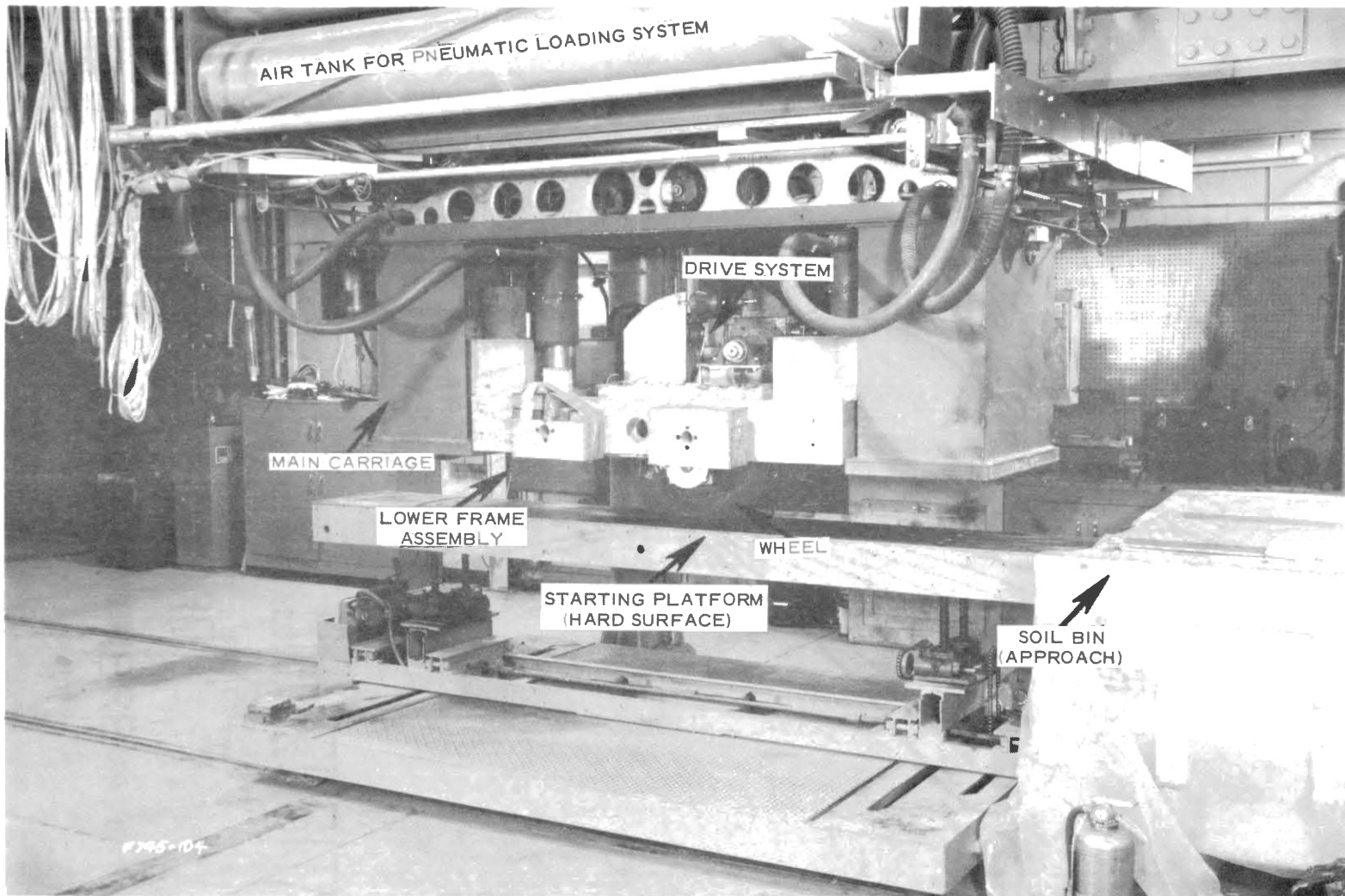
Figure 3.10. Overall View of Dynamometer Carriage.

and yet be free to move up and down. However, for the research described herein the main carriage system was modified so that the wheels could be tested at various turn angles (Melzer, 1976). The major modification is an additional subframe (Figure 3.11) that can be bolted to the basic inner frame (Figure 3.12) of the lower frame assembly at the desired turn angle. Turn angles can be varied from 0 to 20 degrees in five degree intervals. In this configuration, the carriage can accommodate wheels with diameters up to about .65 metres and with widths up to about .22 metres[1]. The wheels can be tested either powered or towed. In the latter case, the chains that connect the drive system with the wheel axle (Figure 3.13) are removed.

The dynamometer system is instrumented to measure the following quantities continuously during each test: wheel load, pull of a powered wheel or towed force of a towed wheel in line with the longitudinal axis of carriage travel, lateral forces exerted by the wheel on the inner carriage frame perpendicular to the direction of travel of the carriage, wheel hub movement, carriage velocity, angular velocity of the wheel, and applied torque (powered tests).

The test wheel axle is rigidly fixed within the inner frame of the lower supporting frame, and the inner frame is suspended from the outer frame at the four corners by load cells that are mounted vertically and serve as hinges. The hinges allow the inner frame to swing longtiudinally, but the movement is opposed by a load cell mounted horizontally between the two frames to measure the horizontal force on the wheel.

_____

[1]This restraint in wheel diameters is probably the major shortcoming of the modified carriage; however, much larger wheels could not be tested because of the overall carriage system was not designed to accommodate excessive lateral forces.
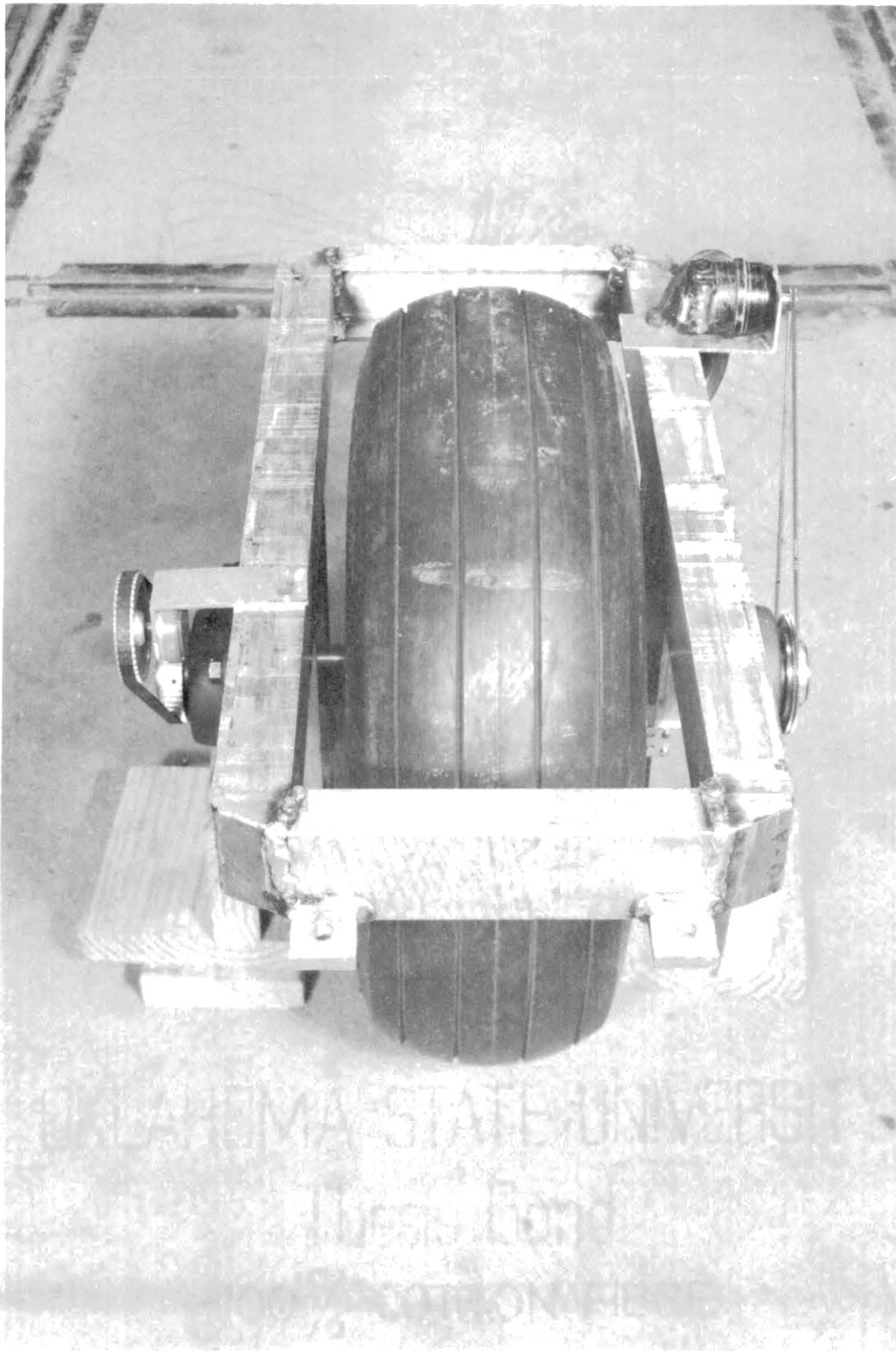
Figure 3.11. Wheel Equipped with 850-10, 8-PR Aircraft Pneumatic Tire
Mounted in Subframe.
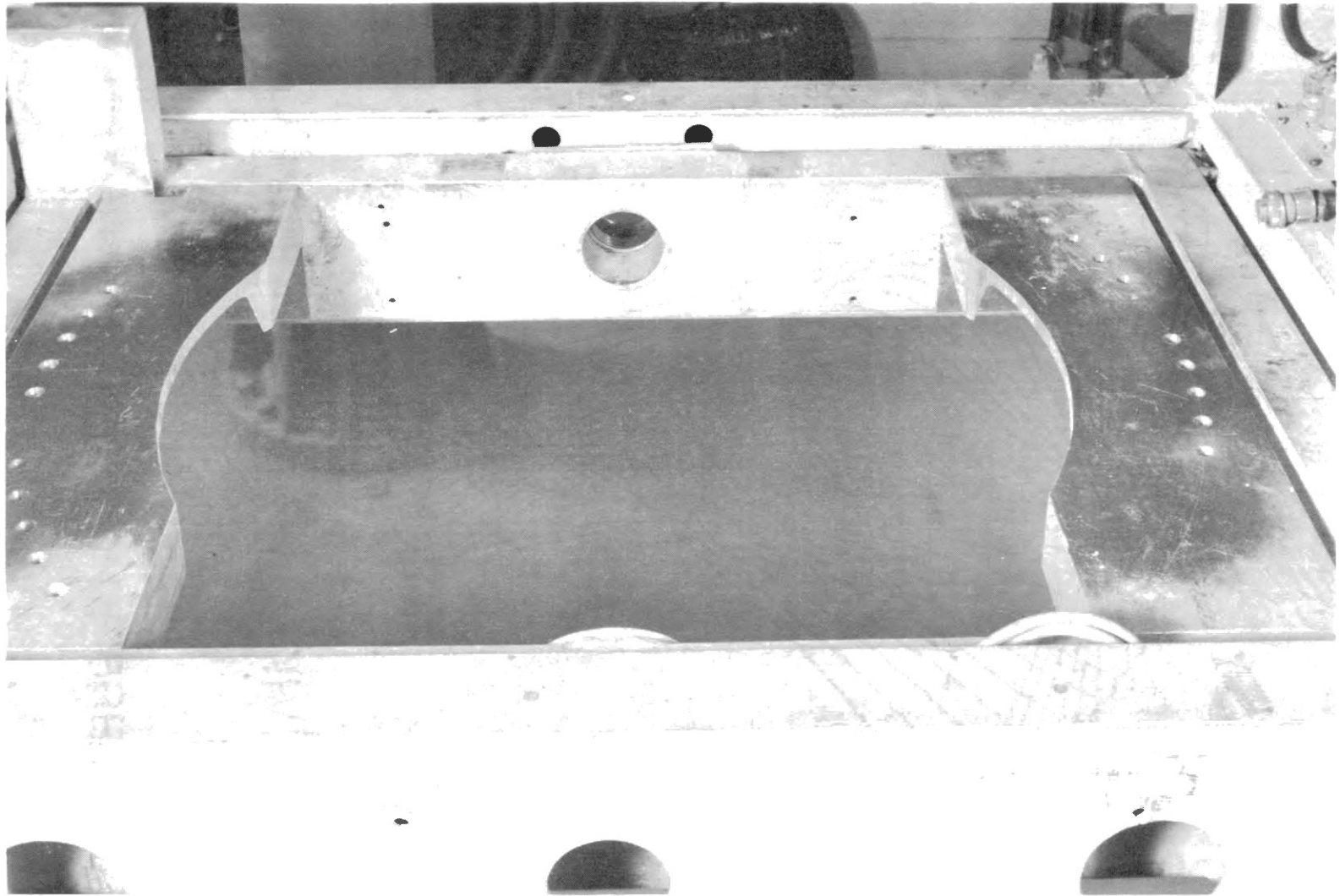
Figure 3.12. Lower Frame Assembly of Dynamometer System (Without Subframe and Wheel).
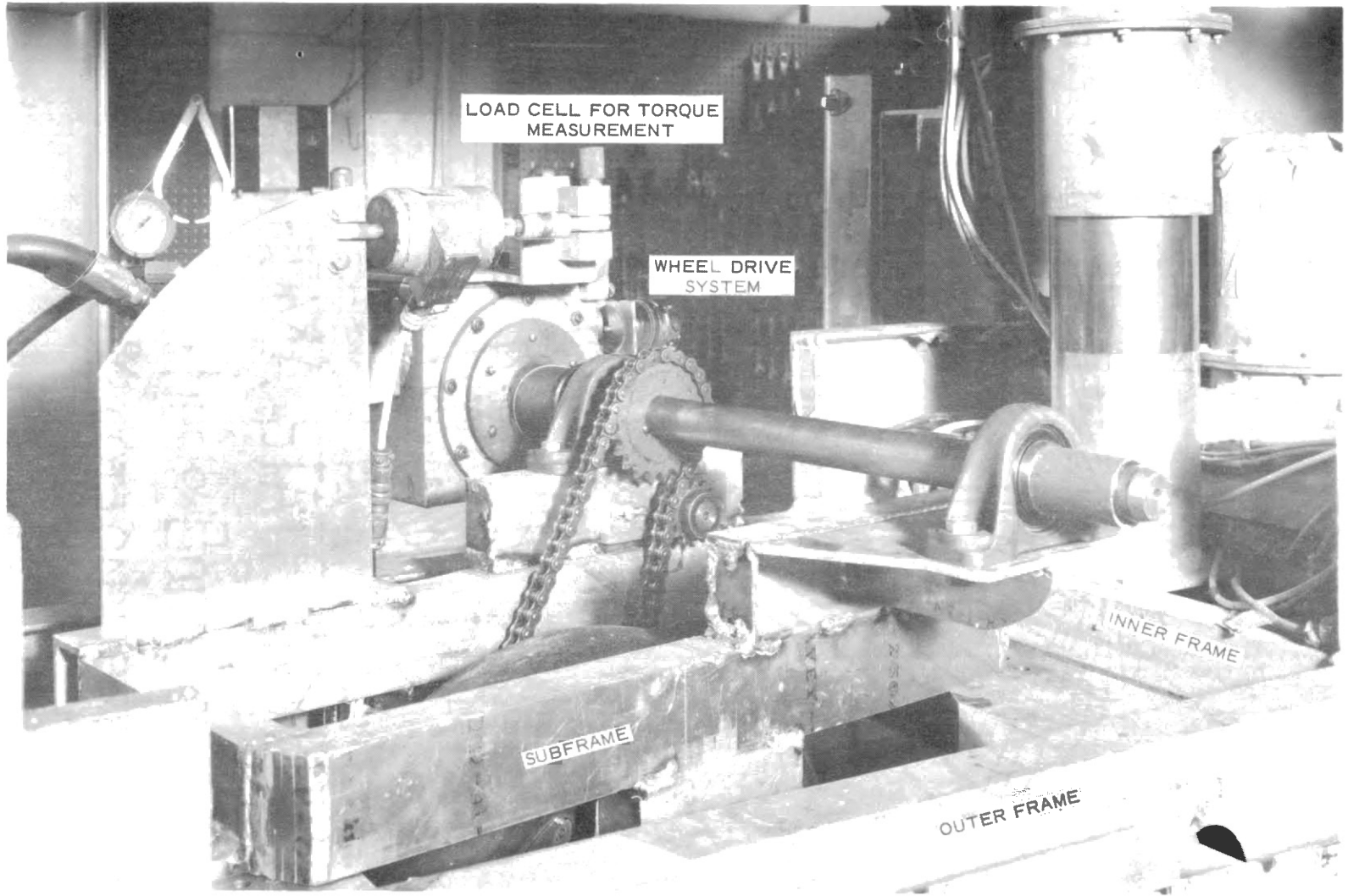
Figure 3.13. Subframe Mounted in Place and Wheel Drive System.

In addition, two load cells are installed parallel to the front and rear ends of the inner frame and connected by rods with the outer frame. These load cells monitor the side forces exerted by the wheel on the inner frame. Each end of the outer frame is attached to a vertical ball-spline shaft that allows the entire assemble to move freely in a vertical direction, but prevent rotation of the assembly in any plane.

Load is applied to the test tire by means of pneumatic cylinders mounted between the upper and lower frames. This air loading system is double-acting, so that an upward force can be used to permit tests at loads less than the static weight of the assemble. The test carriage utilizes one pair of cylinders at the front and another pair at the rear. The air storage tanks, which are visible in the upper portion of Figure 3.10, provide a reserve air supply to compensate for movement of the loading cylinders caused by vertical wheel movement as it progresses down the test lane.

Axial (or hub) movement is measured by a potentiometer connected between the lower frame assembly (Figure 3.11) with the main carriage body. Carriage speed was measured by a tachometer. Angular velocity of the test tire was measured by potentiometer and a tachometer shown mounted in Figure 3.11. Wheel revolutions were monitored by a stationary photoelectric cell and a perforated circular disk that rotates with the axle, and carriage position is indicated by a photo-electric cell mounted on the upper frame, which is activated by tabs spaced .10 metres apart on one of the overhead rails.

The wheel is powered by a hydraulic motor driving through a specifically constructed mechanical transmission mounted on the axle of the wheel. The wheel's rotational speed can be regulated at will,

completely independent of the forward speed of the test carriage. The transmission is restrained from rotating about the axle by a connecting arm in a series with a load cell connected to the support frame. During a test the input torque to the wheel is determined by recording the load cell output and knowing the length (moment arm) of the connecting members.

Data Recording Equipment

Events measured by the instruments mounted on the test carriage originate as electric (analog) signals which are relayed through cables to the signal conditioning and recording equipment (Figure 3.14). The primary recording system is a FM magnetic tape recorder that stores the analog signals in raw form, with no signal conditioning, for further data processing (digitizing). A secondary recording system is a 36-channel, direct-writing oscillograph, which requires signal conditioning. This latter system in addition to providing a backup recording capability, permits a visual inspection of the test data as required to assist in planning subsequent tests, and to rapidly appraise test results. The accuracy of the oscillograph readings depends on the scale used and the expertise of the reader. Only results obtained from the primary recording system were used in the analysis of this test program. The data recorded on magnetic tape was digitized and further processed into engineering units on a digital computer. Using appropriate computer software, the following measured parameters were averaged for each test: lateral forces S' , longitudinal pull P' , wheel hub movement, wheel load W , carriage velocity v_a , and translational velocity v_w of the wheel.
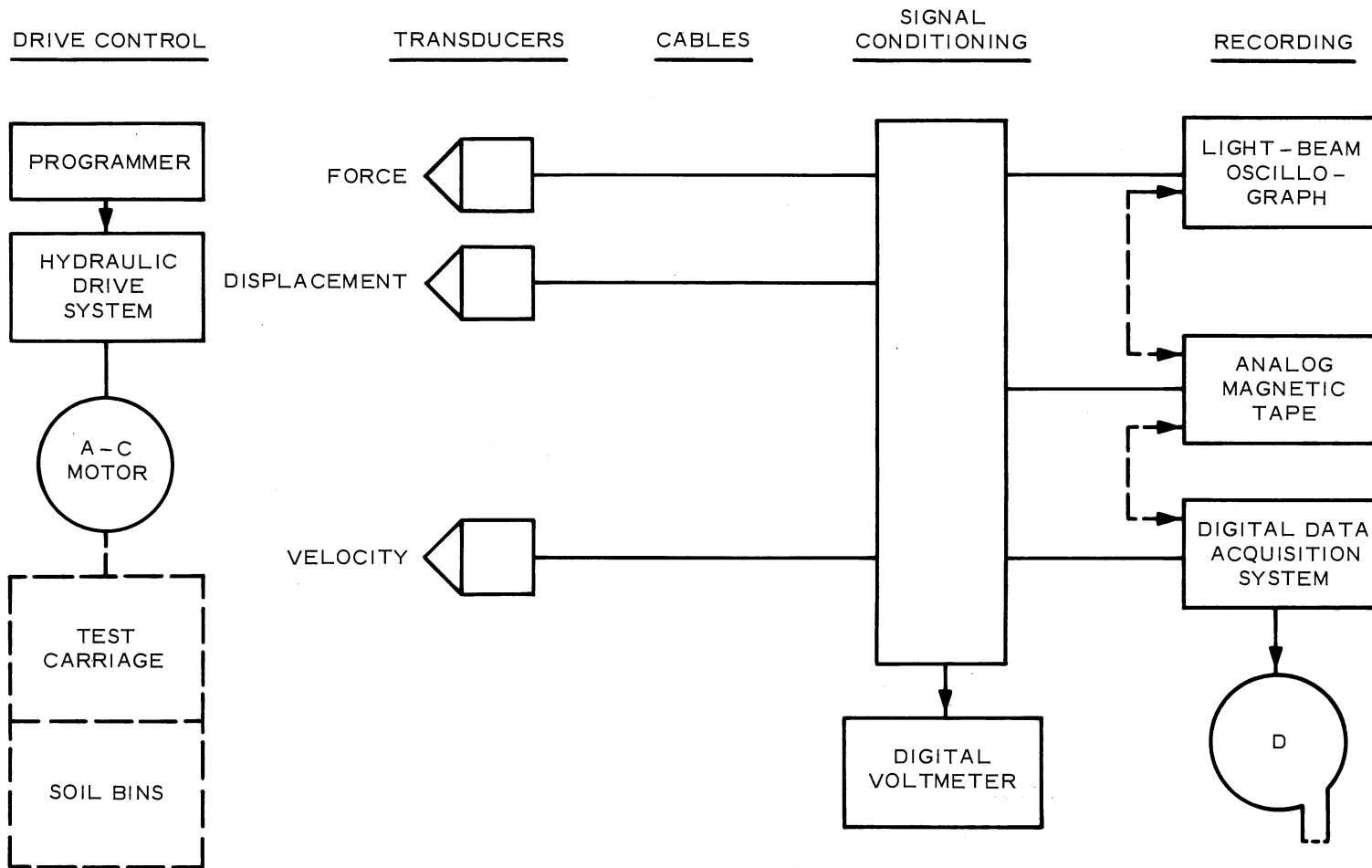
Figure 3.14. Flow Chart for Measurement and Control Systems.

Soil Strength Measurement

Prior to the conduct of each tire test, soil strength was measured at five locations in the soil cars with the WES standard mechanical cone penetrometer (Figure 3.15). The WES cone penetrometer was developed more than 20 years ago as a device to obtain an index of strength of surface soils for trafficability studies and airfield construction. Cone penetrometer reading (resistance values) are not considered basic soil properties but nontheless a convenient measure of soil strength (cone index).

Initially cone index[2] was defined as the average penetration resistance over a depth of 0 to 6 inches in both cohesive and cohesionless soils (Green, 1964). Later, it came to be used to represent the strength of cohesive soils only; for cohesionless soils, the cone gradient was introduced, which is the rate of penetration resistance increase averaged over a depth of 6-inches (Freitag, 1965). Subsequent conversion to metric units results in the terms cone penetration and penetration resistance gradient have replaced cone index and cone index gradient, respectively.

Basically, the instrument consists of a cone with a base diameter of 20.3 millimetres and an apex angle of 30 degrees, attached to a shaft that is about one metre long and has a diameter slightly smaller than the cone. A mechanized cone penetrometer was developed for laboratory

---

[2]Actually cone index is a misnomer because the number is a unit load required to maintain movement of a specifically dimensioned cone in a soil mass and actually has dimension of force per unit area. Originally English units of pounds per square inch were implied but not attached to the number because the same size cone penetrometer was always used in related trafficability studies.
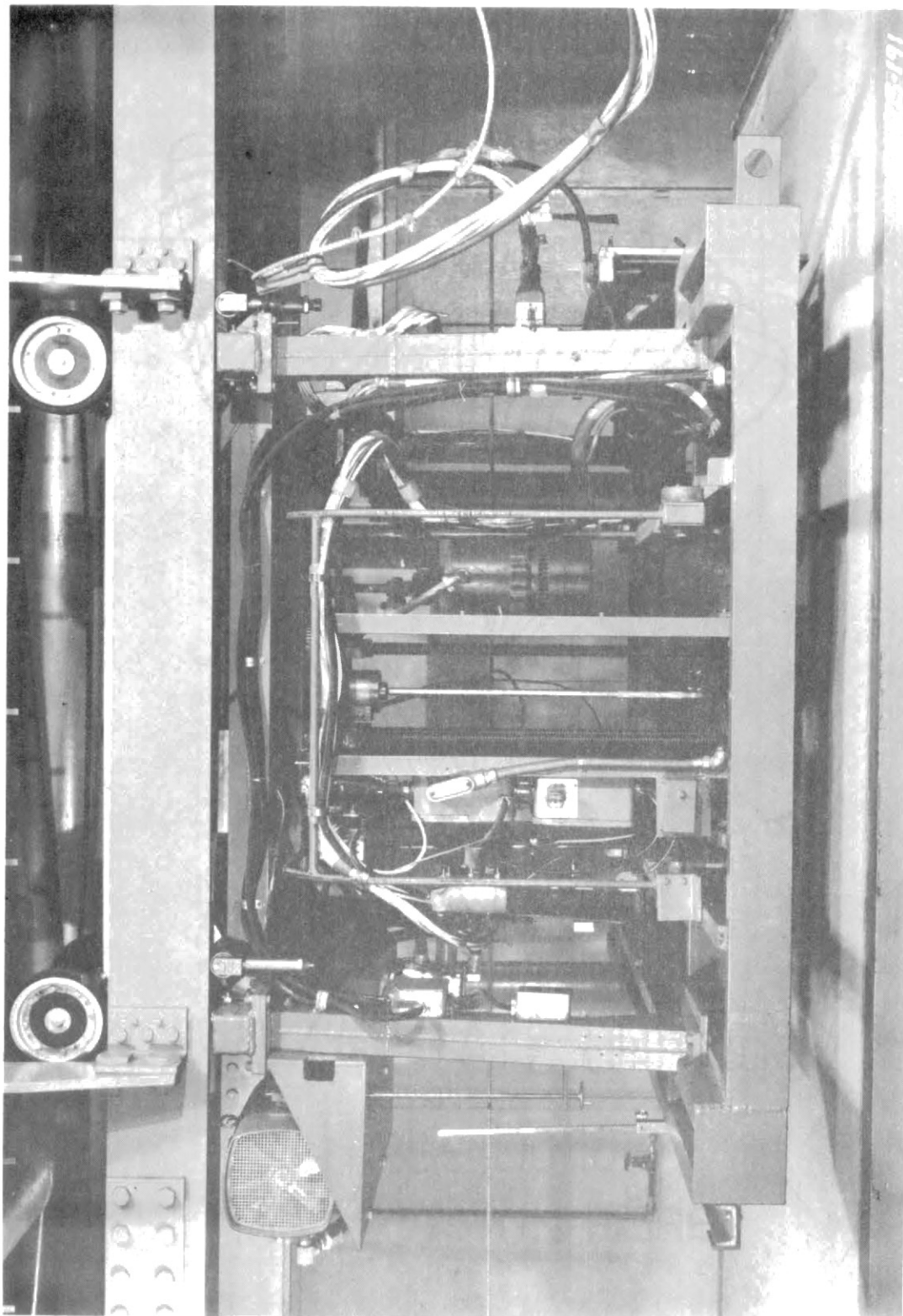
Figure 3.15. Mechanized Cone Penetrometer.

use in mobility related research (McRae, 1965). The penetration rate was 0.03 millimetres per second. The penetration resistance was measured continuously through the 0-150 millimetre depth by a load cell mounted at the top of the penetrometer shaft and recorded directly by an x-y recorder and simultaneously stored on magnetic tape for further processing.

The shear strength of soils having cohesive properties is largely dependent (disregarding or holding constant the effect of previous stress history, structure and mineral composition) upon their density and amount of water present within the voids. If a large percentage of the void space of a loose soil is filled with air (low degree of saturation), an applied load will result in compaction of the soil mass with subsequent strength increases (analogous to local shear failure). If however, the voids are predominantly filled with water (high degree of saturation) an applied load will be largely carried by the pore water and a volume change will occur only as water is squeezed from the mass. For this situation the soil mass would react to rapidly applied loading by yielding when the cohesive resistance is exceeded; hence, the shearing strength of a saturated cohesive soil is independent of the normal stress applied, Figure 3.16a. Cone penetration of a saturated cohesive clay will mobilize the soil's undrained shear strength and after surface effects have been eliminated, the relation between cone penetration resistance and depth is a unique value, as illustrated in Figure 3.16b. Smith (1966) has shown that a very good correlation exists between cone penetration resistance as determined by the WES penetrometer and cohesion as determined by conventional undrained-unconsolidated triaxial compression tests performed on clays molded at sufficient water contents to yield degrees of saturation in excess of 95 percent.
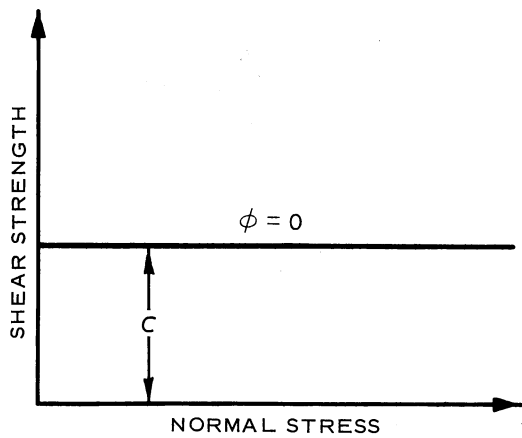
a. MOHR – COULOMB REPRESENTATION
OF PURELY COHESIVE SOIL
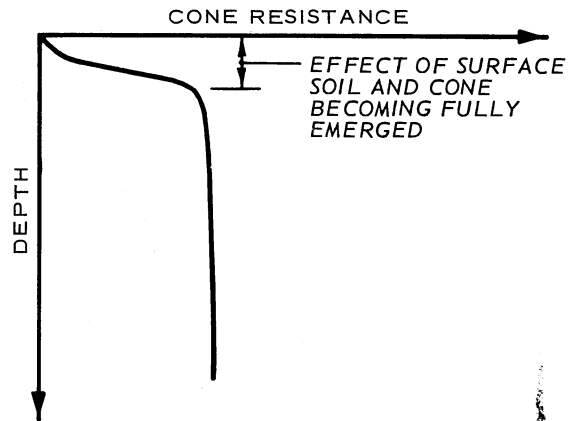
b. PENETRATION RESISTANCE VS
DEPTH OF SATURATED CLAY
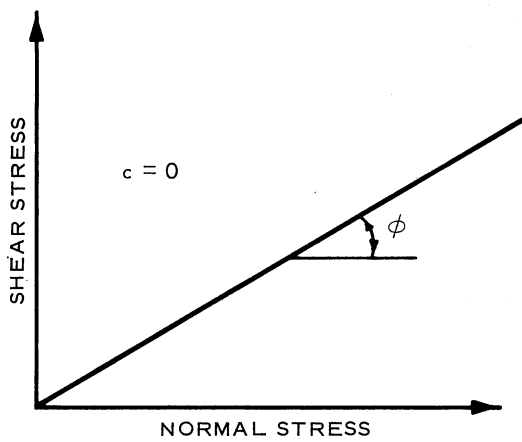
c. MOHR – COULOMB REPRESENTATION
OF PURELY COHESIONLESS SOIL
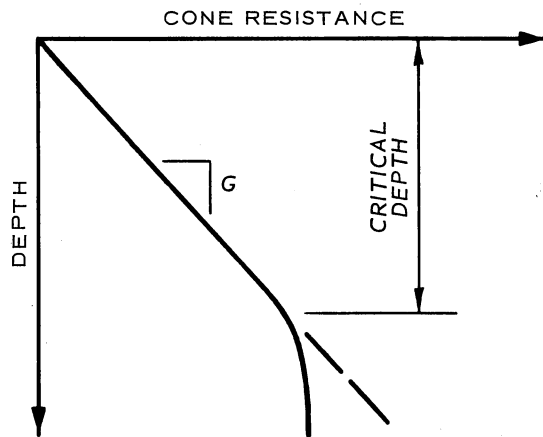
d. PENETRATION RESISTANCE VS DEPTH
OF PURELY COHESIONLESS SOIL

Figure 3.16. Cone Penetration of Soils.

The available shear strength of a cohesionless soil is directly dependent on the applied stress (Figure 3.16c); therefore, constantly increasing forces must be applied to a cone penetrometer as it moves vertically through a sand medium (Figure 3.16d). At shallow depths this increased force is necessary as the sand's shearing resistance is mobilized along the plastic rupture surface as it develops while the cone moves vertically through a sand medium. Theoretically at some "critical" depth (the numerical value depends upon what method selected, e.g. Terzahi, DeBeer, Meyerhoft, etc. bearing capacity for deep foundations and piles) the rupture zone is fully developed and penetration resistance increases only because of the increasing overburden pressure and the increase is therefore much smaller than the above the "critical" depth. Melzer (1971) performed cone penetration tests on three clean fine to medium sands and found that the critical depth using the WES cone penetrometer was in excess of 150 millimetres for medium or dense sands. This is below the depth at which the cone penetration resistance gradient was determined.

The magnitude of the cone penetration resistance at any depth is determined by the soil properties. For soil conditions in which the resistance to penetration is determined only by soil cohesion or only frictional properties the cone penetrometer has been shown to provide good insight to material properties and shear strength. However, the cone penetrometer readings of soils having both frictional and cohesion (most of the real world) do not readily distinguish the relative effect of each component of shear strength.

Test Procedures

The first steps in the testing procedure was to establish zero

positions for all the recording tracks and to record them both on the

oscillograph and magnetic tape recorder. The transducer signal repre-

senting each important variable was then calibrated to ensure that the

instrumentation was working properly and the calibrations recorded.

Before each test the soil surface was leveled and surface profiles

were taken. Cone penetration resistance was measured at five locations

in the test lane of the soil bin before each test to check the uniformity

of the soil and to determine whether the desired soil consistency existed

prior to testing.

Prior to each test the wheel was lowered to a hard-surface platform

adjusted to the average elevation of the test section. Then the desired

load was applied with the pneumatic loading system. The desired tire

deflection in percent of the unloaded section height (15, 25, and 35

percent in this test program) was achieved by measuring the deflected

section height of the loaded tire and adjusting the inflation pressure.

All wheel tests of this study were conducted with a constant-slip

technique. The constant-slip tests were run by maintaining a constant

forward velocity of the dynamometer system and a constant angular veloc-

ity of the wheel, by applying a preselected input torque and measuring

the pull that resulted. An unloaded wheel speed of approximately one

revolution per second was used throughout the test program; the carriage

speed was adjusted to obtain the desired wheel slip.

Test Program

The test program was divided into two parts consisting of 23 tests

performed on near saturated plastic clay and 49 tests performed on air-dried Yuma sand.

Constant-slip, one-pass, powered tests were conducted in the laboratory with a 6.00-9, 4-PR tire. Performance was measured in terms of pull, side force, torque, and sinkage. Wheel load was varied between 1000 and 4000 N. Tire deflections were 15, 25, and 35 percent of unloaded tire section height. Cone penetration resistance, C, was approximately 290 kPa for the clay, and two cone penetration resistance gradients of 2.0 and 3.2 mPa/m in the Yuma sand.

The tests conducted in this program are tabulated in Table II and test results are summarized in Table A.1, Appendix A, for clay tests and Table A.2, Appendix A, for sand tests. Figure A.1 is provided as a descriptor and key for the table headings.

TABLE II

TEST CONDUCTED

No. of Tests	Design Wheel Load N	Tire Deflection %	Design Soil Strength	Wheel Turn Angle Degrees
		Clay Test		
			kPa	
4	2000	35	290	0
1	2000	35	290	5
3	2000	35	290	10
3	2000	35	290	20
3	2000	15	290	5
3	2000	15	290	15
3	2000	25	290	10
1	1000	25	290	10
1	4000	25	290	10
1	3000	35	290	5
		Sand Tests		
			mPa/m	
3	2000	35	2.0	0
4	2000	35	2.0	5
6	2000	35	2.0	10
2	2000	35	2.0	20
1	1000	35	2.0	15
3	1000	35	2.0	20
1	3000	35	2.0	15
3	2000	15	2.0	10
1	2000	15	2.0	20
1	2000	25	2.0	10
1	2000	25	2.0	15
3	2000	35	3.2	5
4	2000	35	3.2	15
4	1000	35	3.2	10
4	1000	35	3.2	15
3	1000	35	3.2	20
1	3000	35	3.2	15
1	2000	15	3.2	15
3	2000	25	3.2	15

CHAPTER IV

ANALYSIS OF TEST DATA

Freitag (1965) showed through the use of dimensional reasoning that the important parameters in predicting the performance of a powered wheel operating in soft soil were wheel load W ; pneumatic tire factors of deflection δ , diameter d , and width b ; and the strength characteristics of the soil as expressed by cone penetration resistance. The most important performance parameters are input torque M , rim pull P , and sinkage z .

$$M , P , z = F (C , W , \delta , d , b) \qquad (4.1)$$

Wheel slip should also be considered an independent variable as done by Smith (1975) for clay and Melzer (1974) for sand. For a turned powered wheel an additional independent variable turn angle α (or more correctly, effective slip angle) would be added and an additional dependent variable side force S would complete the performance parameters.

Tests in Clay

Performance Parameters of Pull and Torque

Sufficient test data were not compiled to permit the incorporation of turn angle α as an independent variable into the clay mobility number. Rather, the effect of turn angle on pull and input torque was determined by developing a comparison of clay mobility numbers as determined from test conditions and as would be computed from measured

68

performance parameters. This is illustrated in Figure 4.1.

The performance prediction equations presented in Chapter II can be used to compute the clay mobility number if two of the three performance measures (pull, input torque, and wheel slip) are known. Three combinations of measured test values are therefore possible for computing the clay mobility number: 1) pull and wheel slip, 2) input torque and pull, and 3) input torque and wheel slip. Since pull and wheel slip might be considered as system output from the input torque, that combination was chosen to compute clay mobility numbers with the following relations:

$$\frac{P}{W} = \frac{1}{2} \log \frac{S}{S_{sp}} \tag{2.7}$$

and

$$S_{sp} = \frac{21}{\left(N'_c\right)^{5/2}} + 0.005 \tag{2.5}$$

solving for N'_c

$$N'_c = \left(\frac{21}{\frac{S}{\log^{-1} \frac{2P}{W}} - 0.005}\right)^{2/5} \tag{4.2}$$

It should be noted that using any two of the three measured test results of input torque, pull, and wheel slip and corresponding relations, the computed values of clay mobility numbers did not differ appreciably as seen in the tabulation in Appendix B.

Figure 4.2 illustrates graphically the relation between the clay mobility number computed from the independent variable (i.e. C , W , δ , d, b) and the two chosen dependent variables of pull and slip for each test conducted. Straight lines have been fitted to the plotted data per turn angle α . The slope of these linear lines, designated
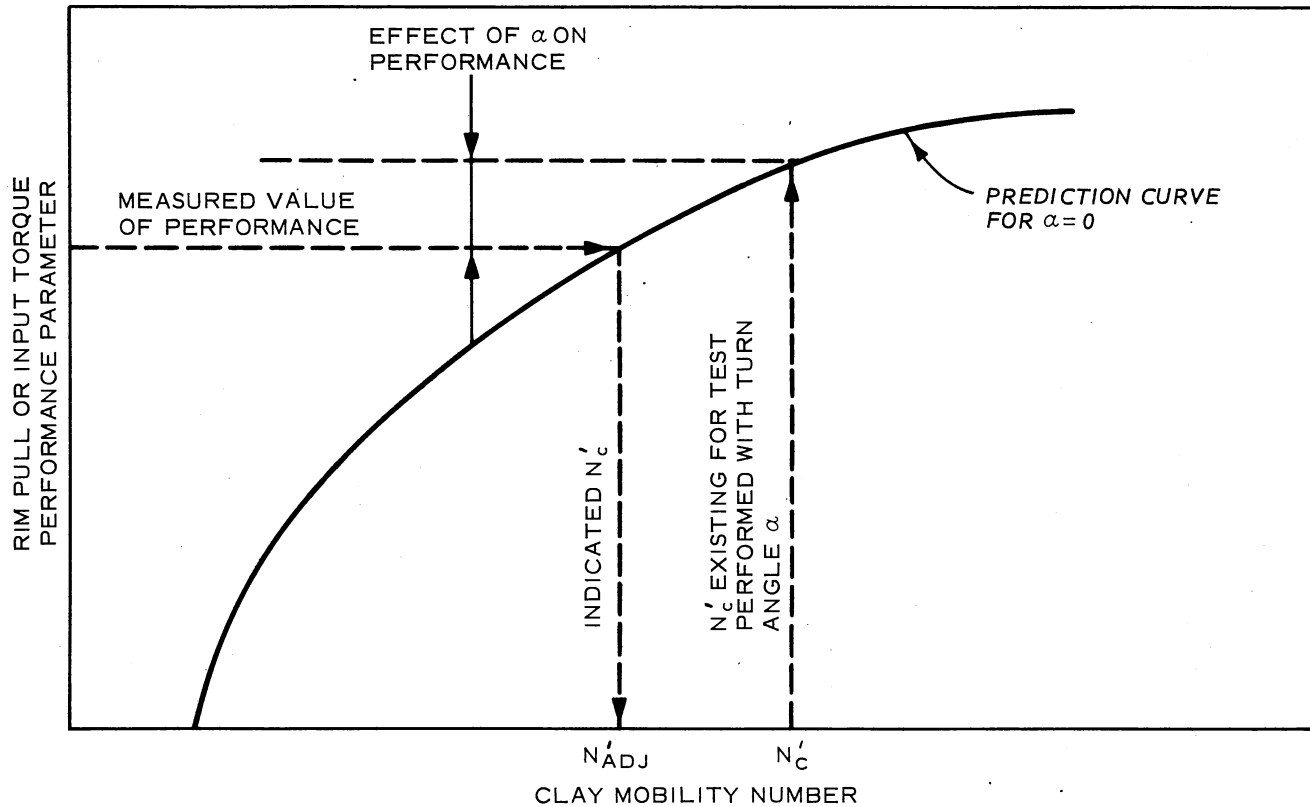
Figure 4.1. Qualitative Comparison of Clay Mobility Numbers as Determined from Test Condition at Turn Angle α and as Indicated by Measured Performance Parameter.
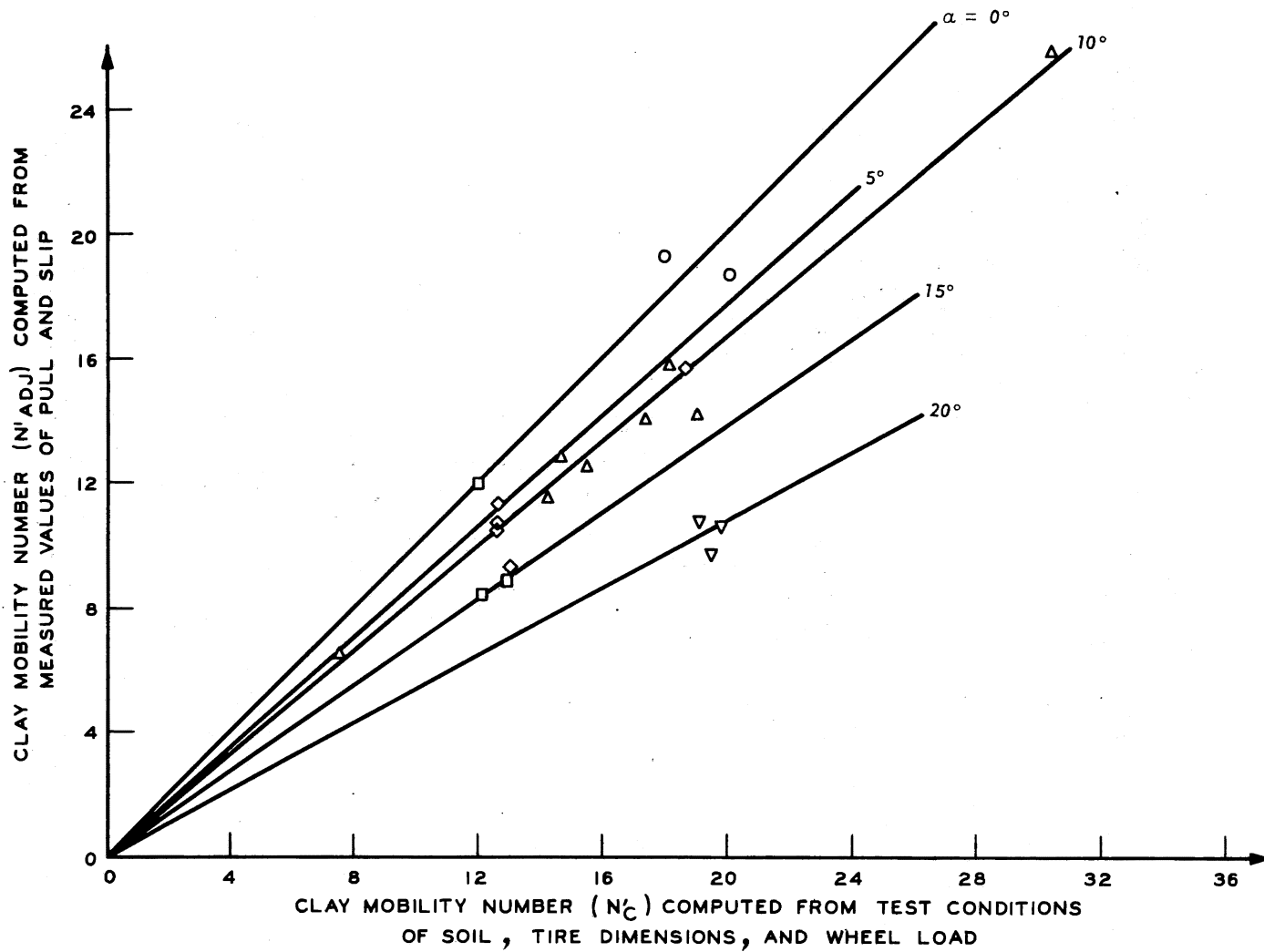
Figure 4.2. Comparison of Clay Mobility Numbers as Computed from Dependent Performance Parameter of Pull Versus Independent Test Variables.

as N'_{ADJ}/N'_c , are plotted for respective turn angles (Figure 4.3). A curve was fitted to the data to permit computation of intermediate values of wheel turn angle α .

$$N'_{ADJ} = (1 - 2.26 \ \alpha^{3/2}) \cdot N'_c \qquad (4.3)$$

Hence, given the independent variables of tire size and deflation, soil strength, and wheel loading N'_c can be computed from Equation 2.3 and with the turn angle α known, N'_{ADJ} is computed from the above relation which in turn is used with Equations 2.4 through 2.7 for computing predicted parameters.

Side Forces Developed in Clay

Pull of a powered wheel operating on a straight line path is proportionate to the clay mobility number N'_c and desired wheel slip (determined by the input torque). For wheels in a turned mode the wheel turn angle α constitutes an additional input variable required to describe the pull. It would appear intuitive that the horizontal side force acting normal to the hub of a turned wheel might be defined by values of the clay mobility number, wheel slip, and turn angle or those same factors on which pull is dependent. Hence pull and side force should be related for given values of the turn angle.

Figure 4.4 is a plot of the side force coefficient S/W versus the pull coefficient P/W for a group of tests having approximately equal clay mobility numbers N'_c between 15 and 18. Also plotted (with solid symbols) are data points obtained from towed wheels in a turned mode as reported by Melzer (1976) which had the stated range of clay mobility numbers. Numbers beside the plotted points indicated percent wheel slip. Based on the limited tests performed linear relations

$$\frac{N'_{ADJ}}{N'_c} = 1 - 2.26 \, \alpha^{3/2}$$

α IN RADIANS
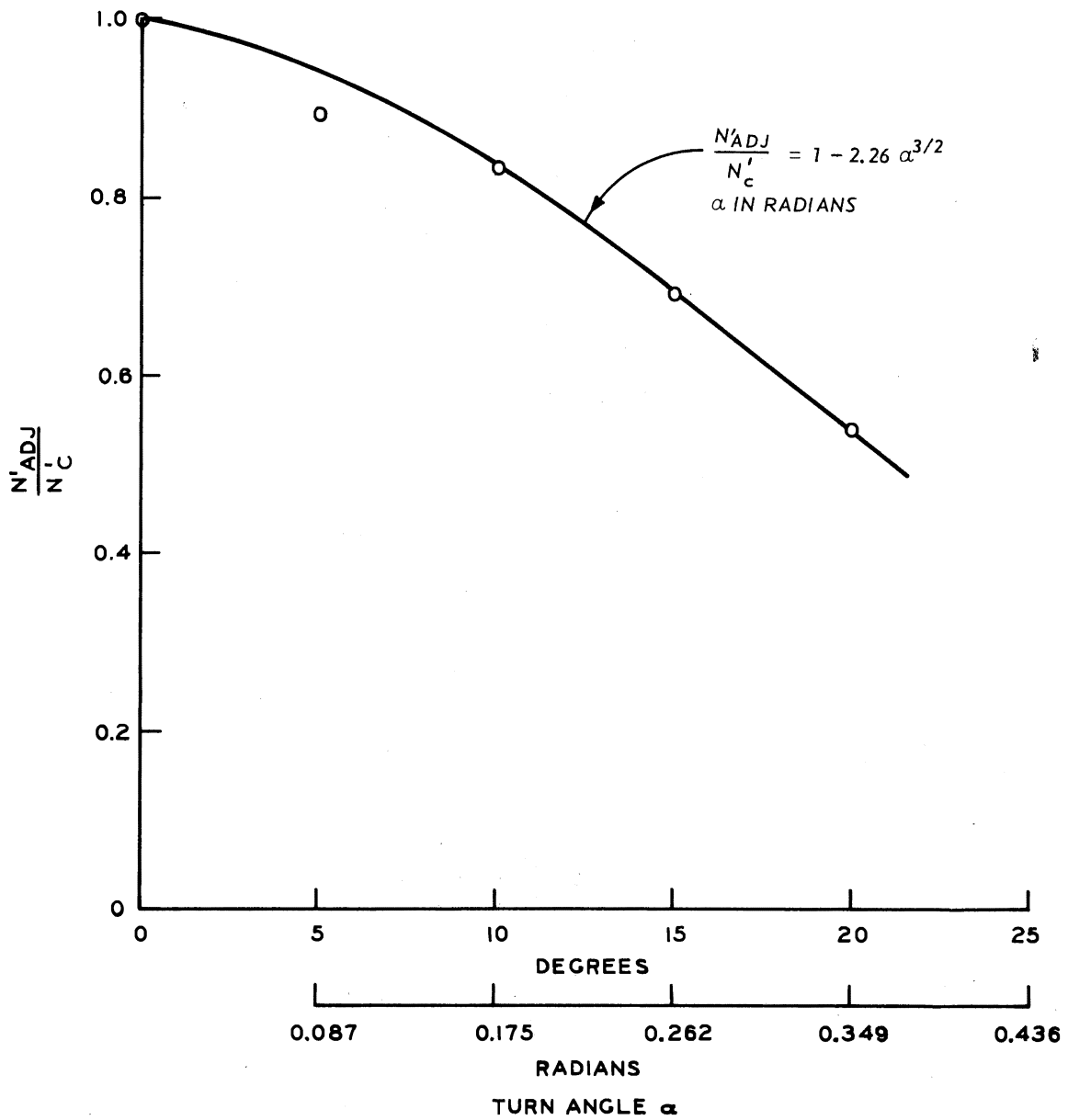
Figure 4.3. Relation between N'_{ADJ}/N'_C and Turn Angle α .
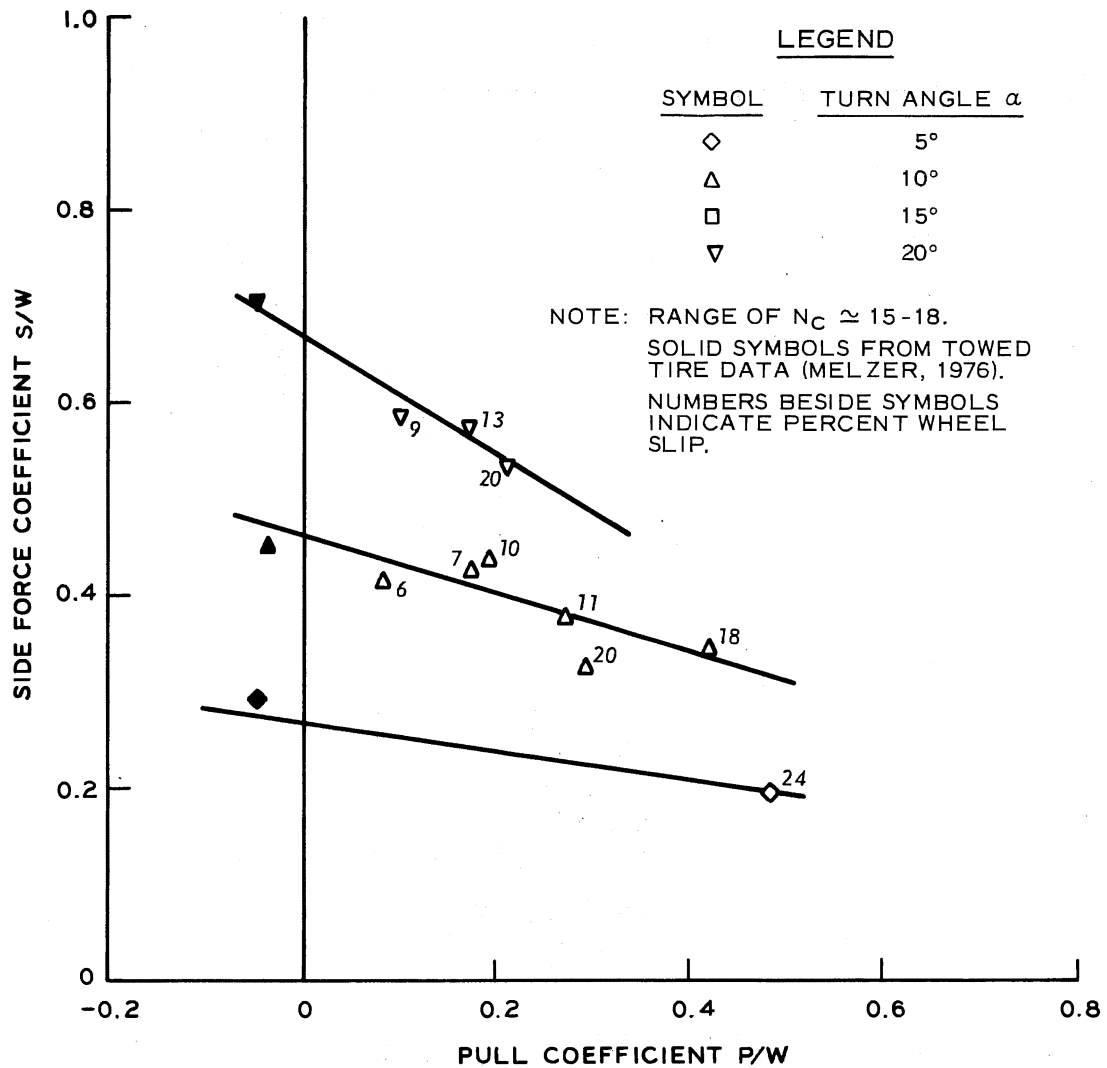
Figure 4.4. Side Force Versus Pull Coefficient for 6.00-9,
4-PR Tire on Clay. Cone Penetration Resistance
C = 290 kPa. Clay Mobility Number $N_c \simeq$ 15 to 18 .

were assumed between side-force and pull coefficient for corresponding values of turn angle. These data would indicate that for a given wheel turn angle and clay mobility number, the effect of increasing the input power (input torque) to a wheel, and thereby increasing the pull, results in a decrease in the side force. The rate of reducing the side forces magnitude increases with increased values of the turn angle α. Also from the towed point to a slip value of approximately 20 percent this relationship can be approximated by a linear function. With sufficient data, isobars of equal wheel slips seemingly could be constructed. These data have that general form of the results reported by Krick (1973) and reviewed in Chapter II except that these data indicate a more pronounced increase in the slope ratio of side force to pull as the wheel turn angle increases.

Figure 4.5 illustrates clay test data in terms of side force coefficient versus pull coefficient, where the wheel turn angle was 10 degrees. Again, towed data having a turn angle of 10 degrees and respective values of clay mobility numbers were extracted from that reported by Melzer (1976). Linear relations have been placed through the data for wheel slips between the towed point and approximately 20 percent slip. These data indicate that for a given wheel turn angle α the relation of side force coefficient versus pull coefficient are parallel lines displaced higher along the ordinate as the clay mobility number increases.

It would seem reasonable to assume that as 100 percent slip (wheel in full spin) is approached the side force will approach zero while the pull coefficient will assume some finite value approximated by
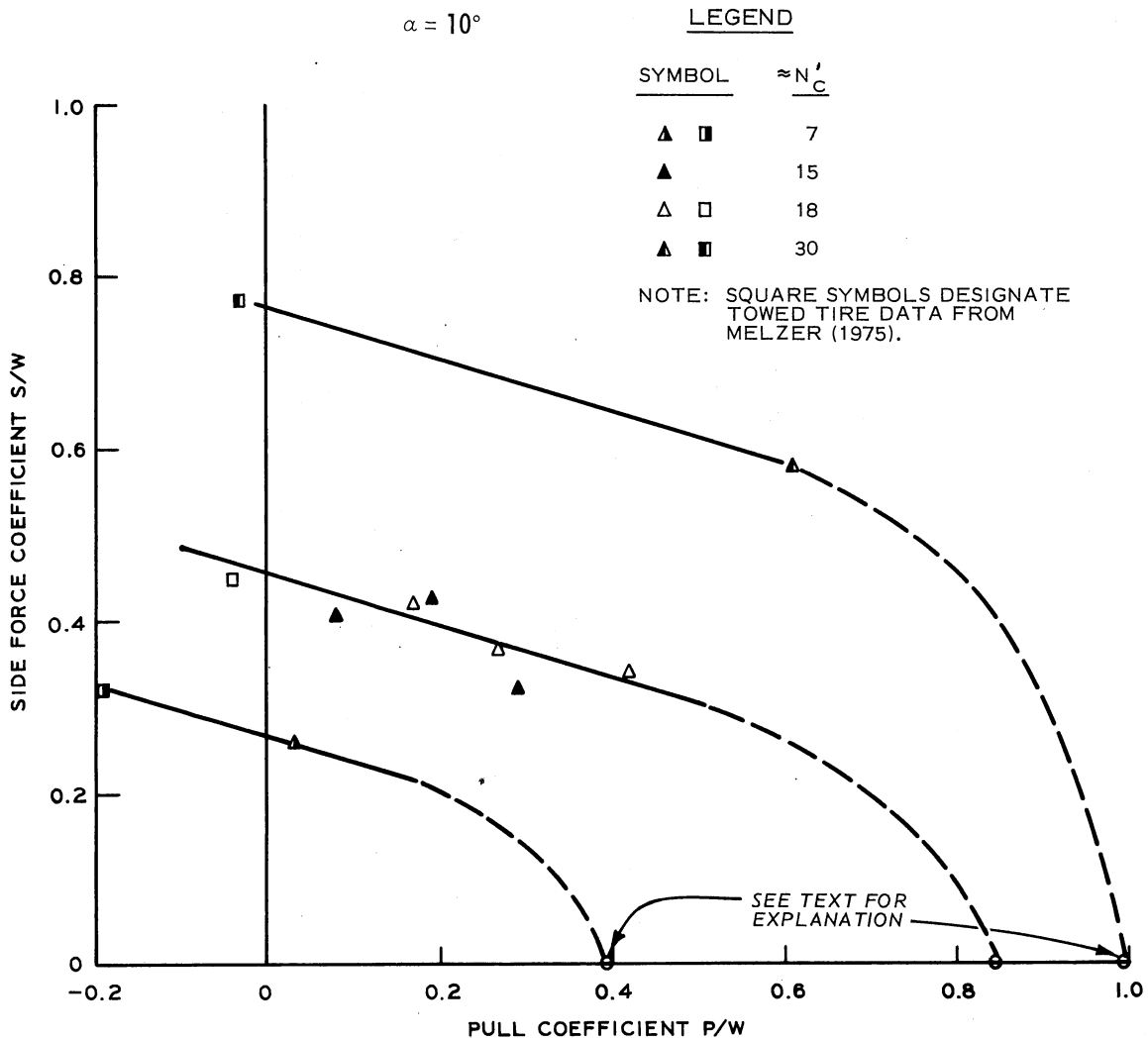
Figure 4.5. Effect of Variation in Clay Mobility Number on Side -
Force Versus Pull Coefficient for 6.00-9, 4-PR Tire
at 10 Degrees Turn Angle. Cone Penetration Number C
= 290 kPa.

Equation 2.7. Pull coefficients of 0.39, 0.88, and 1.0 correspond to a wheel slip of 100 percent and clay mobility numbers of 7, 18, and 30, respectively. These pull coefficient values form the end points for the three sets of data illustrated in Figure 4.5. The dashed lines illustrate a potential path of S/W versus P/W at slip values in excess of 20 percent.

From the above discussion two assumptions are made for justifying the remaining development of predicting side forces.

1) The relation between S/W and P/W at any turn angle is linear for wheel slip values between the towed point and 20 percent (Figure 4.4).

2) For a given turn angle the relation between S/W versus P/W is linear for a given clay mobility number and parallel but vertically displaced as the clay mobility number is varied (Figure 4.5).

Slopes of the three lines shown in Figure 4.4 are plotted against the respective turn angle α in Figure 4.6. A straight line was passed through the origin having a slope of 1.72.

The value of side force coefficients when the pull coefficients are zero were read from Figures 4.4 and 4.5 and plotted in Figure 4.7 and 4.8, respectively. Figure 4.7 illustrates that the side force coefficient, when the pull is zero and the clay mobility number is constant, increases with increasing values of turn angle α. The trend indicated that for higher values of turn angle α, the S/W at zero pull may decrease. Figure 4.8 indicates that if the turn angle is held constant, and for the test conditions upon which these findings are based, S/W at zero pull increases as the clay mobility number increases. This trend would not continue indefinitely but most likely
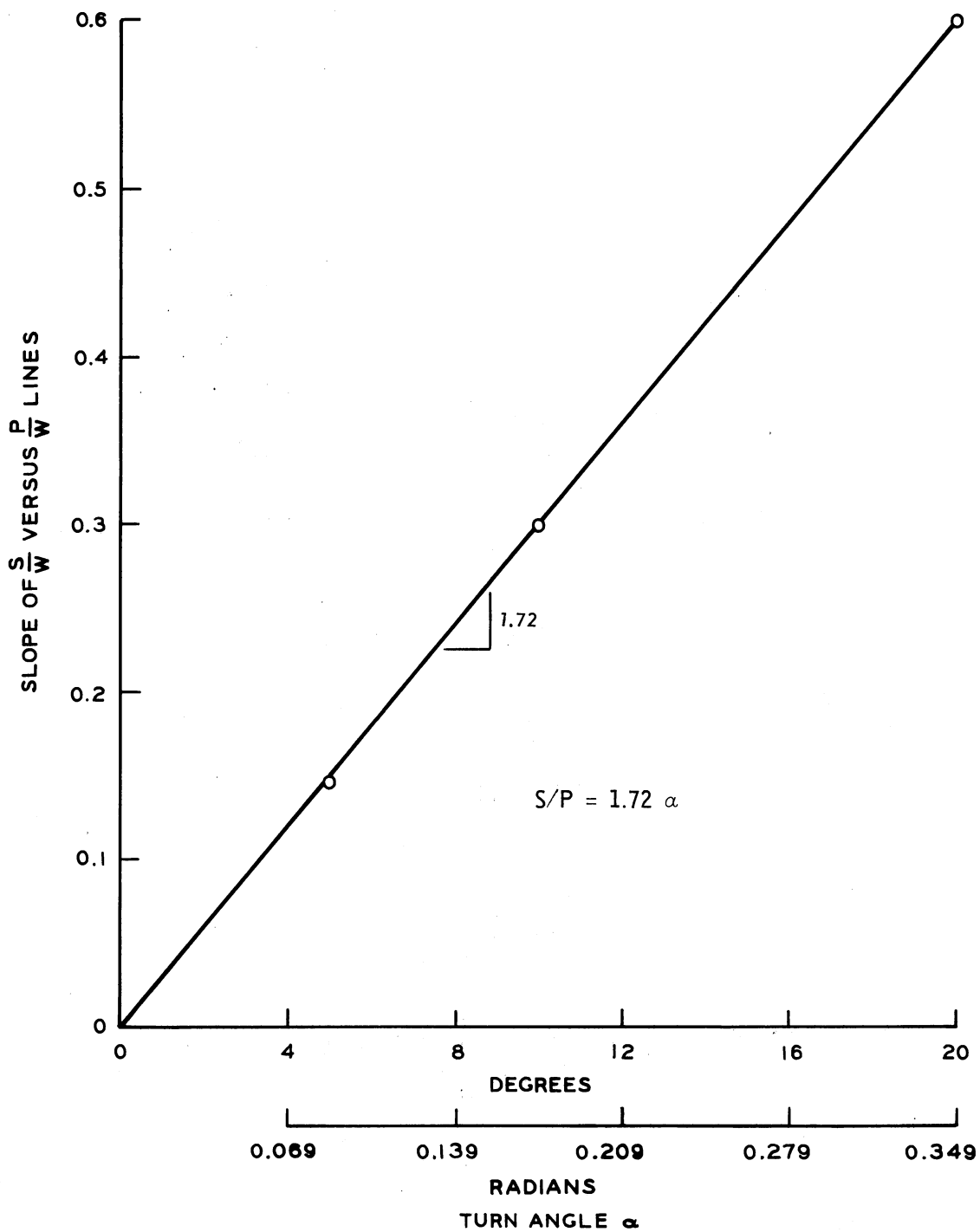
Figure 4.6.   Relation Between   Δ(S/W)/Δ(P/W)   and Turn Angle   α .   Cone
            Penetration Resistance   C = 290 kPa . Clay Mobility
            Number N_c' ≃ 15 to 18 .

Figure 4.7.   Side Force Coefficient at Zero Pull Versus
               Turn Angle α . Data Points Extrapolated
               from Figure 4.4.   Clay Mobility Number
               N'_c = 15 to 18 .
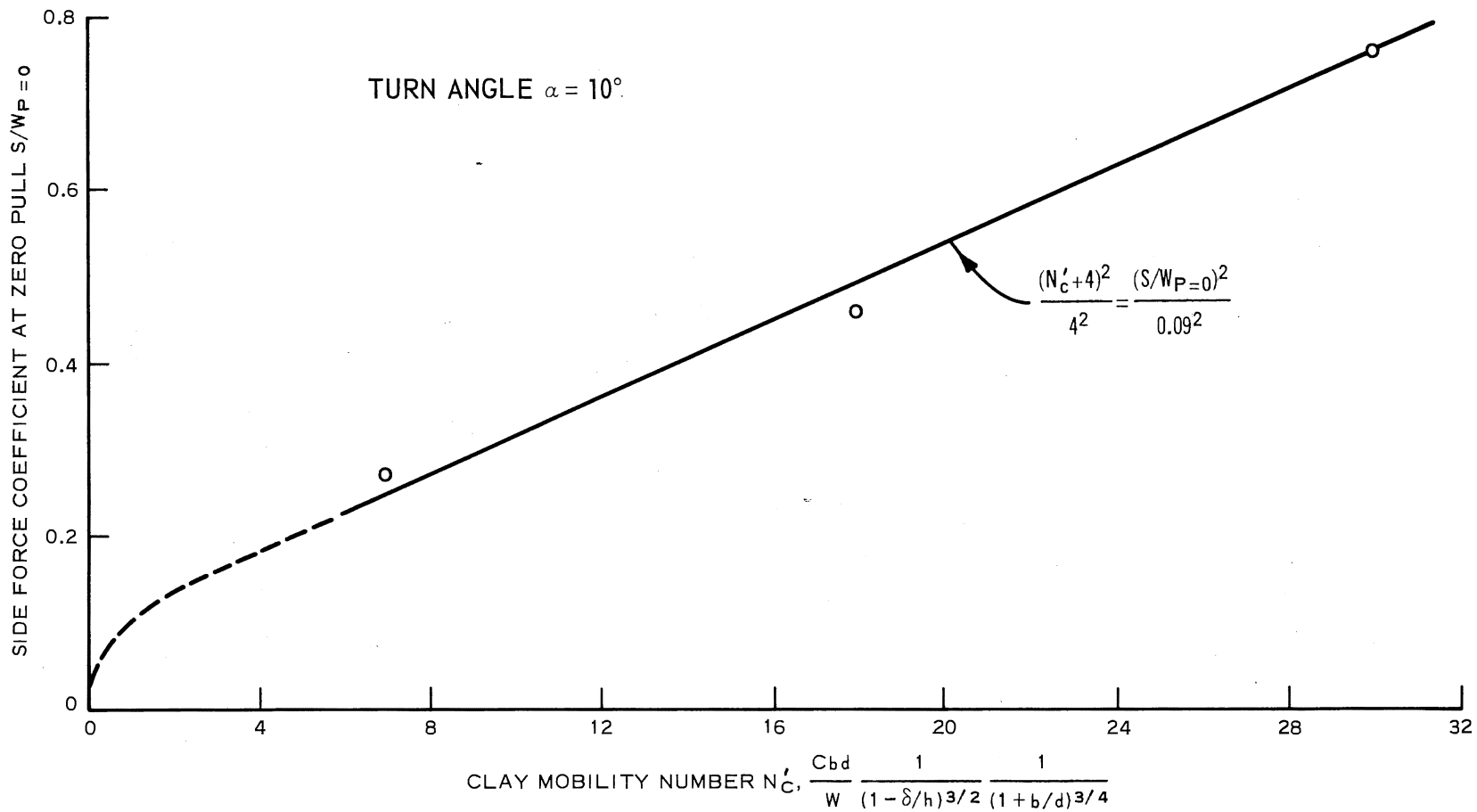
Figure 4.8. Side Force Coefficient at Zero Pull Versus Clay Mobility Number for a Turn Angle of 10 Degrees.

would begin to decrease at some nominal value of the clay mobility number N_c'. As N_c' approaches an infinitely large number, as would occur when the operating surface approached a hard, semi-rigid medium (i.e. cone penetration resistance becomes very large), the side force would be reduced primarily because the friction properties of the tire-surface would dominate performance rather than from passive earth pressure failure and side friction on the tire that must accompany a turned tire partially sunk as it corners in a plastic soil medium.

The relations developed from Figures 4.7 and 4.8 permit the side force coefficient at zero pull, per increment of turn angle, to be computed for any clay mobility number. For a turn angle of 10 degrees:

$$\frac{S}{W}\genfrac{}{}{0pt}{}{\alpha = 10}{P = 0} = \left(\frac{\left(N_c' + 4\right)^2}{16} \cdot 0.0081\right)^{1/2} \tag{4.4}$$

and for a clay mobility number of approximately 15 to 18:

$$\frac{S}{W}\genfrac{}{}{0pt}{}{N_c' = 18}{P = 0} = 3.37\,\alpha - 4.24\,\alpha^2 \tag{4.5}$$

From Figure 4.4 when $N_c' = 18$ and $\alpha = 10$ degrees $(S/W)_{P\,=\,0}$ is equal to 0.46 which is used to normalize when the two previous equations are combined to give the side force coefficient at zero pull per turn angle and clay mobility number, or:

$$\frac{S}{W}\genfrac{}{}{0pt}{}{}{P = 0} = \left(\frac{\left(N_c' + 4\right)^2}{16} \cdot 0.0081\right)^{1/2} \left(3.37\,\alpha - 4.24\,\alpha^2\right)\frac{1}{0.46} \tag{4.6}$$

The side force coefficient at zero pull constitutes the ordinate intercept with 1.72 α , where α is expressed in radians, expressing the slope of the S/W versus P/W relation. Hence for a given turn

angle and clay mobility number:

$$\frac{S}{W} = \frac{S}{W}\bigg|_{P=0} - (1.72\ \alpha)\ \frac{P}{W}^{\alpha} \tag{4.7}$$

Sinkage in Clay

Sinkage coefficient z/d (vertical hub movement value divided by the inflated but unloaded wheel diameter) as a function of the clay mobility number and wheel turn angle is depicted in Figure 4.9. The line drawn on each plot of Figure 4.9 represents the cumulative results of previous test programs in which numerous combinations of the independent variables were considered; however the wheels were always at zero turn angle and the wheel slip very close to 20 percent (Turnage, 1972). The data from this program are shown as plotted points with the respective wheel slip noted beside each datum point. For a given turn angle, z/d decreases with increasing N_c' as expected. Insufficient data prevents meaningful analysis as to the influence of turn angle on sinkage at a specific N_c' value; although the data suggests that α is of secondary importance in that the previous described relation reported by Turnage (1972) amply depicts results from this study. This data also suggests that over the slip range (0 to 20 percent) used in this test program, wheel slip does not appreciably influence sinkage.

Summary

For a given set of independent variables expressed as the clay mobility number N_c' and the wheel turn angle, forces acting on a pneumatic tire are computed as follows:

The adjusted clay mobility number accounting for turn angle α
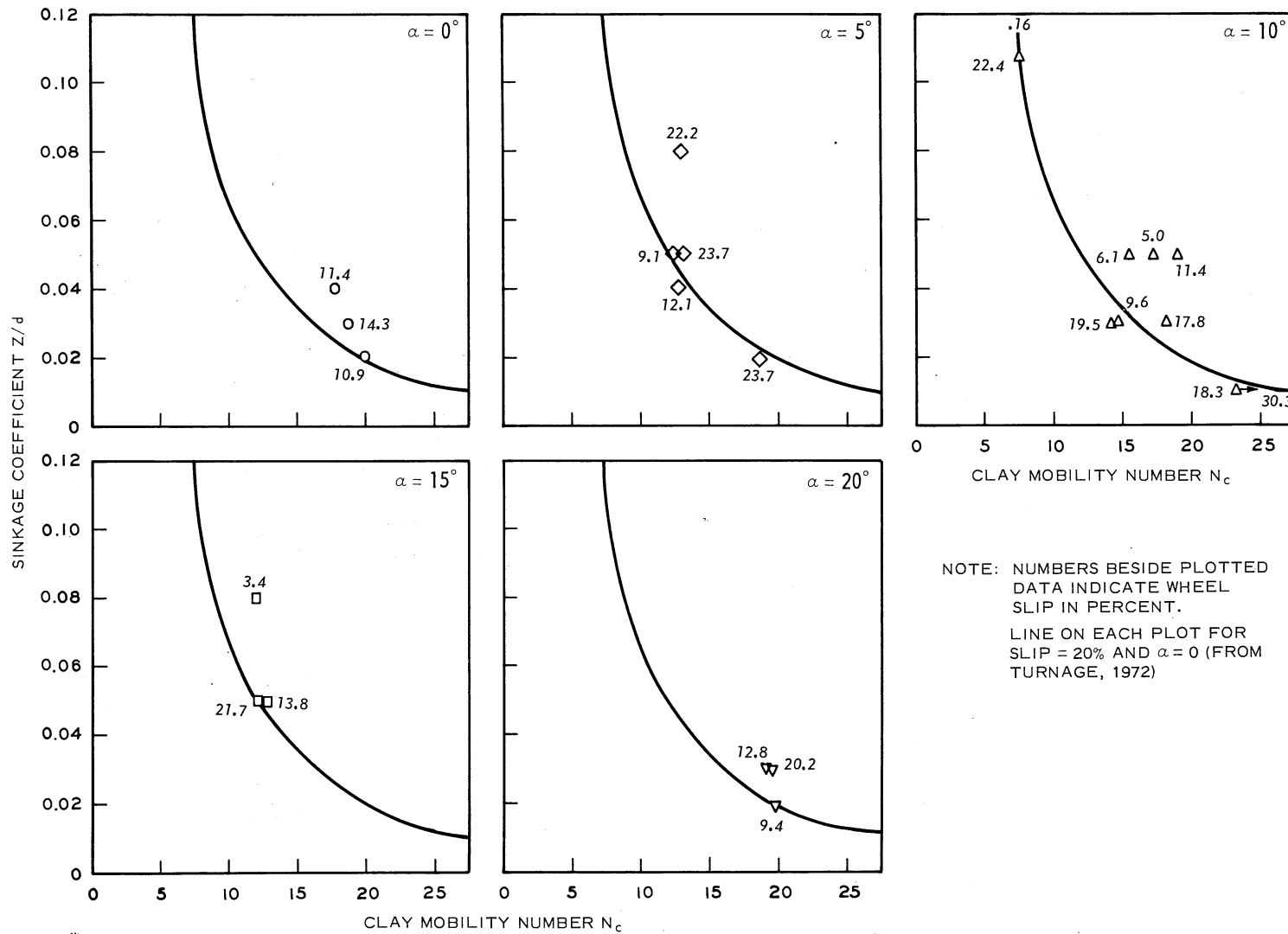
Figure 4.9. Sinkage Coefficient as Functions of Clay Mobility Number and Turn Angle.

$$N'_{ADJ} = N'_c \left(1 - 2.26\ \alpha^{1.5}\right) \tag{4.3}$$

Slip at the self-propelled point

$$\left(S_{sp}\right)^\alpha = \frac{21}{\left(N'_{ADJ}\right)^{2.5}} + 0.005 \tag{2.5}$$

The input torque coefficient at the self-propelled point

$$\left(\frac{M_{sp}}{Wr_a}\right)^\alpha = \frac{12}{\left(N_{ADJ}\right)^2} + 0.007 \tag{2.6}$$

The pull coefficient in the plane of the wheel

$$\left(\frac{P}{W}\right)^\alpha = 0.5\ \log\left(\frac{S}{S_{sp}}\right) \tag{2.7}$$

Input torque coefficient is determined by equating Equations 2.6 and 2.7

$$\left(\frac{M}{Wr_a}\right)^\alpha = \left(1 + \frac{b}{d}\right)^{1/4} \left(\frac{P}{W}\right)^\alpha + \left(\frac{M_{sp}}{Wr_a}\right)^\alpha$$

and finally the side force coefficient

$$\left(\frac{S}{W}\right)^\alpha = \left(\frac{S}{W}\right)_{P\ =\ 0} - (1.72\ \alpha) \left(\frac{P}{W}\right)^\alpha \tag{4.7}$$

Values of actual laboratory test conditions were substituted into the above equations to obtain predictions of the performance coefficients pull, side force, and input torque. Table III provides a tabulated comparison of computed coefficients with those measured during the course of testing. The comparisons provided in Table III were determined by taking the absolute difference of the corresponding predicted and measured performance coefficient divided by the larger of the two terms and expressed as a percentage. Considering all 23 tests conducted in this program, 74 percent of the pull coefficients, 89 percent of the

TABLE III

COMPARISON OF PREDICTED PERFORMANCE PARAMETERS WITH CORRESPONDING
TEST RESULTS FOR TESTS CONDUCTED ON CLAY SURFACE

Test No.	Clay Mobility Number N_c	Turn Angle α	Pull Coefficient, P/W			Side Force Coefficient S/W			Input Torque Coefficient, M/Wr_a		
			Test Value	Pre-dicted	Dif-ference %	Test Value	Pre-dicted	Dif-ference %	Test Value	Pre-dicted	Dif-ference %
A-73-0048-3	18.84	0.	0.34	0.44	24.28	0.	0.	0.	0.42	0.51	17.90
A-73-0049-3	20.00	0.	0.38	0.41	6.84	0.	0.	0.	0.47	0.47	0.28
A-73-0050-3	17.87	0.	0.40	0.37	7.88	0.	0.	0.	0.49	0.44	9.35
A-73-0051-3	17.34	10.00	0.17	0.19	8.84	0.42	0.42	0.87	0.28	0.27	3.25
A-73-0052-3	18.97	10.00	0.27	0.32	15.66	0.37	0.42	11.79	0.38	0.40	3.71
A-73-0053-3	18.08	10.00	0.42	0.40	5.41	0.34	0.38	9.03	0.53	0.48	8.35
A-73-0054-3	19.75	20.00	0.10	0.09	9.08	0.58	0.71	19.32	0.12	0.21	41.00
A-73-0055-3	19.50	20.00	0.21	0.25	15.12	0.53	0.61	13.73	0.30	0.38	19.92
A-73-0056-3	19.08	20.00	0.17	0.14	19.33	0.57	0.66	13.76	0.020	0.27	23.58
A-73-0057-3	18.61	5.00	0.48	0.52	8.94	0.19	0.21	7.84	0.58	0.61	3.72
A-73-0058-3	12.59	5.00	0.11	0.14	17.26	0.22	0.19	13.50	0.24	0.24	1.31
A-73-0059-3	12.63	5.00	0.14	0.20	31.67	0.22	0.18	15.29	0.26	0.31	15.30
A-73-0060-3	13.00	5.00	0.21	0.35	39.74	0.14	0.17	13.04	0.37	0.46	20.26
A-73-0061-3	11.96	15.00	-0.07	-0.25	79.16	0.45	0.58	21.25	0.03	-0.09	30.67
A-73-0062-3	12.06	15.00	0.15	0.15	0.80	0.44	0.40	10.22	0.30	0.34	11.25
A-73-0063-3	12.93	15.00	0.08	0.09	7.51	0.42	0.45	6.23	0.18	0.25	29.14
A-73-0064-3	15.44	10.00	0.08	0.09	16.55	0.41	0.41	00.19	0.14	0.18	21.85
A-73-0065-3	14.64	10.00	0.19	0.16	13.53	0.43	0.37	14.69	0.28	0.26	5.94
A-73-0066-3	14.23	10.00	0.29	0.30	5.08	0.32	0.32	0.49	0.41	0.42	2.63
A-73-0067-3	7.54	10.00	0.03	0.01	69.20	0.26	0.26	2.12	0.22	0.32	30.26
A-73-0068-3	30.32	10.00	0.61	0.60	1.14	0.58	0.59	1.94	0.74	0.67	10.03

TABLE III (CONTINUED)

Test No.	Clay Mobility Number N_c	Turn Angle α	Pull Coefficient, P/W			Side Force Coefficient S/W			Input Torque Coefficient, M/Wr_a		
			Test Value	Pre-dicted	Dif-ference %	Test Value	Pre-dicted	Dif-ference %	Test Value	Pre-dicted	Dif-ference %
A-73-0069-3	12.60	5.00	0.29	0.35	15.11	0.12	0.16	22.97	0.42	0.46	8.13
A-73-0070-3	18.97	0.	0.19	0.08	56.74	0.	0.	0.	0.25	0.13	48.94

side force coefficients, and 70 percent of the input torque coefficients
had percent differences of 20 percent or less. Figure 4.10 through 4.12
contain the plotted test values of pull, side force, and input torque
coefficients versus percent wheel slip. Tests having similar test con-
ditions were grouped to permit meaningful representation. Superimposed
are lines computed from prediction Equations 2.5, 2.6, 2.7, 4.3, and
4.7. Input values to these equations were determined from the desired
test conditions as provided in Table I which differ slightly from the
individual or average test conditions being represented. Effective
work is not developed by a powered wheel until positive pull is realized.
This program was concerned with the performance of a powered wheel
between the self-propelled slip and about 20-percent wheel slip; hence,
performance relations are not shown on Figures 4.10 through 4.12 for
wheel slip values less than that occuring when the pull is zero.

<center>Sand Tests</center>

Performance Parameters of Pull and Torque

Each condition for the powered turned wheel tests performed in
Yuma sand (Table A.2, Appendix A) can be expressed in terms of a sand
mobility number N_S , and wheel slip s , and wheel turn angle α .
Substituting values of P/W , M/Wr_a , and s from each test into
Equation 2.9 and 2.10, sand mobility numbers were detemined per test
and reported in Table B.2, Appendix B. These computed sand mobility
numbers combine those independent variables (i.e. test conditions) that
yielded predictions of performance parameters P/W and M/Wr_a for a
powered wheel traveling without a turn slip angle. With the complete
absence of test variation, experimental error, and difference between

Figure 4.10. Influence of Turn Angle on Performance Parameters. Tire Deflection
$\delta/h = 0.35$, Design Wheel Load W = 2,000 N .
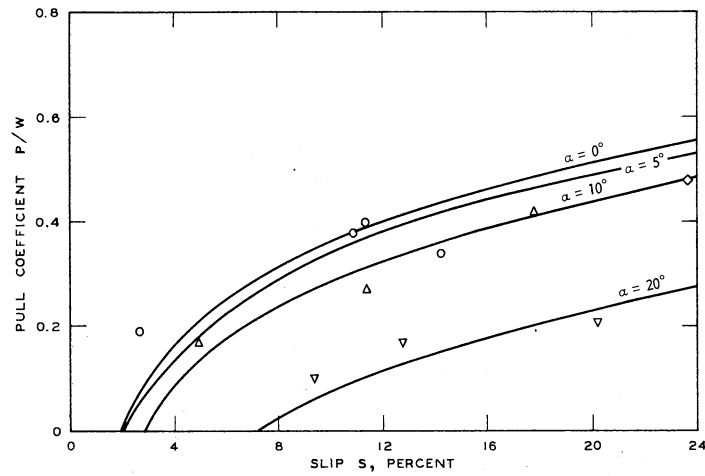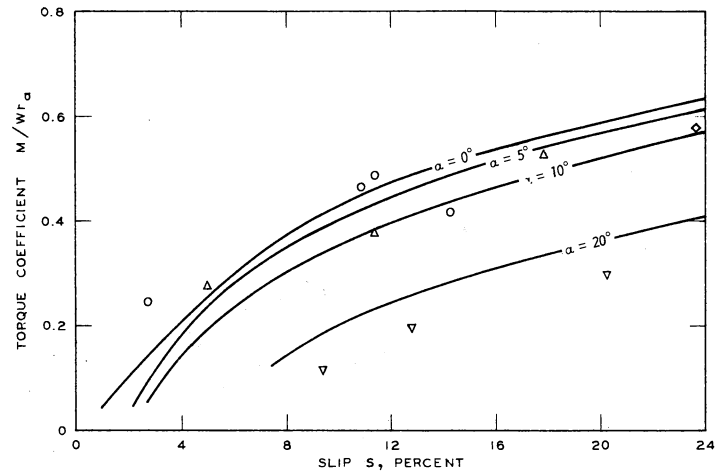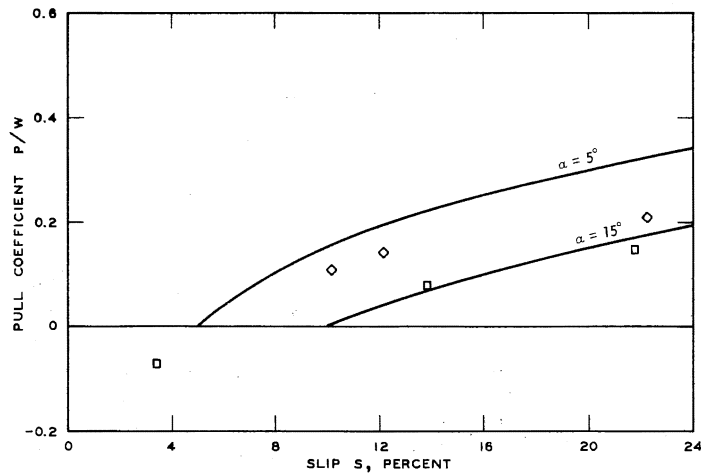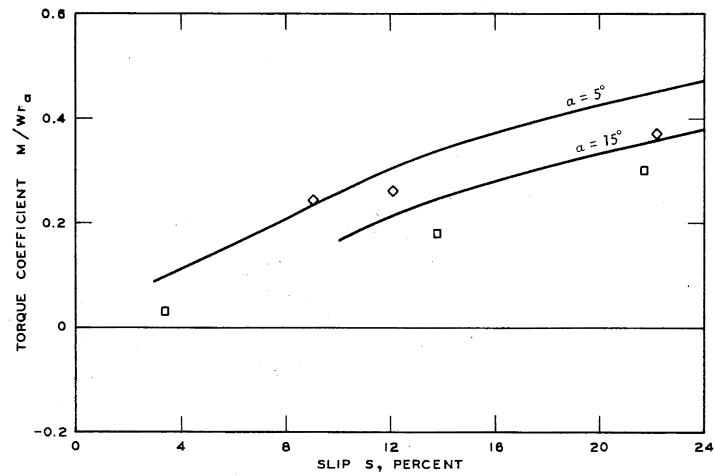
a. PULL COEFFICIENT

b. TORQUE COEFFICIENT
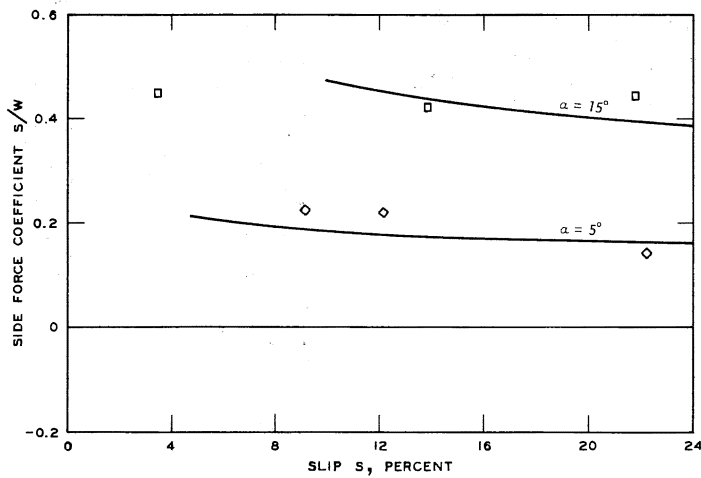
c. SIDE FORCE COEFFICIENT

LEGEND

SYMBOL	TURN ANGLE α
○	0°
◇	5°
△	10°
□	15°
▽	20°

Figure 4.11. Influence of Turn Angle on Performance Parameters. Tire Deflection $\delta/h = 0.15$, Design Wheel Load $W = 2,000$ N .
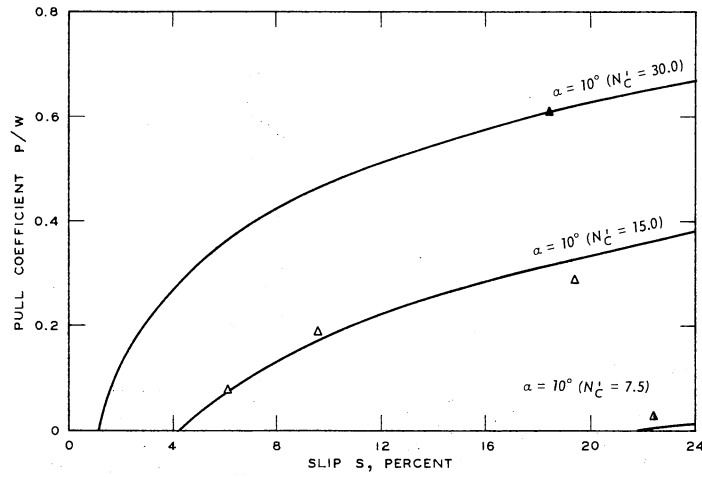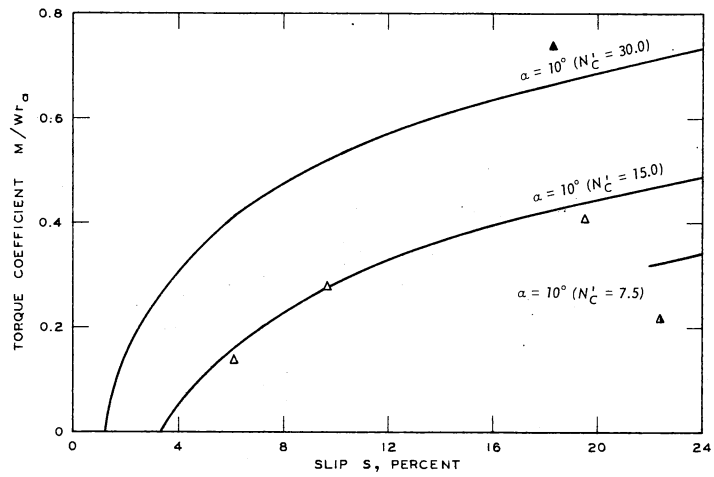
a. PULL COEFFICIENT

b. TORQUE COEFFICIENT
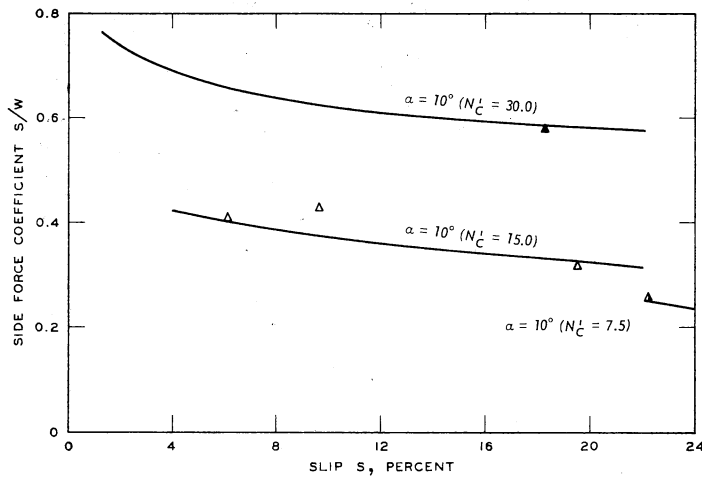
c. SIDE FORCE COEFFICIENT

LEGEND

SYMBOL	DESIGN WHEEL LOAD, N
▲	1000
△	2000
▲	4000

Figure 4.12.   Influence of Turn Angle and Wheel Load on Performance Parameters.
Tire Deflection $\delta/h = 0.25$, Turn Angle $\alpha = 10$ Degrees.

experimental curves and generalized equations, the N_S computed from

Equations 2.9 and 2.10 would be identical. Unfortunately, such is not

the nature of man or machine. Since pull and wheel slip are considered

as output from the respective torque applied to the wheel, the sand

mobility number computed from test values of P/W and s are plotted

in Figure 4.13 against N_S as computed from actual test conditions and

grouped accordingly to wheel turn angle. Since the computed sand

mobility numbers are derived from pull coefficients on powered wheels

having the added resistance of side forces, these values would seemingly

be less than test conditions would suggest for a powered wheel underway

with the absence of a turn angle. Furthermore, large differences would

be expected to occur as the wheel turn angle increased and larger side

forces developed. Hence the plotted values of computed versus test con-

dition sand mobility numbers in Figure 4.13 should lie below the 45

degree diagonal lines.

Examination of Figure 4.13 reveals that for wheel turn angles up to

10 degrees, the sand mobility number determined from measured pull and

slip are often greater than those N_S expressed by test conditions.

Furthermore, a distinct relation (neither linear like that noted in

Figure 4.2 for the clay data nor otherwise) for each wheel turn angle

between the two values of sand mobility numbers is not apparent although

a general trend does exist for larger differences between the two sand

mobility numbers being developed as the wheel turn angle α increases.

Since the sand turn tire data would not lend itself to analysis with

the generalized procedure just discussed a more specific method was

selected that involved developing the pull and torque data to investigate

the variation of the coefficients of Equations 2.9 and 2.10 as affected
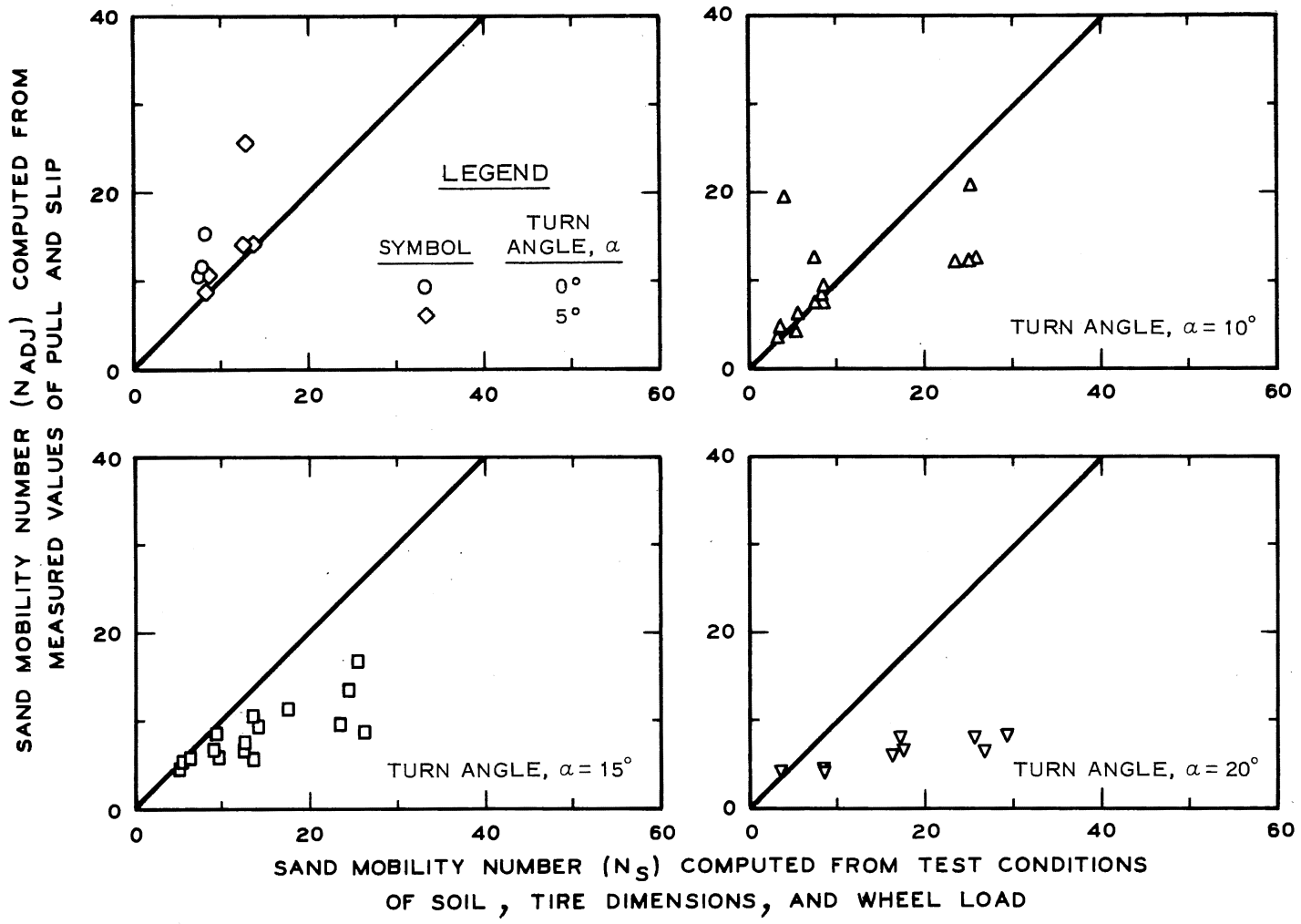
Figure 4.13. Comparison of Sand Mobility Numbers as Computed from Dependent Performance Parameter of Pull Versus Independent Test Variables.

by the influence of the side slip angle. The procedure began by placing

smooth curves through data points of P/W and M/Wr$_a$ versus wheel

slip s ; tests having approximately equal sand mobility numbers were

plotted together for meaningful comparisons. These curves served as the

bases for developing more fundamental relations of P/W and M/Wr$_a$

versus N$_S$ at certain values of wheel slip; in turn these curves were

measured against the respective relation at zero wheel turn angle to

permit a comparative analysis.

Measured values of pull and torque obtained during the powered

turn tire tests performed in Yuma sand are presented in therms of P/W

and M/Wr$_a$ versus wheel slip s in Figure 4.14 through 4.19.

Performance parameters in terms of P/W and M/Wr$_a$ from the various

tests are comparative only if the independent variables are alike or

approximately equal. The independent variables are represented in terms

of the sand mobility number and increase from 3.5 to 26.3 in six unequal

increments as designated in Figure 4.14 to 4.19, respectively. The

dashed line drawn through each figure represent predicted values of P/W

and M/Wr$_a$ at zero wheel turn angle across the slip ranges investigated

in this test program using Equations 2.9 and 2.10, respectively. The

solid lines were judged to best fit the plotted data points and experi-

mental trends.

Examination of pull coefficient versus wheel slip at specified

sand mobility number and wheel turn angle indicates that the pull

increases with increased values of slip. The effect of increasing the

turn angle is seen to reduce the pull at specific values of wheel slip.

The general slopes of the P/W versus s plots indicate that at the

higher wheel slip values the rate of decrease in pull begins to diminish
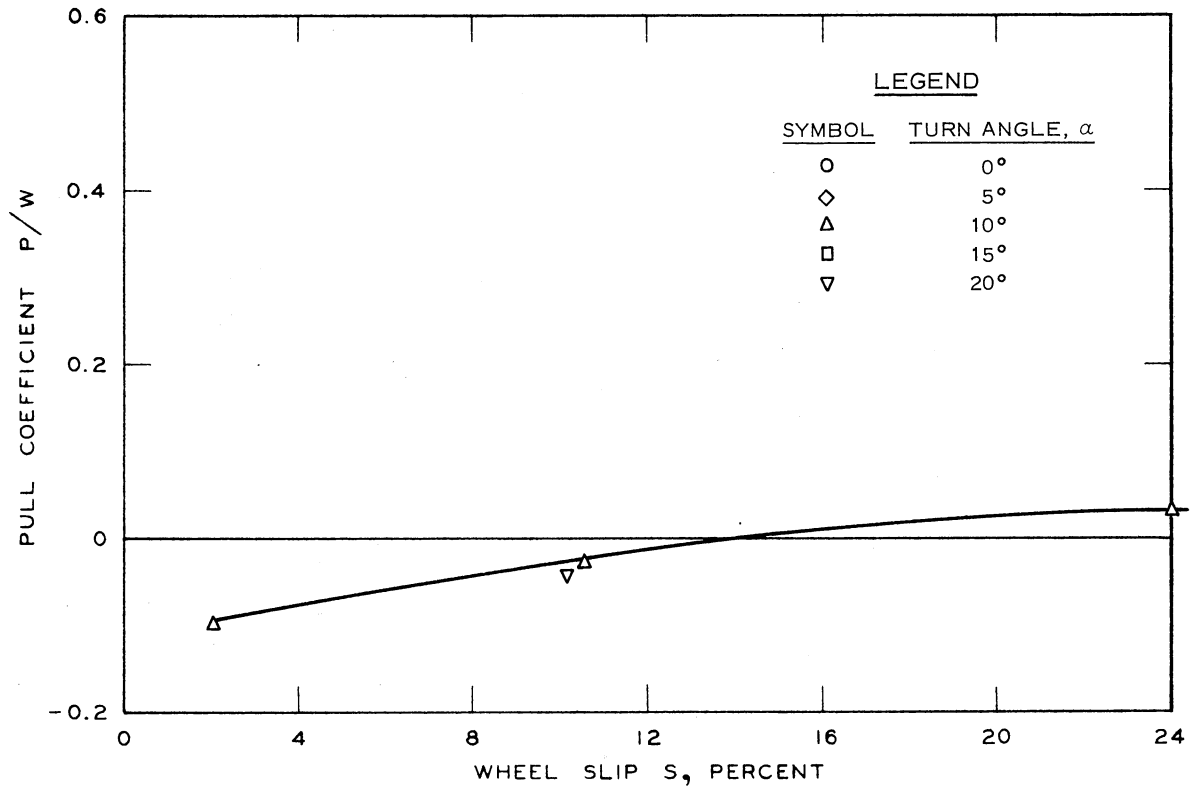
a. PULL COEFFICIENT
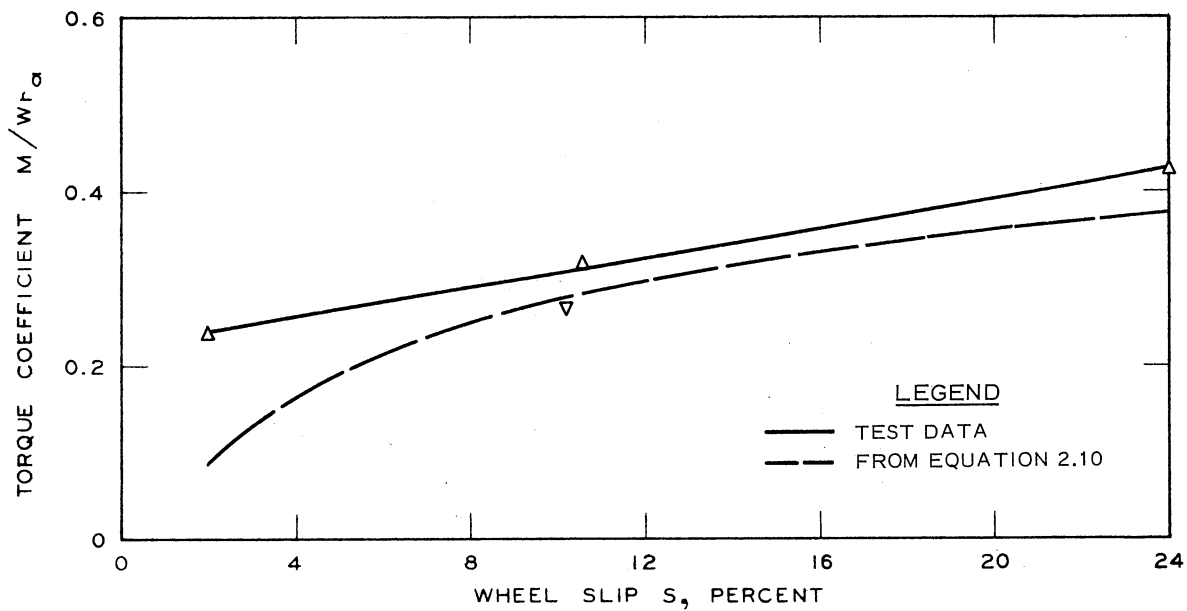
b. TORQUE COEFFICIENT

Figure 4.14.   Influence of Turn Angle on Pull and Torque Coefficients.
Average Cone Penetration Resistance Gradient   G = 2.0 ,
Tire Deflection δ/h = 0.15 , Design Wheel Load
W = 2,000 N .   Desired Sand Mobility Number = 3.5 .
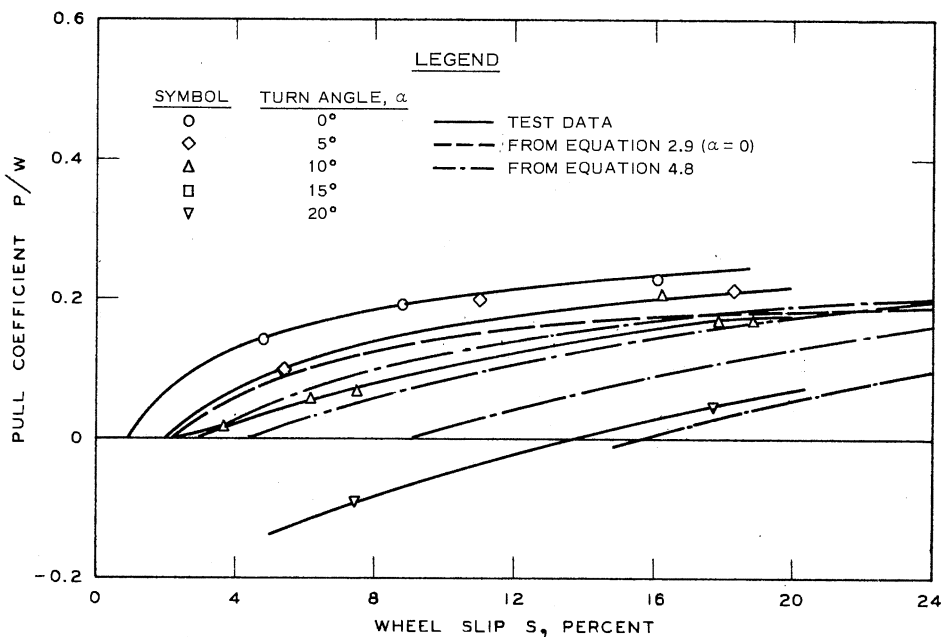
a. PULL COEFFICIENT
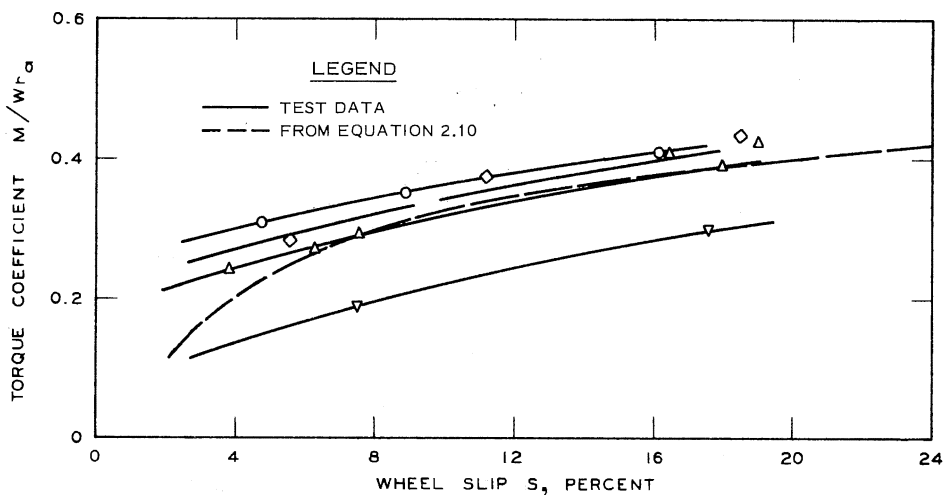
b. TORQUE COEFFICIENT

Figure 4.15. Influence of Turn Angle on Pull and Torque
Coefficients. Average Cone Penetration
Resistance Gradient G = 2.0 , Tire
Deflection δ/h = 0.35 , Design Wheel
Load W = 2,000 N . Desired Sand Mobil-
ity Number = 8.2 .

a. PULL COEFFICIENT

b. TORQUE COEFFICIENT

Figure 4.16.   Influence of Turn Angle on Pull and Torque Coefficients.
Average Cone Penetration Resistance Gradient   G = 3.2 ,
Tire Deflection δ/h = 0.25 , Design Wheel Load
W = 2,000 N .   Desired Sand Mobility Number = 9.4 .

a. PULL COEFFICIENT

b. TORQUE COEFFICIENT

Figure 4.17. Influence of Turn Angle on Pull and Torque Coefficients.
Average Cone Penetration Resistance Gradient G = 3.2 ,
Tire Deflection δ/h = 0.35 , Design Wheel Load
W = 2,000 N . Desired Sand Mobility Number = 13.2 .

a. PULL COEFFICIENT

b. TORQUE COEFFICIENT

Figure 4.18. Influence of Turn Angle on Pull and Torque Coefficients.
Average Cone Penetration Resistance Gradient G = 2.0 ,
Tire Deflection δ/h = 0.35 , Design Wheel Load
W = 1,000 N . Desired Sand Mobility Number = 16.4 .

a. PULL COEFFICIENT

b. TORQUE COEFFICIENT

Figure 4.19. Influence of Turn Angle on Pull and Torque Coefficients.
Average Cone Penetration Resistance Gradient G = 3.2 ,
Tire Deflection δ/h = 0.35 , Design Wheel Load
W = 1,000 N . Desired Sand Mobility = 26.3 .

for any turn angle. If at 100 percent slip the side force is reduced to zero, then on any turn angle the P/W versus s relation will approach the respective P/W versus s relations for a zero turn angle as the wheel slip increases (of course comparative sand mobility numbers are necessary). Values of the pull coefficient were interpreted from the P/W versus s relations shown in Figures 4.14a to 4.19a at wheel slips of 5, 7.5, 10, 15, and 20. The values of P/W for each of the particular wheel slips with the corresponding turn angles and sand mobility numbers, were plotted (Figures 4.20 through 4.24) in the form of P/W versus N_S and curves drawn through points representing similar turn angles. Equations of the form

$$\frac{P}{W}_\alpha = A_\alpha - \frac{A_\alpha B_\alpha}{N_S - C_\alpha + B_\alpha} \tag{4.8}$$

were established for each of the plotted curves with the aid of computer programming. Notice that Equation 4.8 is the identical form to Equation 2.9, which was established to predict the pull coefficient for any sand mobility number and wheel slips up to 20 percent. The final task was to develop relations to define the influence of independent variables of N_S , S , and α on the coefficients A_α , B_α , and C_α of Equation 4.8 which differed in magnitude from the related coefficients in Equation 2.9.

Table IV lists the values of coefficients A_α , B_α , and C_α from Equation 4.8 for various wheel slips and wheel turn angles. Figures 4.25 to 4.27 illustrate how coefficients A_α , B_α , and C_α vary with wheel slip and turn angle. Also shown are the equations established to approximate the plotted points into continuous functions. Hence with the coefficients defined, Equation 4.8 to predict the pull coefficient
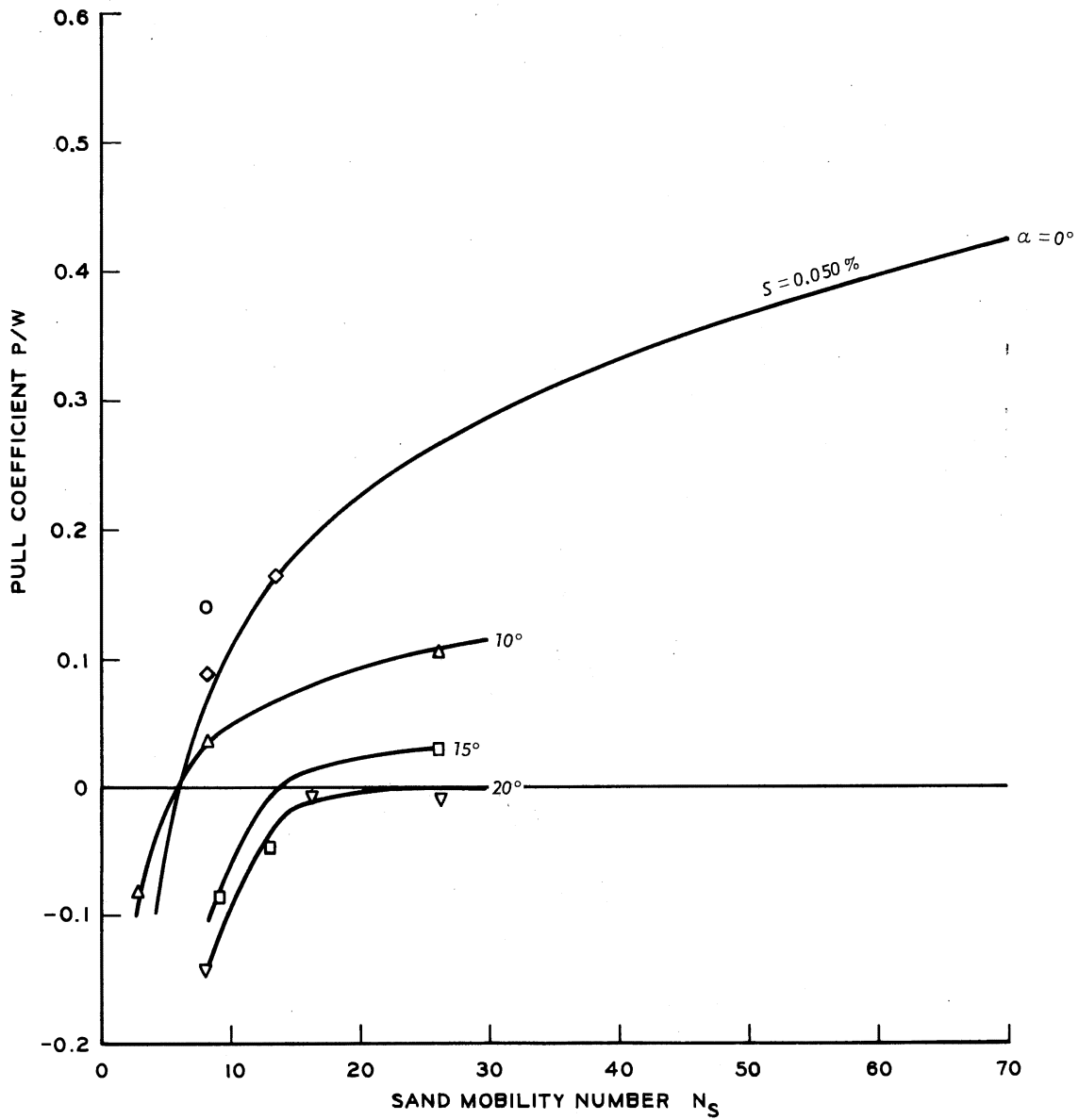
Figure 4.20. Pull Coefficient Versus Sand Mobility Number, Wheel Slip = 5 Percent.
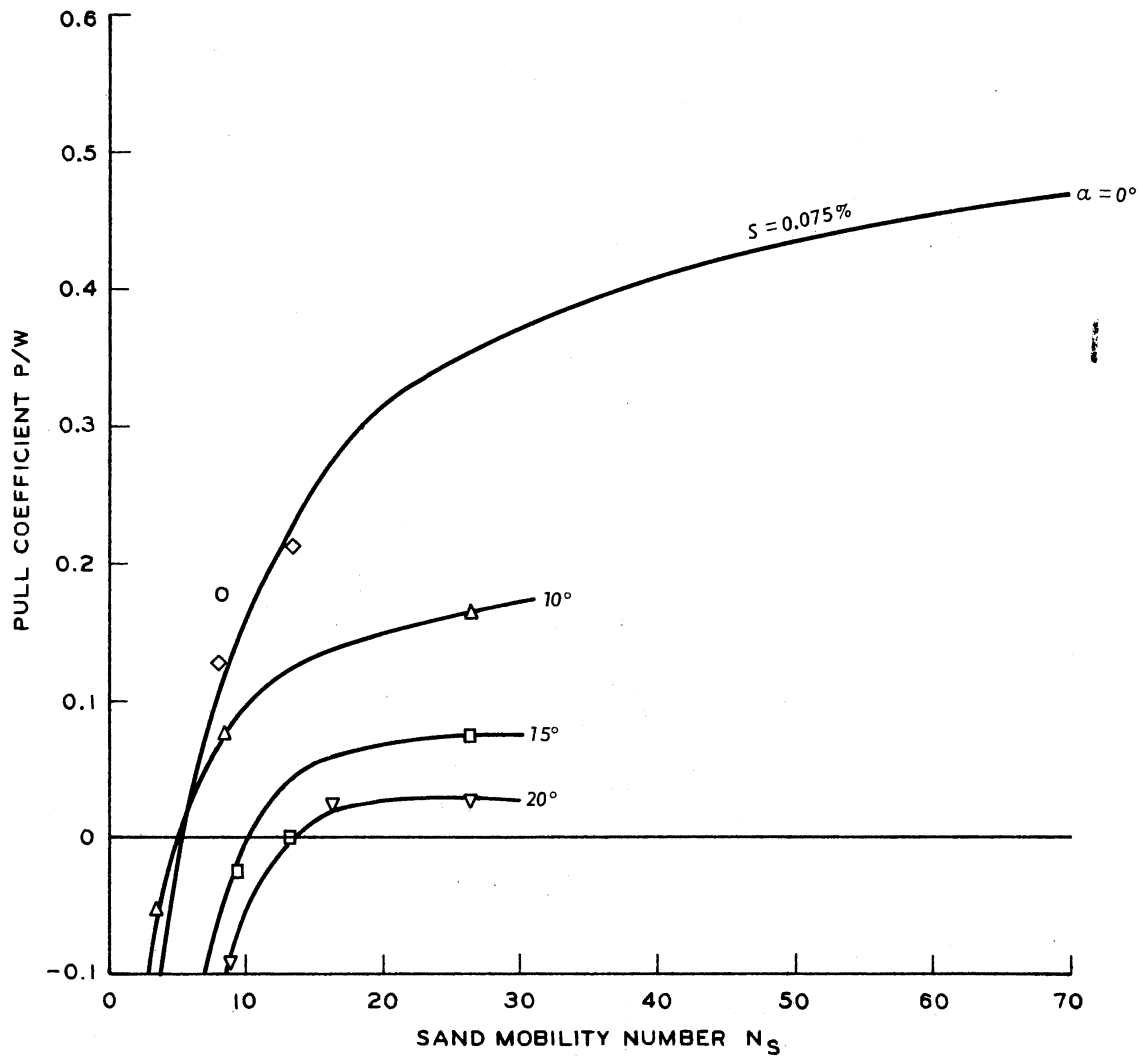
Figure 4.21. Pull Coefficient Versus Sand Mobility Number,
Wheel Slip = 7.5 Percent.
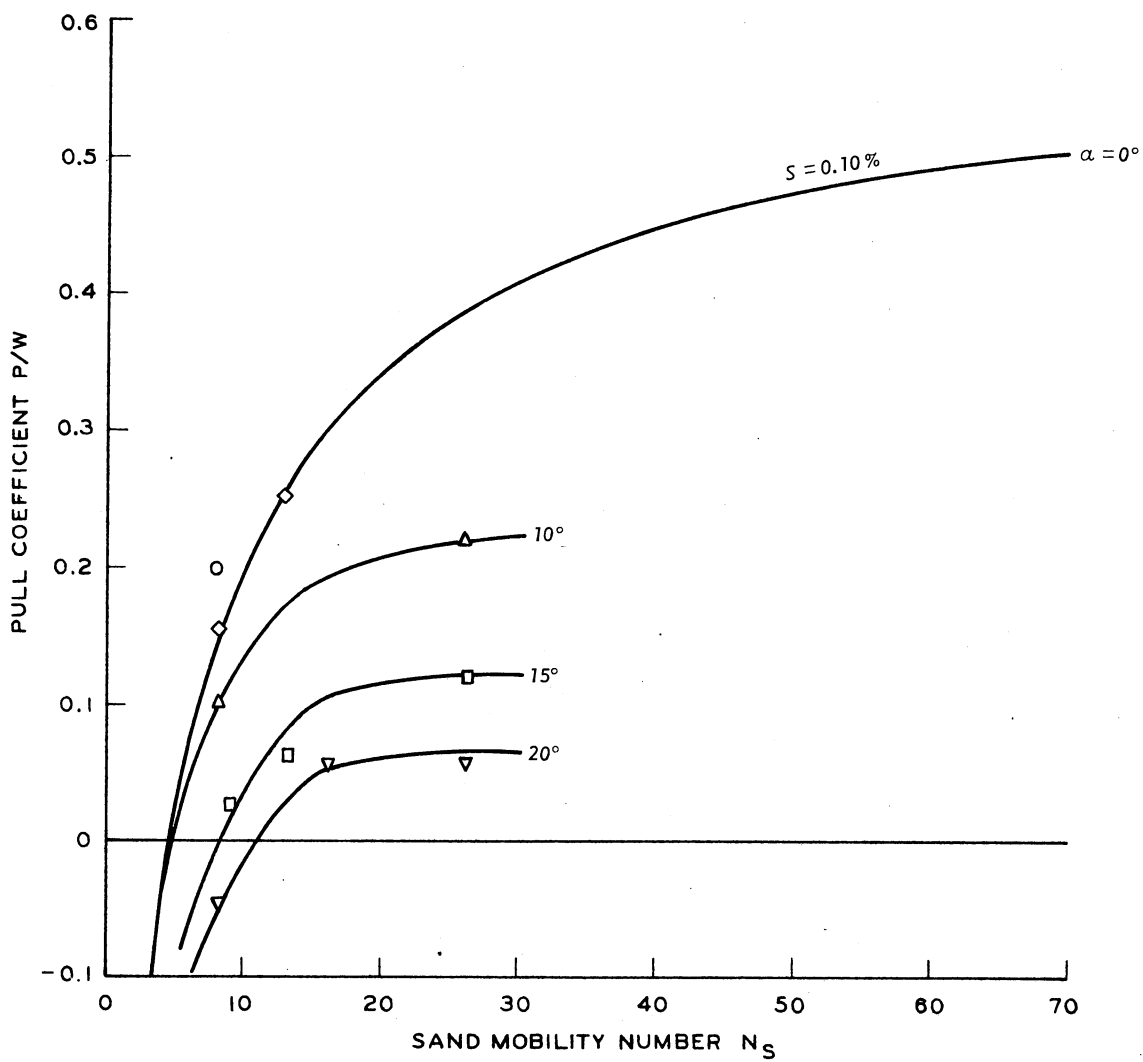
Figure 4.22.   Pull Coefficient Versus Sand Mobility Number,
Wheel Slip = 10 Percent.
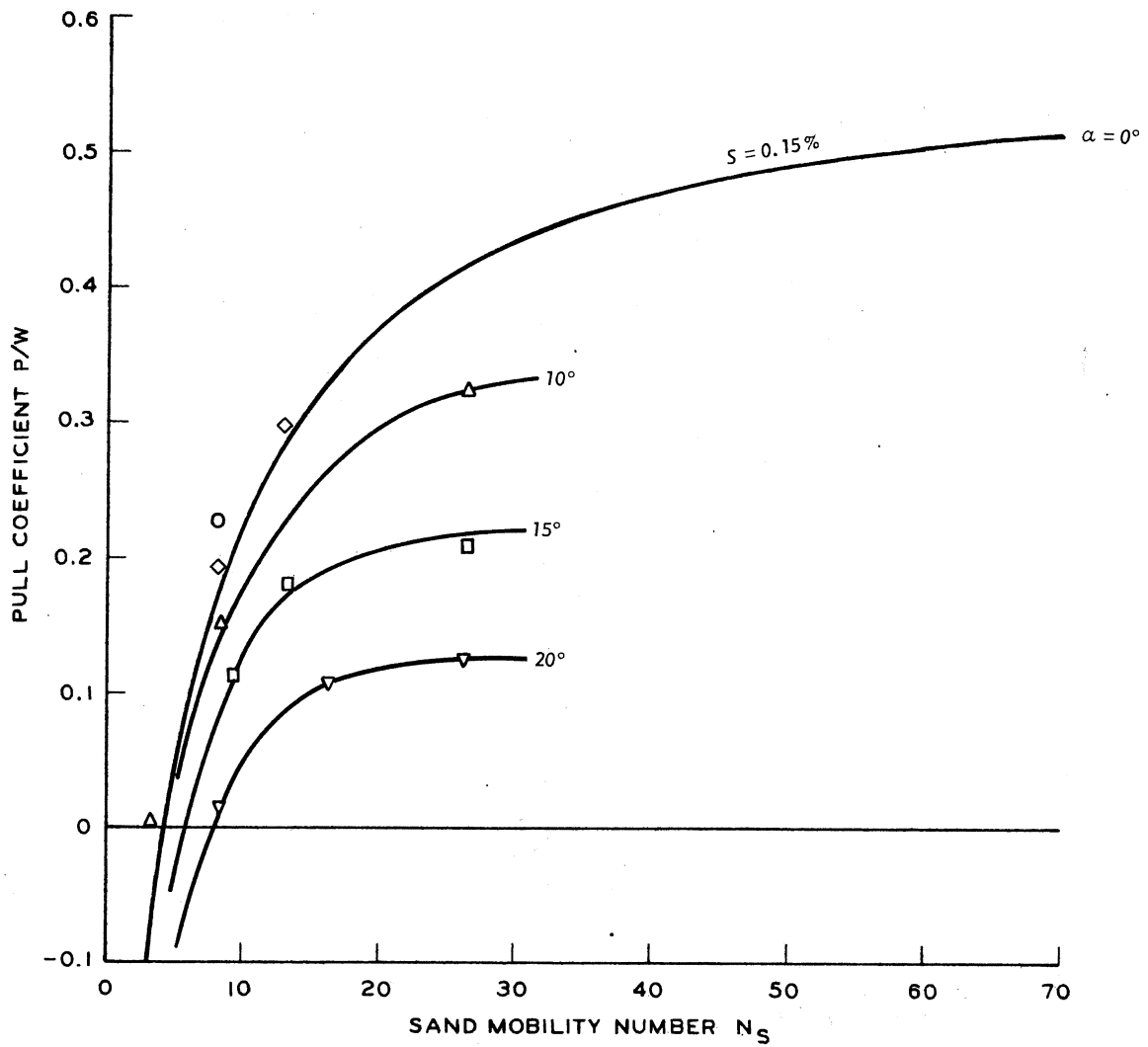
Figure 4.23. Pull coefficient Versus Sand Mobility Number,
Wheel Slip = 15 Percent.
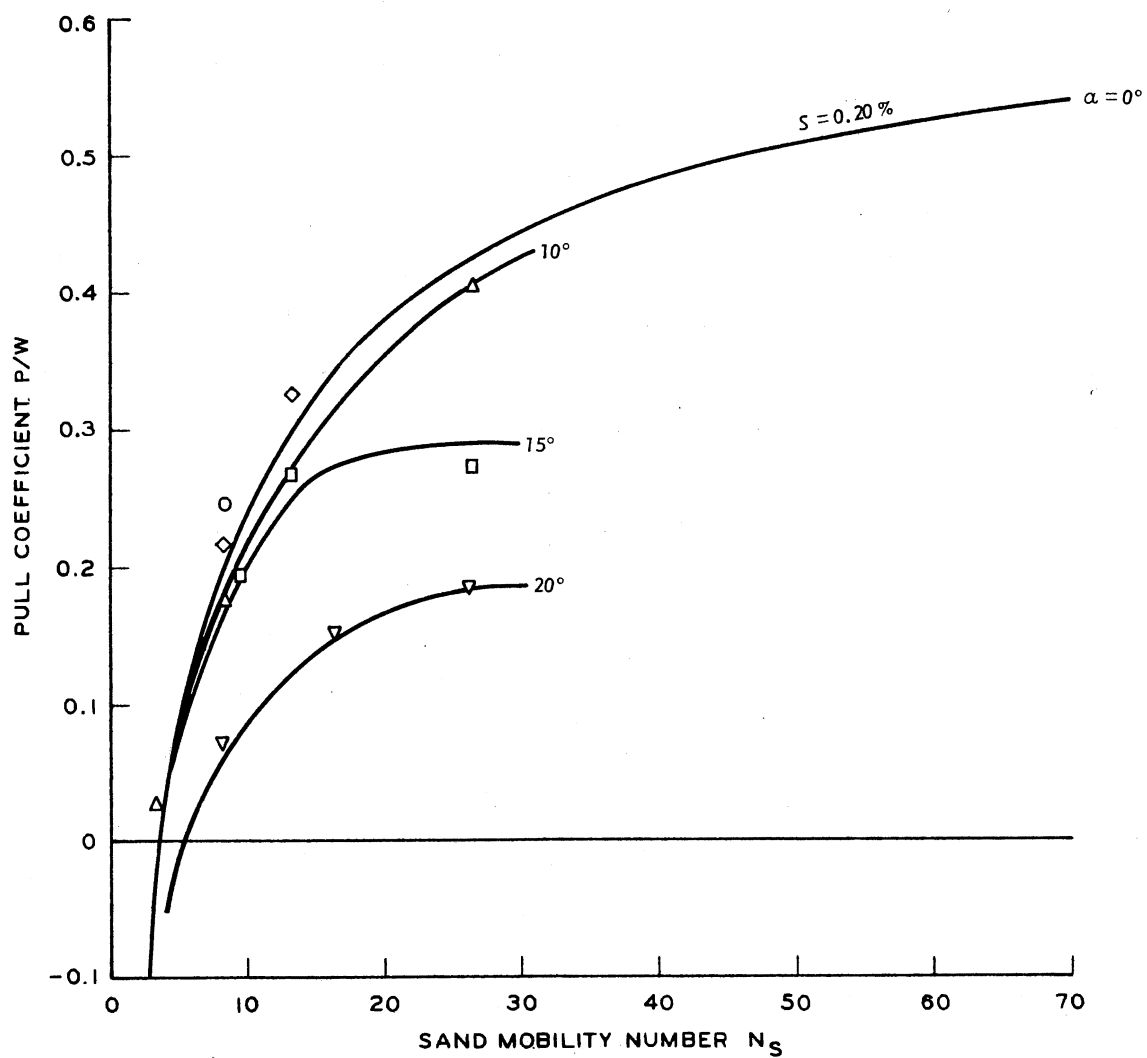
Figure 4.24. Pull Coefficient Versus Sand Mobility Number,
Wheel Slip = 20 Percent.
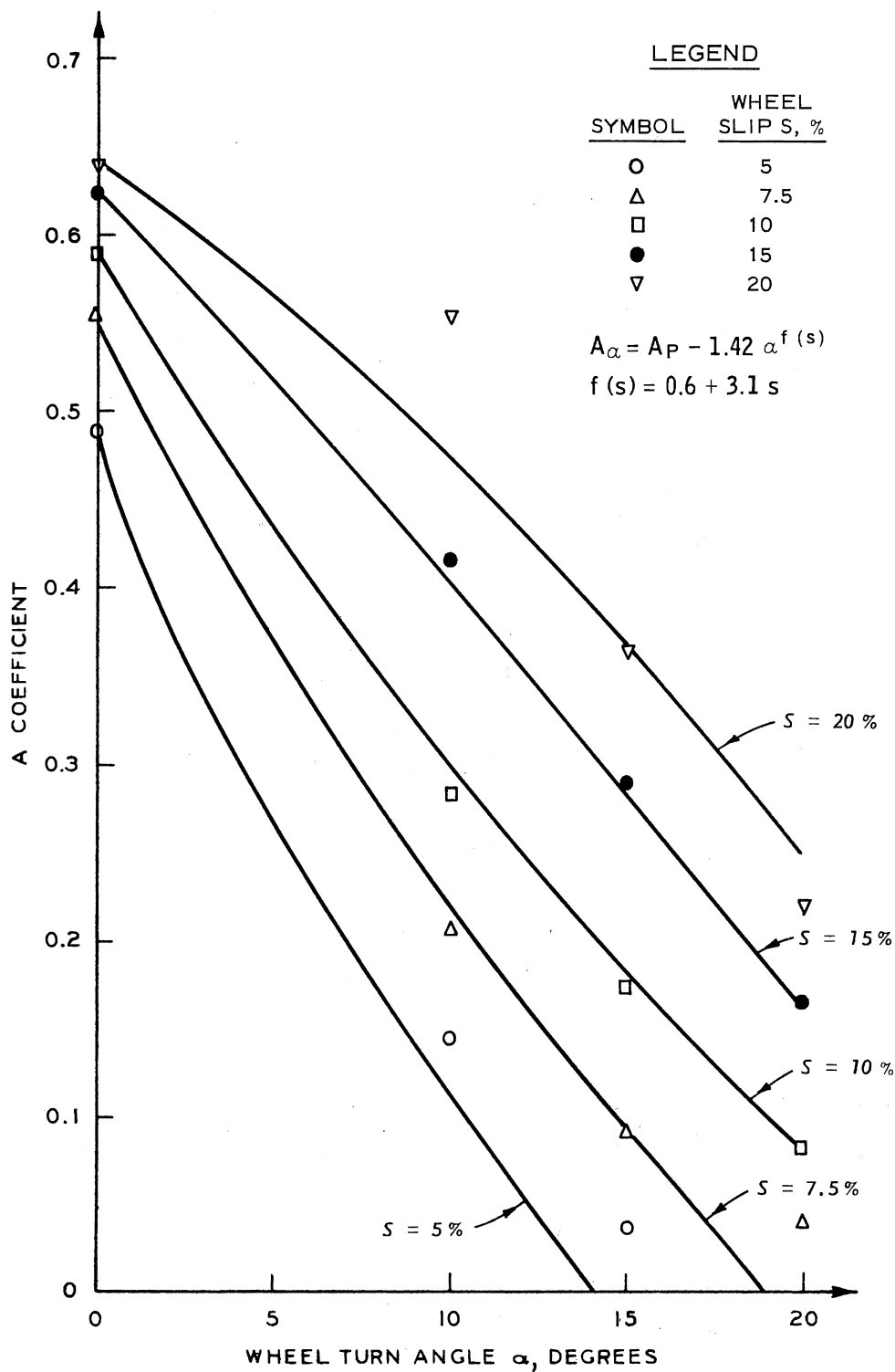
Figure 4.25. Effect of Wheel Turn Angle and Wheel Slip on A_p Coefficient.
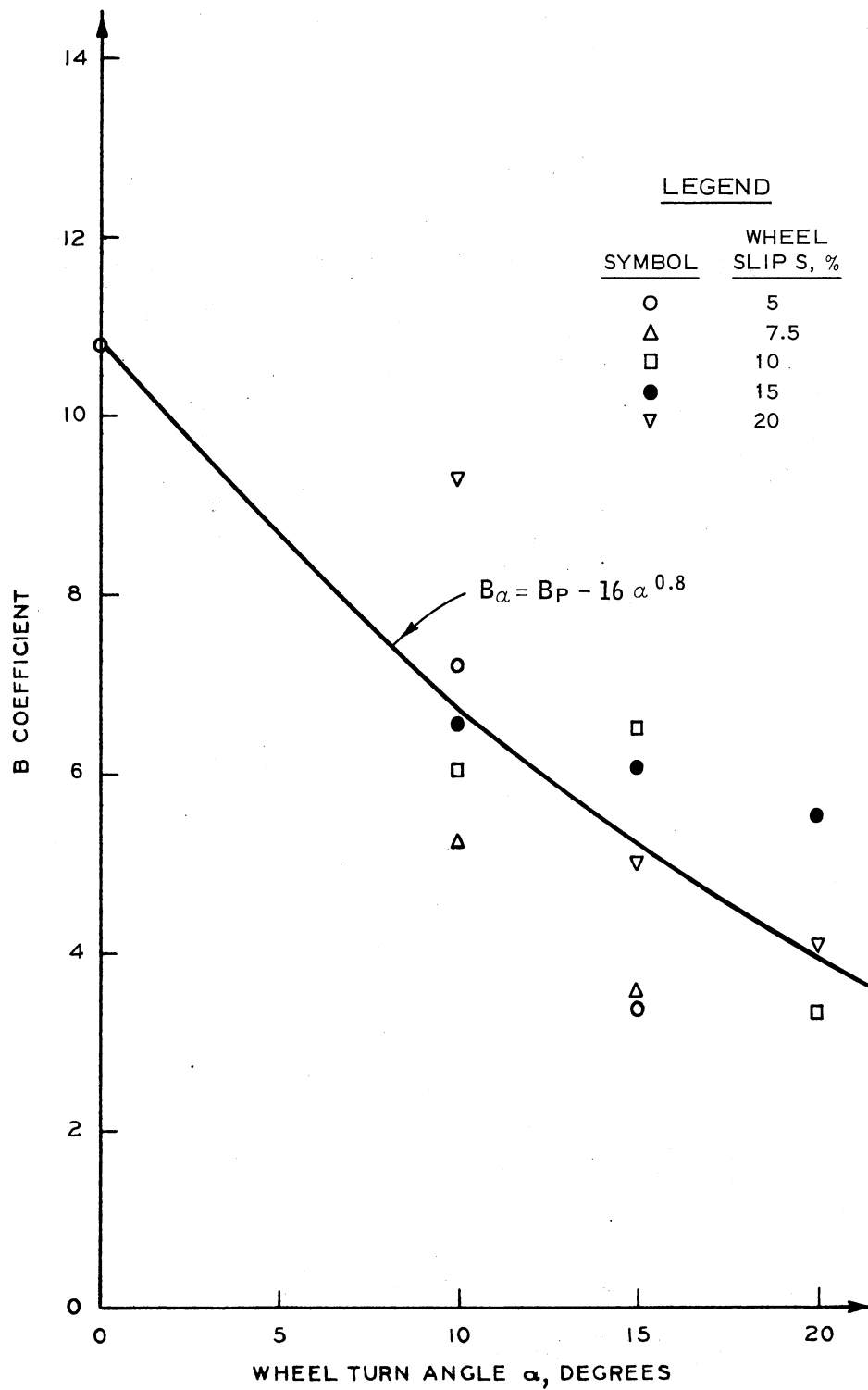
Figure 4.26. Effect of Wheel Turn Angle and Wheel Slip on B_p Coefficient.
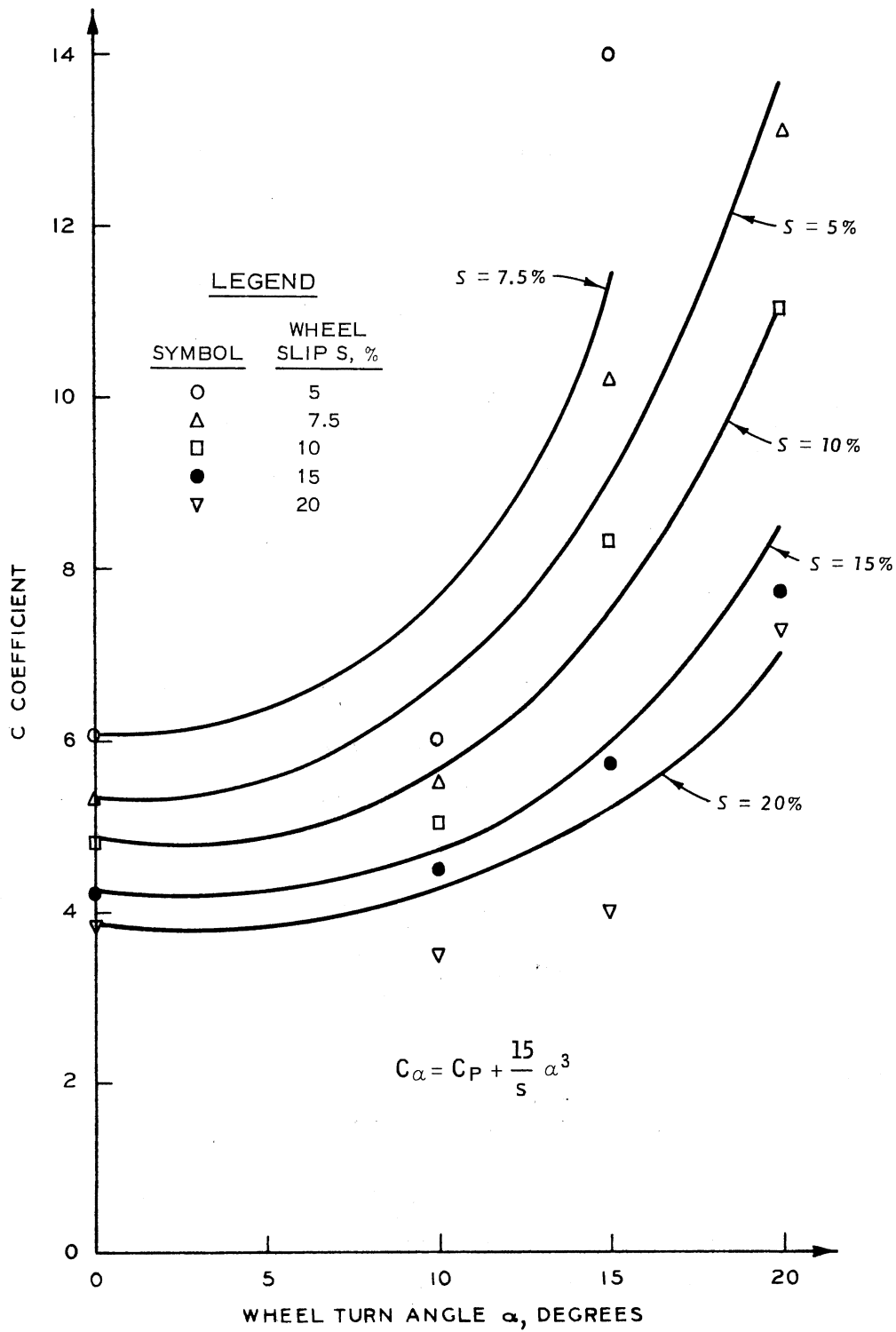
Figure 4.27. Effect of Wheel Turn Angle and Wheel Slip on C_p Coefficient.

for various combinations of N_S , slip, and α becomes

$$\frac{P}{W}\Big|_\alpha = A_\alpha - \frac{A_\alpha B_\alpha}{N_S - C_\alpha + B_\alpha} \qquad (4.8)$$

where

$$A_\alpha = A_P - 1.42\ \alpha^{(0.6\ +\ 3.1\ s)}$$

$$B_\alpha = B_P - 16\ \alpha^{0.8}$$

and

$$C_\alpha = C_P + \frac{15}{S}\ \alpha^3$$

TABLE IV

VARIATION OF COEFFICIENT USED
IN EQUATIONS 2.9 and 4.8

Wheel Slip %	Turn Angle α Degree	Coefficients		
		A	B	C
5.0	0	0.490	10.8	6.05
	10	0.142	7.22	6.0
	15	0.0379	3.36	14.0
	20	--	--	--
7.5	0	0.557	10.8	5.3
	10	0.207	5.21	5.5
	15	0.0907	3.54	10.2
	20	0.0396	3.46	13.1
10.0	0	0.590	10.8	4.80
	10	0.285	6.05	5.0
	15	0.173	6.51	8.3
	20	0.0817	3.34	11.0
15.0	0	0.623	10.8	4.20
	10	0.418	6.56	4.5
	15	0.290	6.07	5.7
	20	0.166	5.57	7.7

TABLE IV (CONTINUED)

Wheel Slip %	Turn Angle α Degree	Coefficients		
		A	B	C
20.0	0	0.640	10.8	3.81
	10	0.556	9.30	3.5
	15	0.365	5.02	4.0
	20	0.221	4.10	7.3

Equation 4.8 in the above expanded version was used to formulate the long-short dashed lines illustrated in Figures 4.14a through 4.19a. Figures 4.14b through 4.19b illustrate the torque coefficient versus slip at various sand mobility numbers and a range of wheel turn angles. Several occurances seem apparent. First over the slip range tested, M/Wr_a increases gradually and somewhat linearily as slip increases for a given N_S and α . For a given wheel slip and sand mobility number, M/Wr_a decreases as the wheel turn angle increases. On a percentage or proportionate bases this decrease in M/Wr_a is not as large as that noted for the P/W performance parameter. The most discerning feature of the M/Wr_a · versus wheel slip s plots is that the base line (i.e. α = 10) predicted by Equation 2.10 frequently lie below the plotted data for a turn angle of five degrees and on occasion plot below the data points corresponding to a 10 degree turn angle. Examination of the basic data used by Turnage and Melzer in developing M/Wr_a versus N_S and reported herein with Figures 2.5 and 2.7 indicates that for N_S values less than 20 (the majority of the powered turn wheel sand tests

were performed with N_s less than 20) and for a given wheel slip, the torque coefficients from individual tests varied approximately $\pm$ 30 percent from the smooth curve drawn through the data points. Comparisons of the data points of Figure 4.14b through 4.19b with the respective base line predictions of Equation 4.10 indicates that more than 80 percent of the M/Wr_a test data is within $\pm$ 20 percent of that value predicted by Equation 4.10 at respective values of wheel slip. Since the difference between the test data and the predicted value is less than the variation of the basic data from Equation 2.10 was developed, it does not seem appropriate to refine the data further and in effect wheel turn angle is considered insignificant in computing torque inputs to a powered wheel operating in loose sand.

Side Forces Developed in Sand

Figure 4.28 illustrates plots of the side force coefficient S/W versus the pull coefficient P/W ; individual plots contain related data having about equal sand mobility numbers N_s . The linear relations fitted to the plotted data points verify the finding established for the clay data; namely, that for positive wheel slip values up to 20 percent, S/W versus P/W for a given α and N_s can be expressed linearily. Further, the slope of the line is constant for a given angle and displaced vertically upward on the plot as N_s increases. The numbers beside the plotted points indicate wheel slip s ; and, as with the clay data, shows that as the input power (as expressed and implied by wheel slip) to the wheel is increased, the pull becomes greater and the magnitude of the side force decreases.

Slopes of the lines drawn through the data points in Figure 4.28
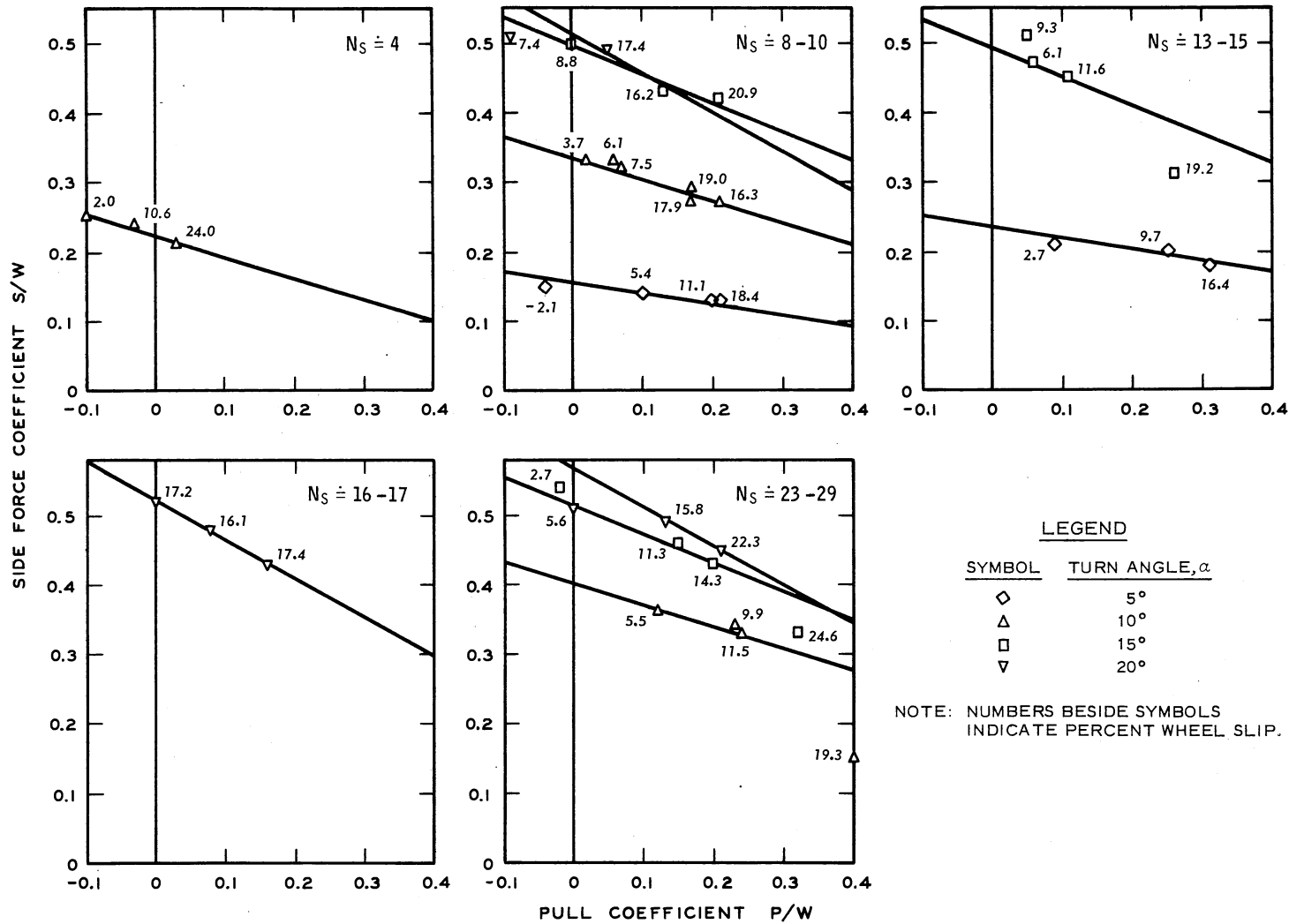
Figure 4.28. Side Force Versus Pull Coefficient for 6.00-9, 4-PR Tire on Sand for Various Values of Sand Mobility Number N_s .

are plotted against the respective turn angle α in Figure 4.29. A straight line was passed through the origin and the plotted points having a slope of 1.65 (note that this value is only slightly below the 1.72 reported on Figure 4.6 from similar clay data).

The values of side force coefficients developed at zero pull were selected from Figure 4.28 and plotted in Figure 4.30. Figure 4.30 indicated that the side force coefficient, when the pull is zero and the sand mobility number is about the same, increases with increasing values of turn angle α. Further, if the turn angle is held constant, S/W at zero pull increases as the sand mobility number increases. A second degree polynominal curve was fitted to data points having N_S of 8.3 to 9.4 and a second polynominal curve for those tests having a N_S of 26.3. These curves imply that N_S is of secondary importance to the development of side forces for powered wheels operating in loose sand. If the coefficients of the two polynominals are assumed to vary linearily for intermediate values of the sand mobility number then a general equation can be written to relate the side force coefficient at zero pull

$$\frac{S}{W}_{P\ =\ 0} = (2.3 + 0.03\ N_S)\ \alpha - (2.4 + 0.065\ N_S)\ \alpha^2 \qquad (4.9)$$

The side force coefficient at zero pull is the ordinate intercept of the S/W versus P/W relation and the slope 1.65 α expresses the slope of the S/W versus P/W relation. Hence for a given turn angle and sand mobility number the two performance parameters are related as

$$\left(\frac{S}{W}\right)^{\alpha} = \left(\frac{S}{W}\right)_{P\ =\ 0} - (1.65\ \alpha)\ \left(\frac{P}{W}\right)^{\alpha} \qquad (4.10)$$
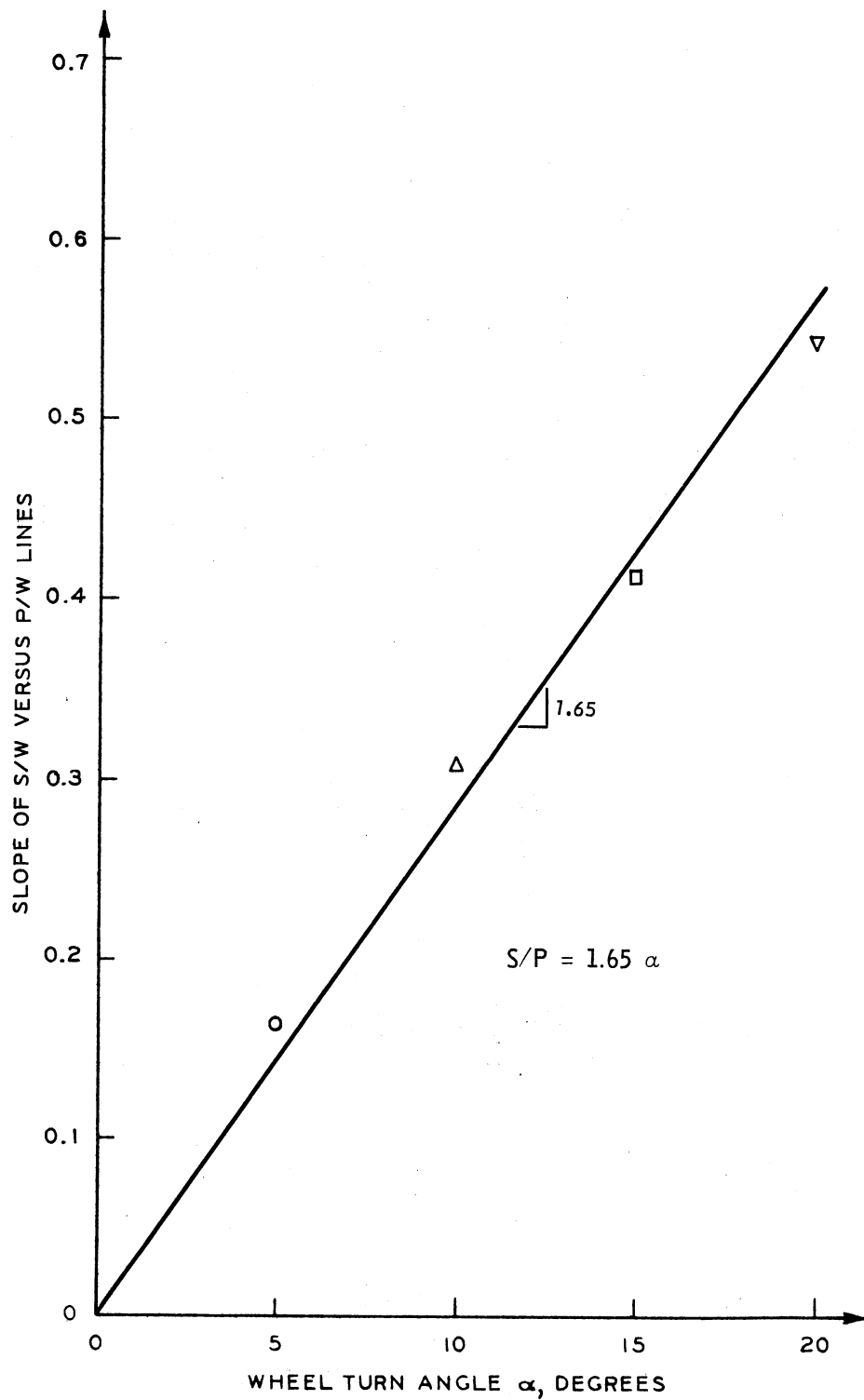
Figure 4.29.   Relation Between Δ(S/W)/Δ(P/W) and Turn
Angle, α , for Sand.
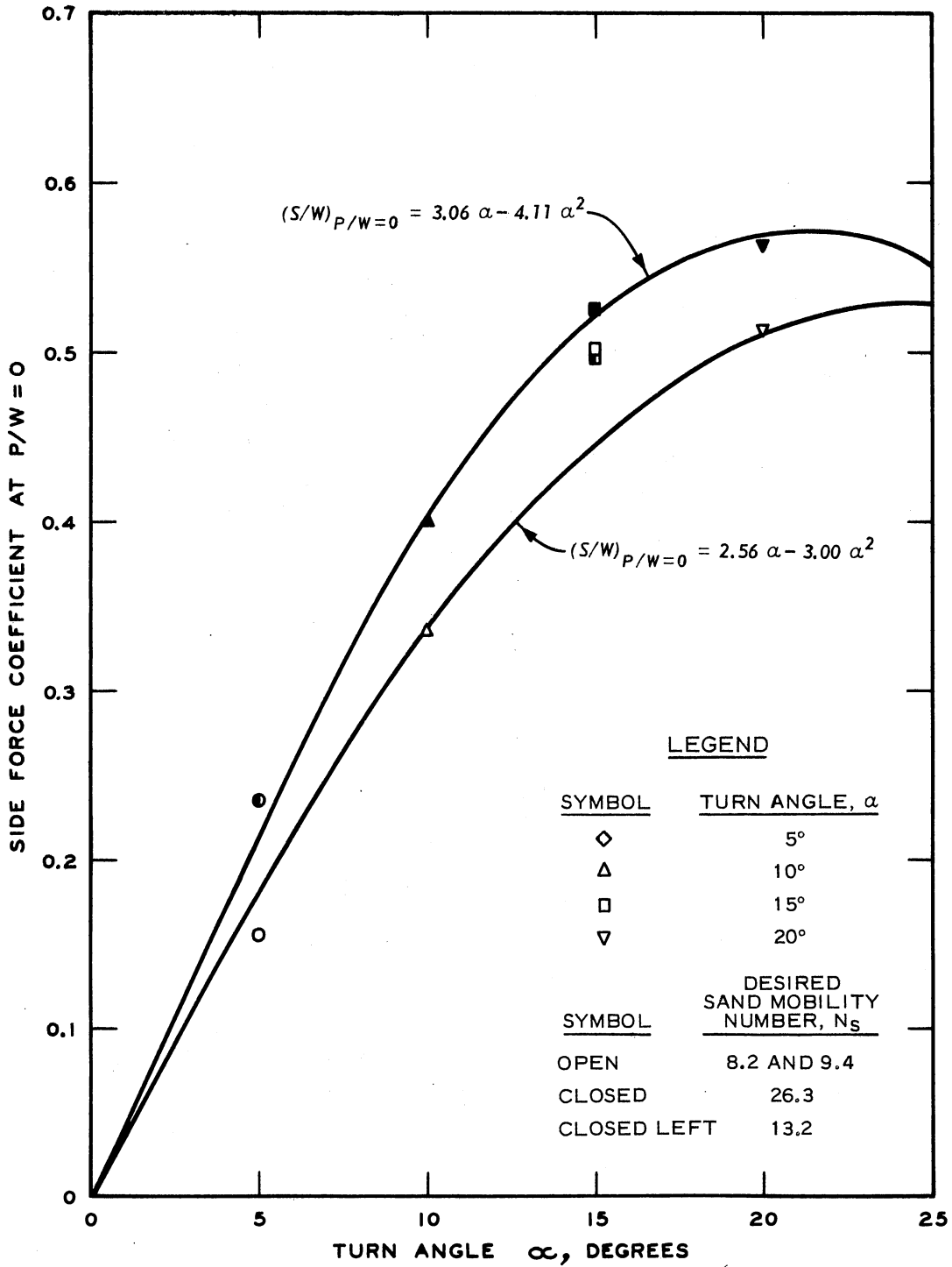
Figure 4.30. Side Force Coefficient at P/W = 0 Versus Turn Angle, α , for Sand.

Figures 4.31 through 4.36 contain the plotted test values of side force coefficient versus percent wheel slip. Again the tests are grouped on each plot having similar test conditions (i.e. sand mobility number approximately the same). Superimposed are broken lines determined from Equation 4.10 along with solid lines visually fitted to the data. For the sand tests conducted with turn angles other than zero, Equation 4.10 predicted the side force within 20 percent or less of the test value in 40 and our 46 tests or 83 percent.

Sinkage in Sand

Sinkage coefficient (z/d) as a function of the sand mobility number and wheel turn angle is illustrated in Figure 4.37. As expected, z/d decreases for a given turn angle with increasing N_S . The broken lines on each plot of Figure 4.37 represents results from previous test programs where the turn angle was zero and the wheel slip about 20 percent (Turnage, 1972). Data obtained with wheel turn angles of 10, 15, and 20 degrees indicate that for a given sand mobility number, sinkage increases with increasing turn angle. This is readily apparent from the summary plot provided in Figure 4.37. The number beside each datum point is the wheel slip in percent, and, as with the clay results, sinkage is not significantly influenced by wheel slips up to 20 percent.

Summary

For a given set of independent variables expressed as the sand mobility number N_s , the wheel slip, and the wheel turn angle forces acting on a pneumatic tire are computed as follows:

The input torque coefficient in the plane of the wheel
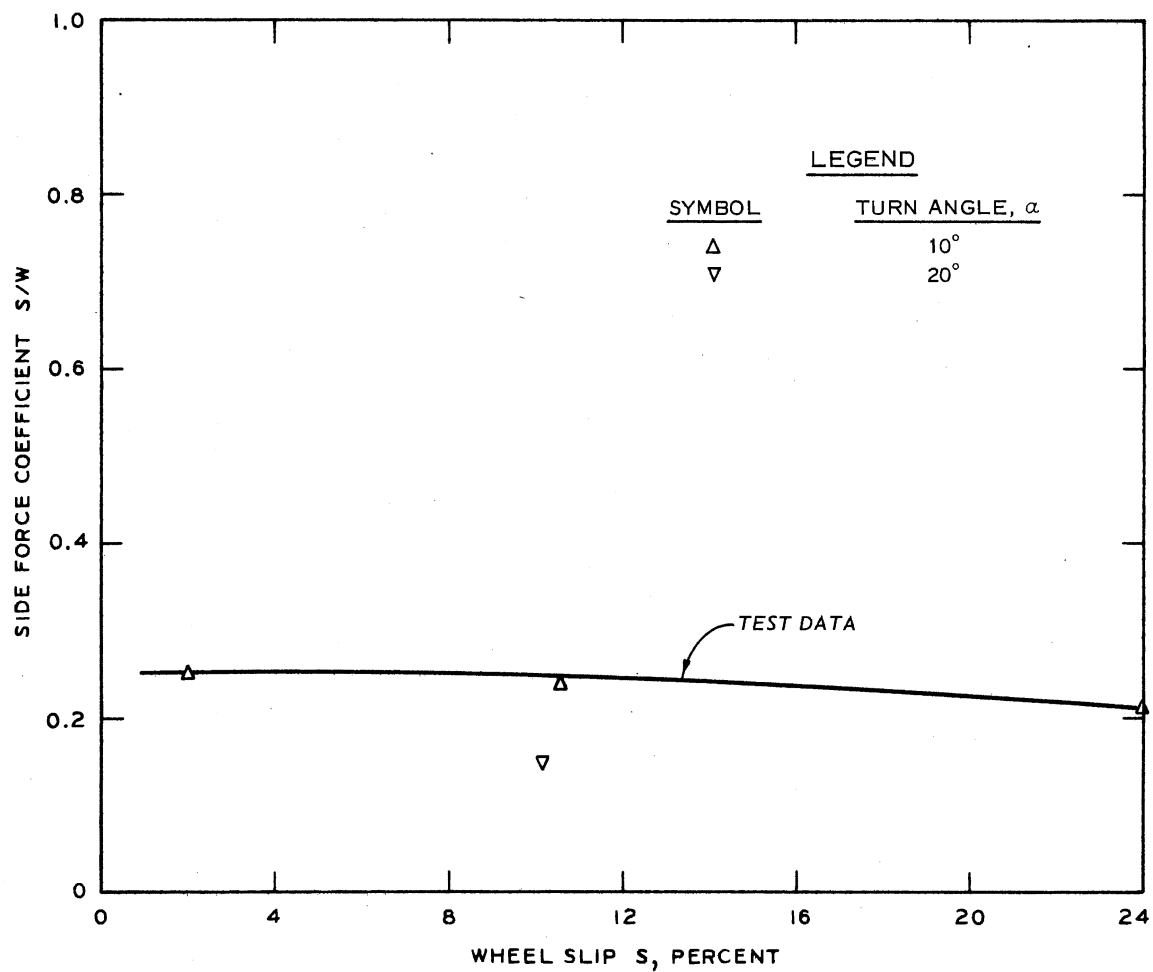
Figure 4.31.   Influence of Turn Angle on Side Force Coefficient.
Average Cone Penetration Resistance Gradient
$G = 2.0$, Tire Deflection $\delta/h = 0.15$, Design
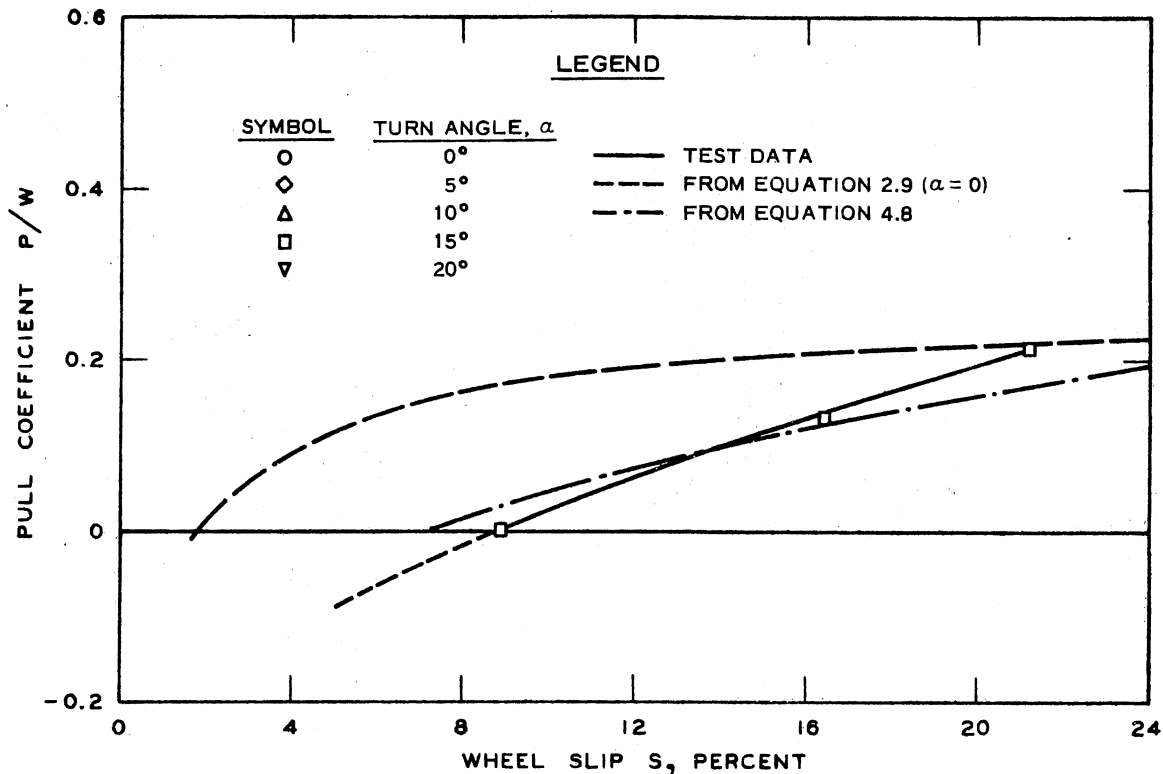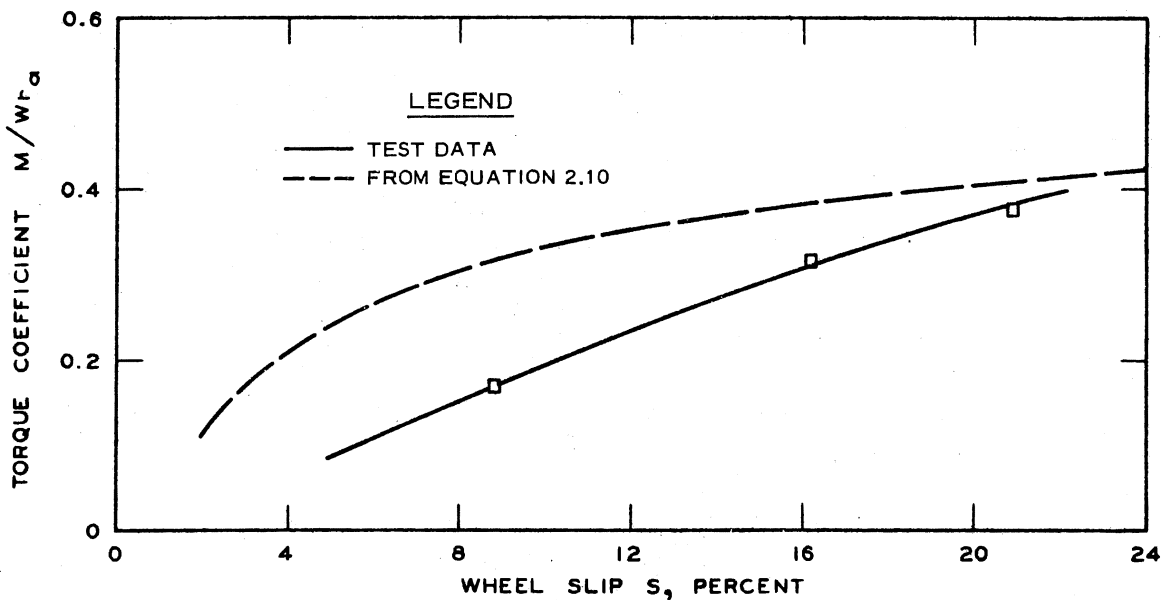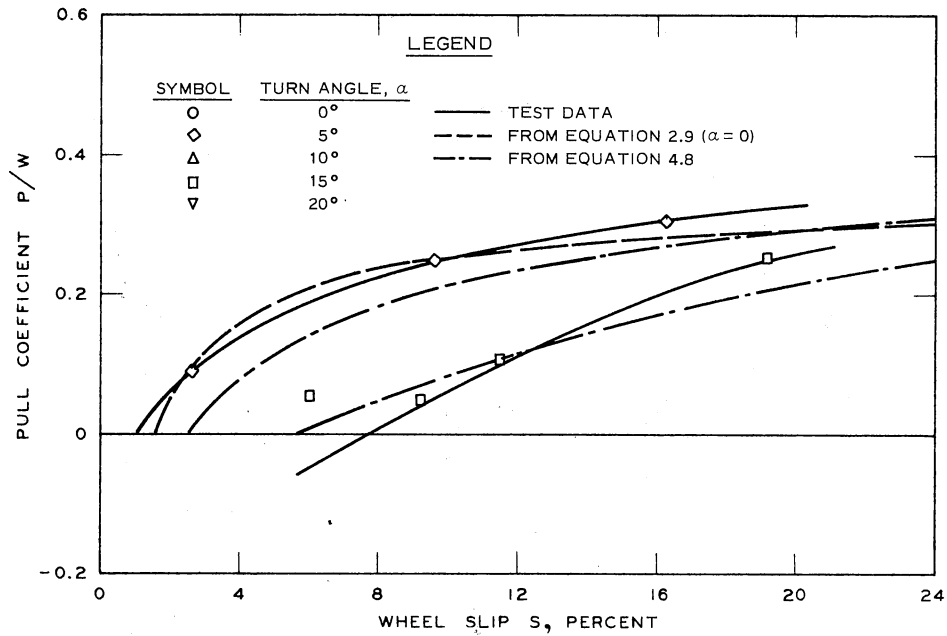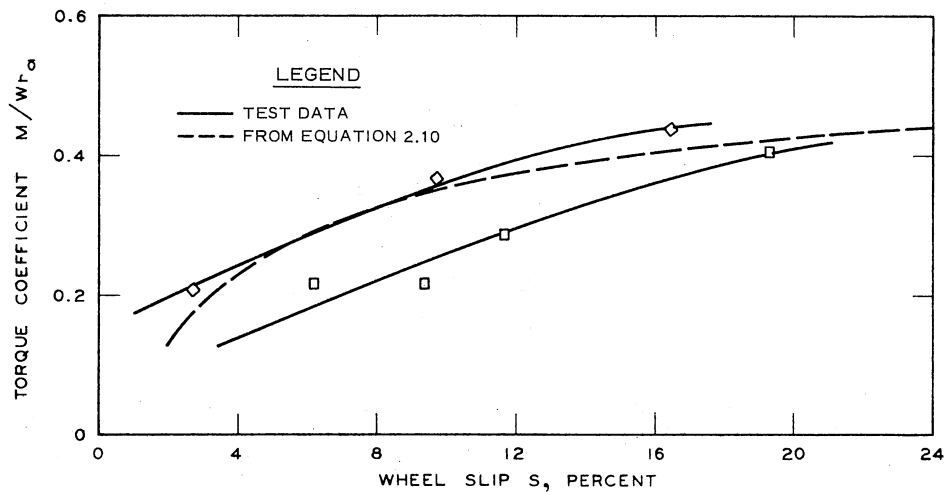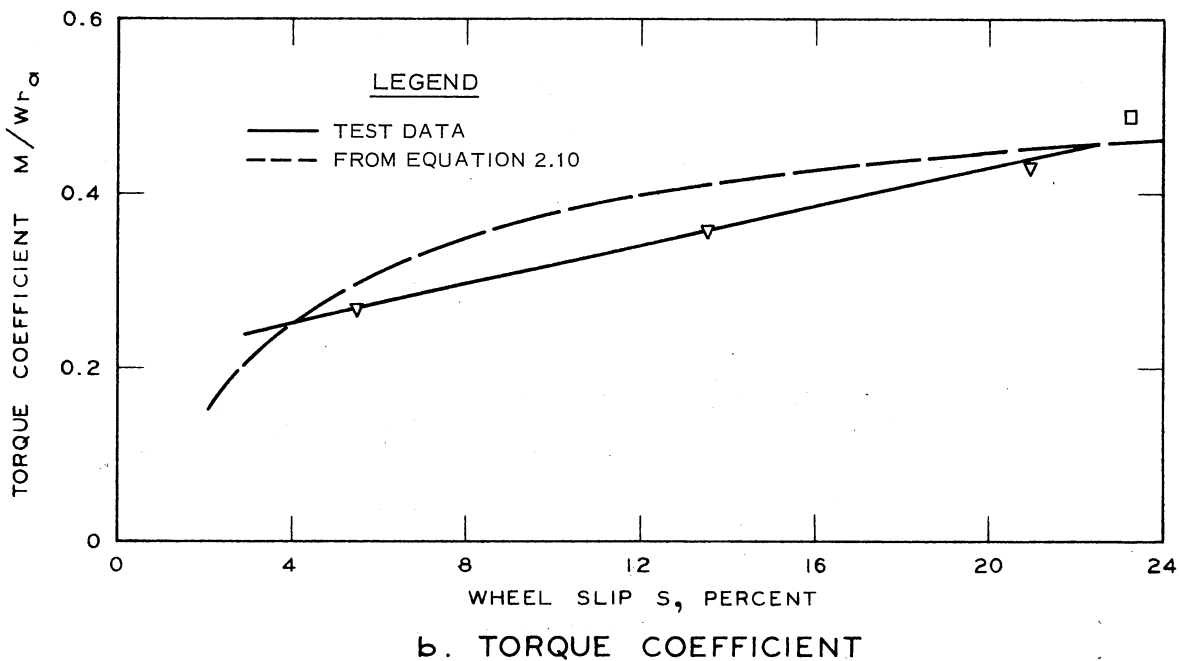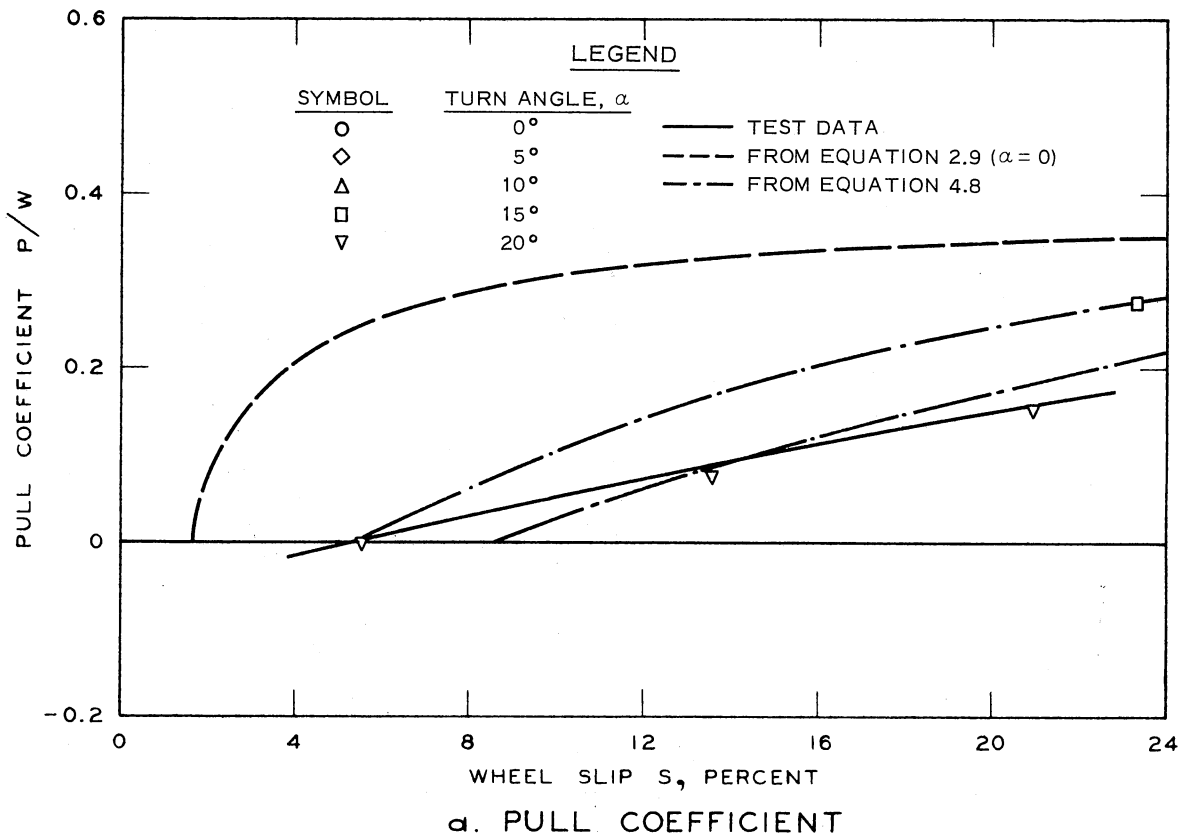Wheel Load $W = 2,000$ N .   Desired Sand Mobility
Number $N_s = 3.5$.
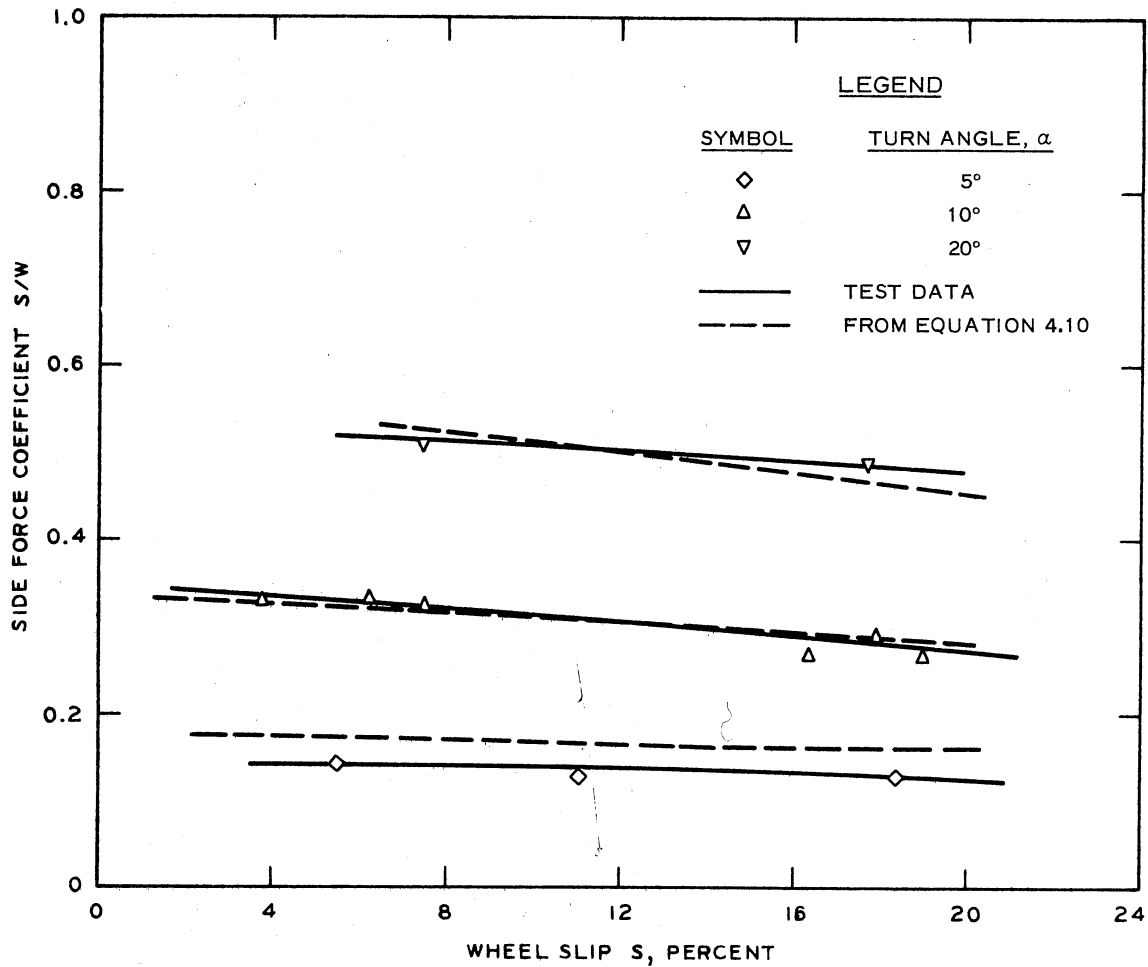
Figure 4.32. Influence of Turn Angle on Side Force Coefficient.
Average Cone Penetration Resistance Gradient
G = 2.0 , Tire Deflection δ/h = 0.35 , Design
Wheel Load W = 2,000 N . Desired Sand Mobility
Number N_s = 8.2 .
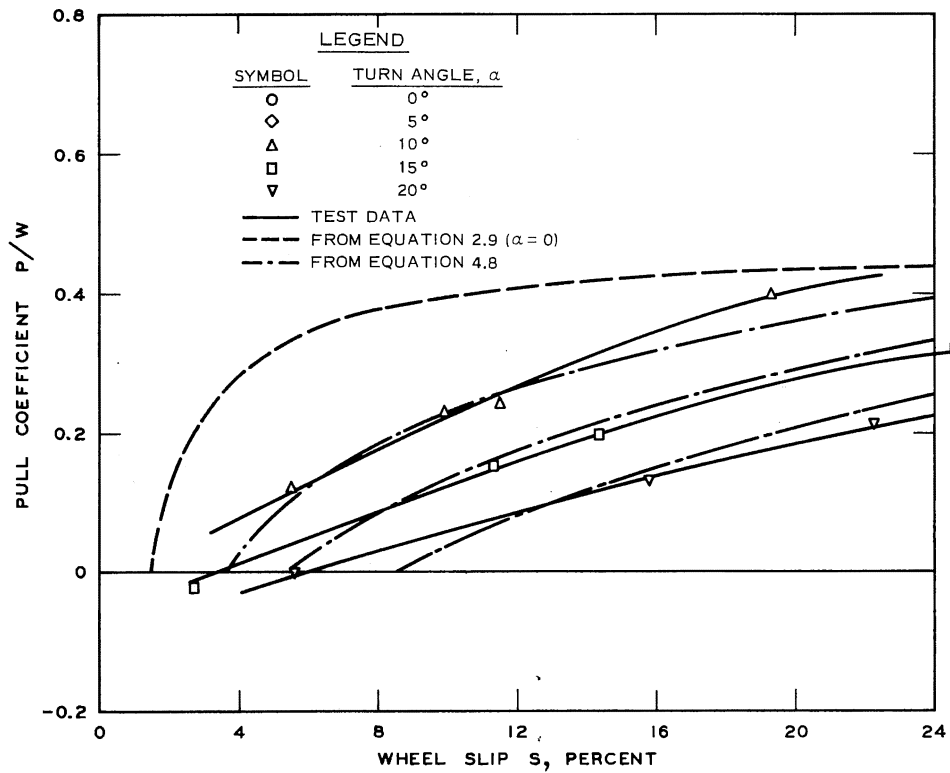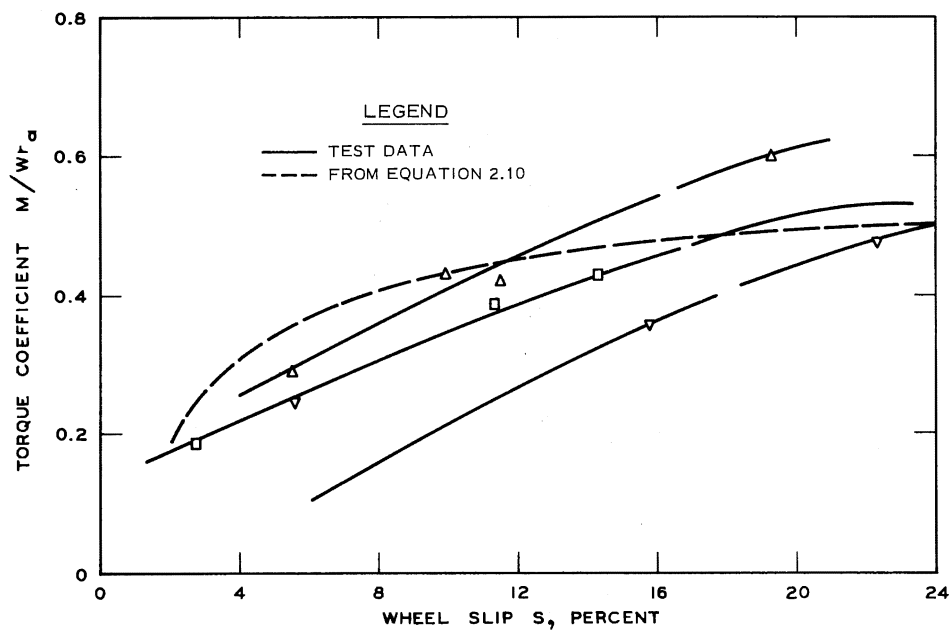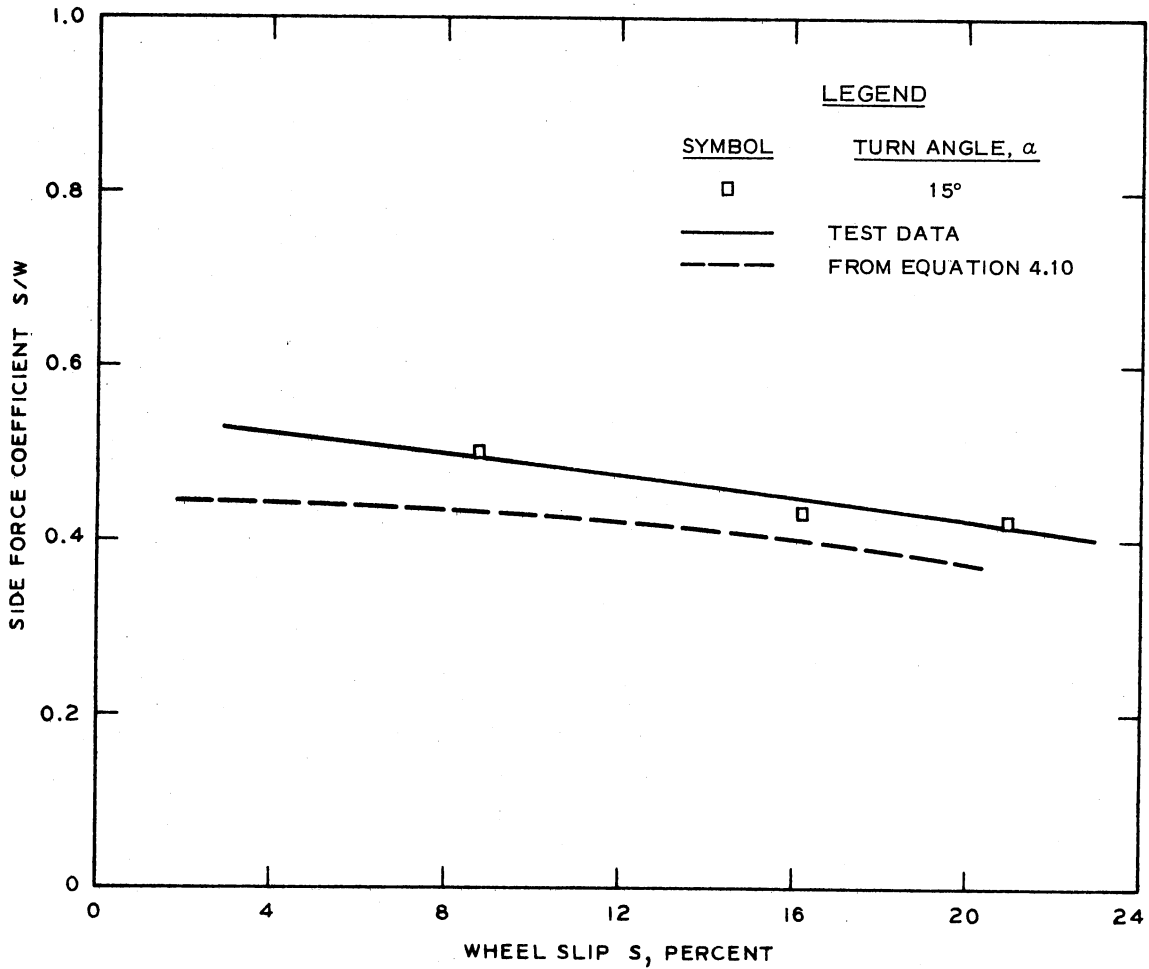
Figure 4.33. Influence of Turn Angle on Side Force Coefficient.
Average Cone Penetration Resistance Gradient
$G = 3.2$, Tire Deflection $\delta/h = 0.25$, Design
Wheel Load $W = 2,000$ N . Desired Sand
Mobility Number $N_s = 9.4$.
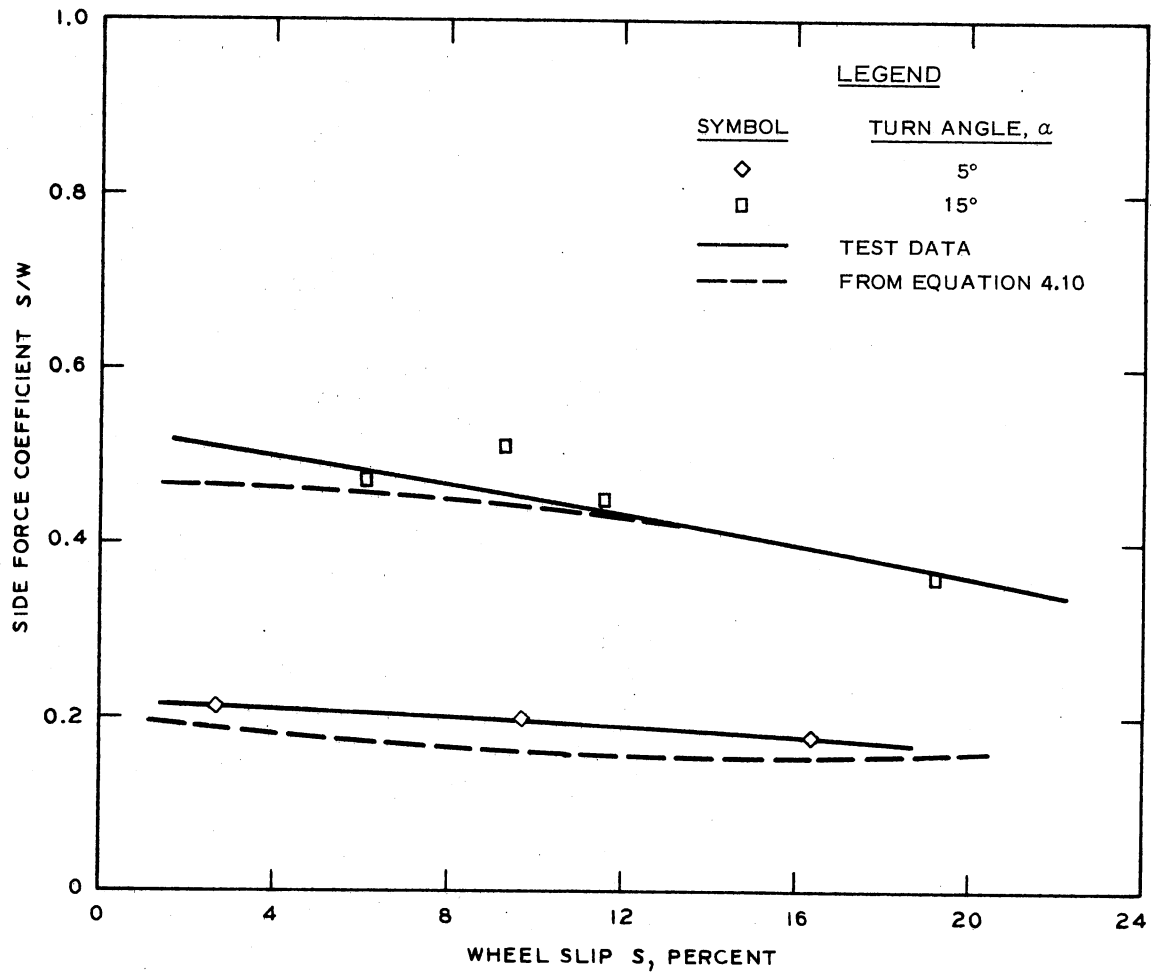
Figure 4.34.   Influence of Turn Angle on Side Force Coefficient.
Average Cone Penetration Resistance Gradient
$G = 3.2$, Tire Deflection $\delta/h = 0.35$, Design
Wheel Load $W = 2,000$ N .   Desired Sand Mobility
Number $N_s = 13.2$.
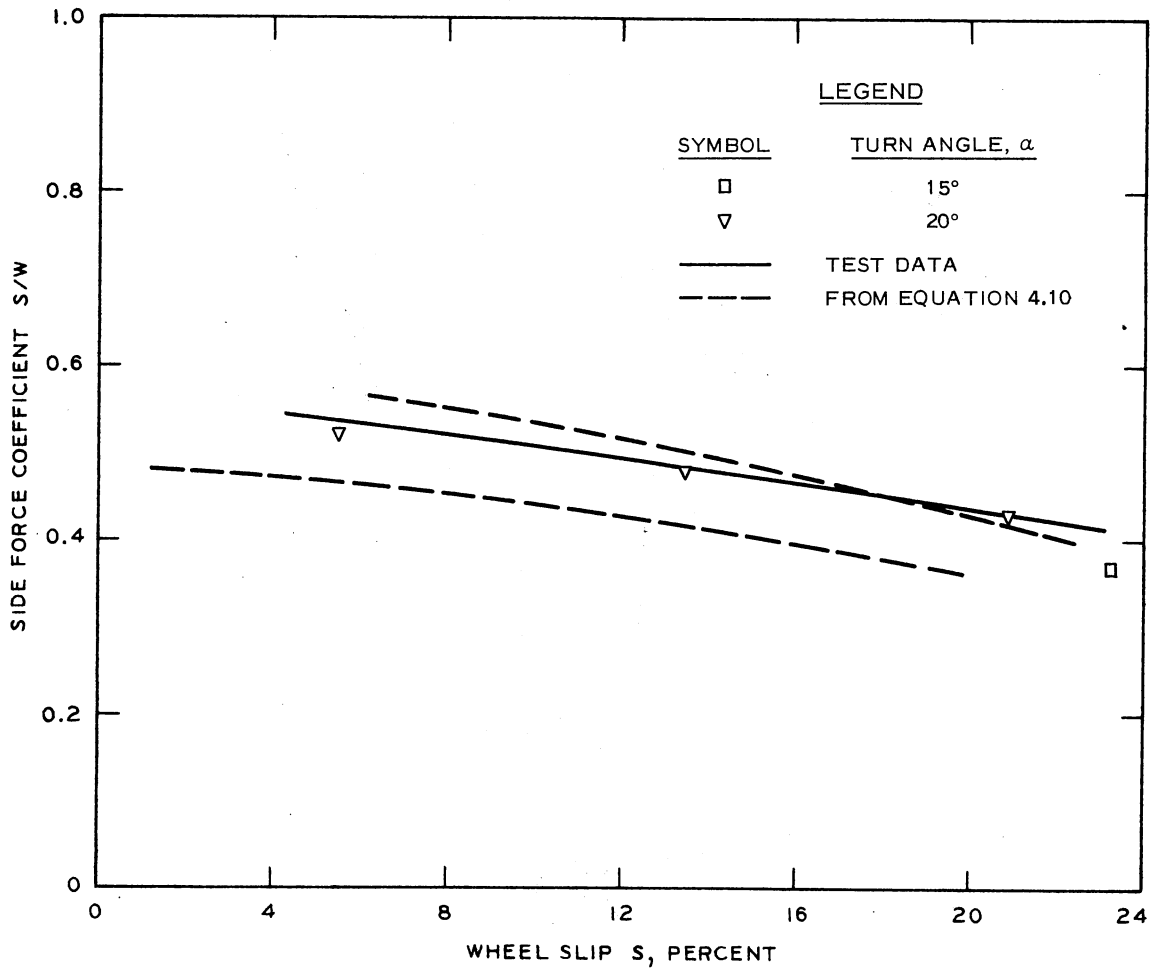
Figure 4.35. Influence of Turn Angle on Side Force Coefficient.
Average Cone Penetration Resistance Gradient
$G = 2.0$, Tire Deflection $\delta/h = 0.35$, Design
Wheel Load $W = 1,000$ N . Desired Sand Mobility
Number $N_s = 16.4$.
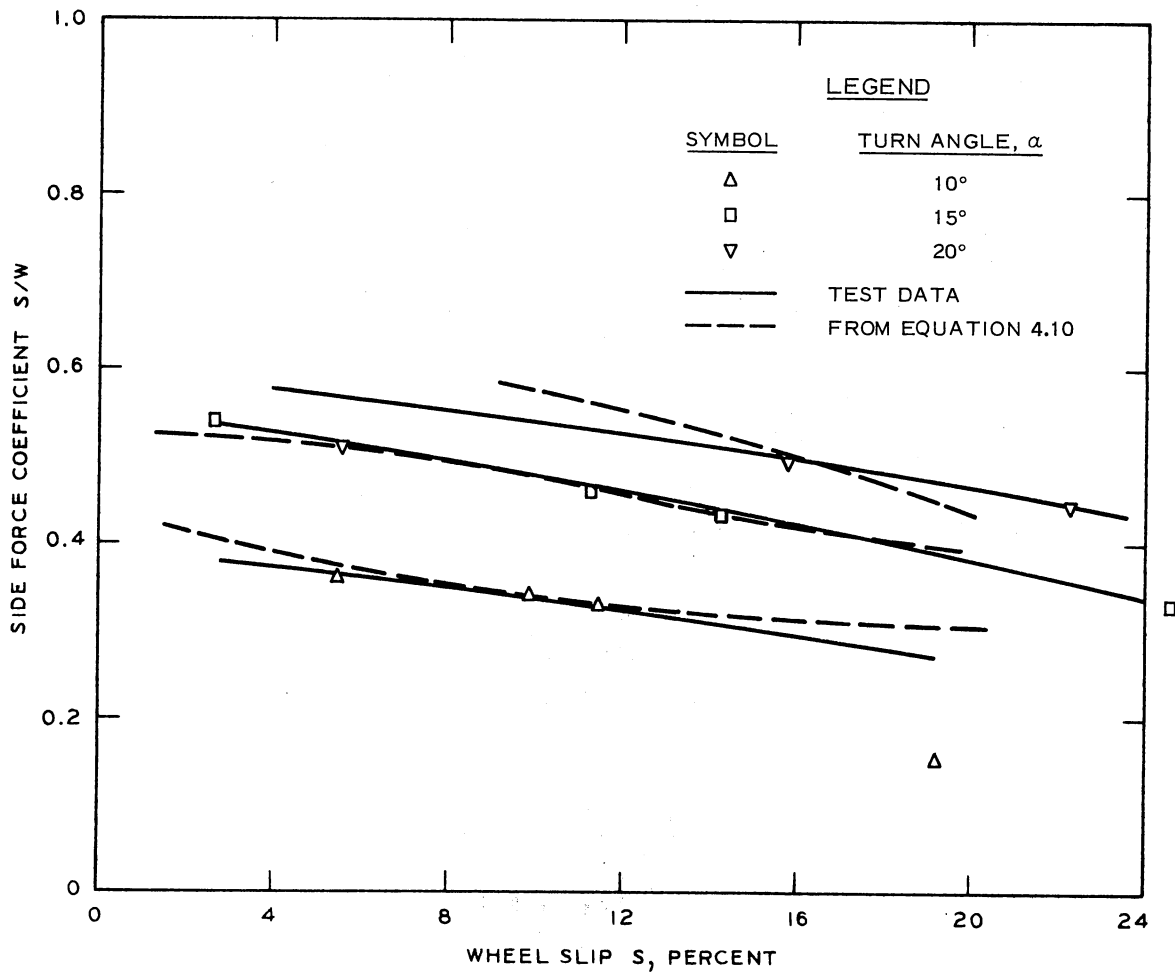
Figure 4.36. Influence of Turn Angle on Side Force Coefficient. Average Cone Penetration Resistance Gradient G = 3.2 , Tire Deflection δ/h = 0.35 , Design Wheel Load W = 1,000 N . Desired Sand Mobility Number N_s = 26.3 .
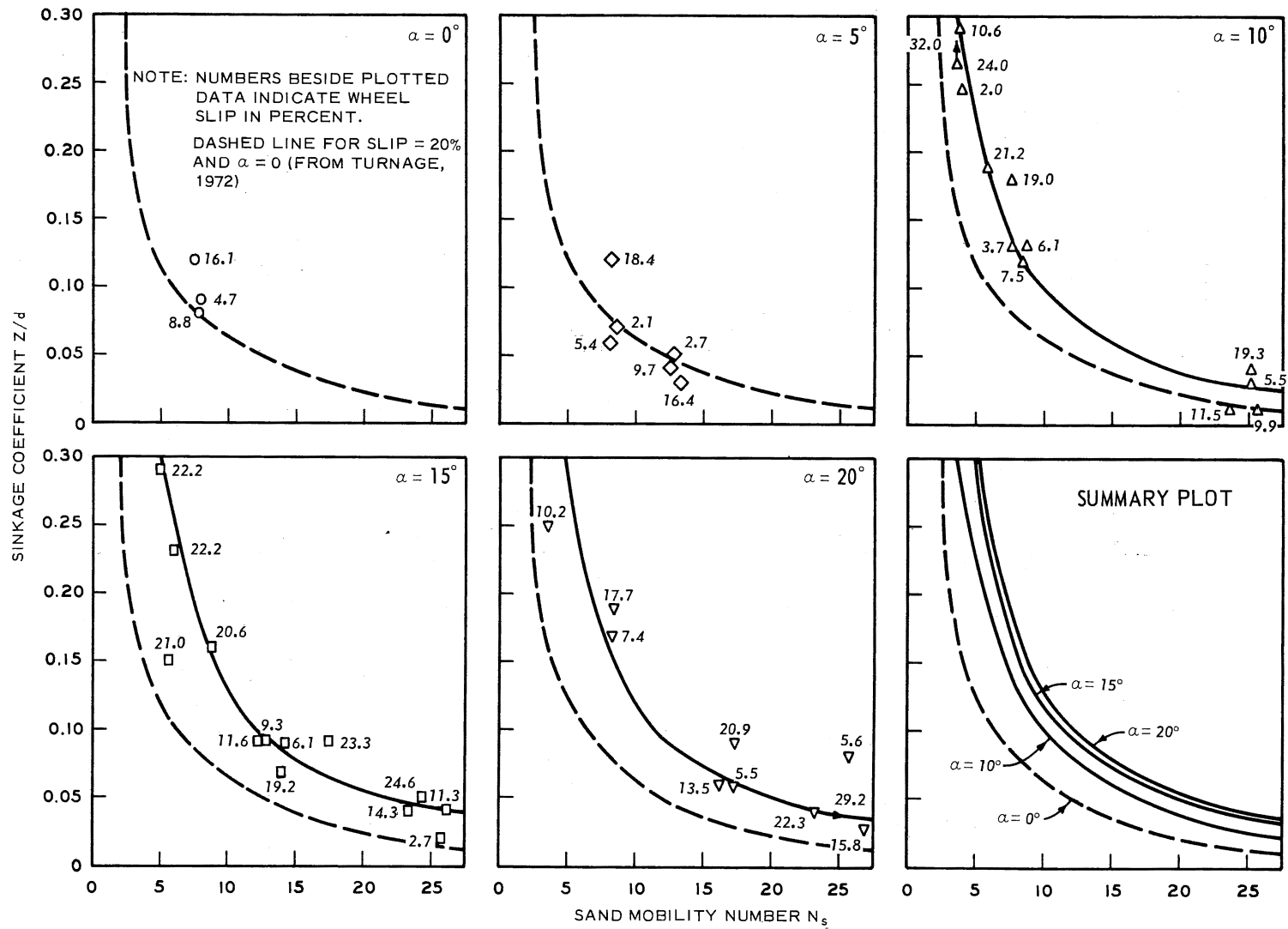
Figure 4.37. Sinkage Coefficient as Functions of Sand Mobility Number and Turn Angle.

$$\left(\frac{M}{Wr_a}\right)^\alpha = \frac{M}{Wr_a} = A - \frac{AB}{N_S - C + B}$$

where

$A = 0.66$

$B = 4.71 + 1.72/s$

$C = -10$

The pull coefficient in the plane of the wheel

$$\left(\frac{P}{W}\right)^\alpha = A_\alpha - \frac{A_\alpha B_\alpha}{N_S - C_\alpha + B_\alpha}$$

where

$A_\alpha = A_P - 1.42\ \alpha^{(0.6 + 3.1\ s)}$

$B_\alpha = B_P - 16\ \alpha^{0.8}$

$C_\alpha = C_P + \frac{15}{s}\ \alpha^3$

and

$A_P = 0.69 - \frac{0.01}{s}$

$B_P = 10.8$

$C_P = \frac{2.23}{s^{1/3}}$

and finally the side force coefficient perpendicular to the plane of the wheel

$$\left(\frac{S}{W}\right)^\alpha = \left(\frac{S}{W}\right)_{P\ =\ 0} - (1.65\ \alpha)\left(\frac{P}{W}\right)^\alpha$$

CHAPTER V

RELATIONS APPLIED TO A SIMPLIFIED MODEL

Control and Stability of a Four Wheeled

Vehicle in a Flat Turn

Introduction

The directional stability and control of a four wheeled vehicle operating on soft soils is studied by means of a simplified theoretical analysis which takes into account the variation of the cornering performance of pneumatic tires.

The problem of directional stability and control in a flat turn is formulated with steady-state dynamical equations of motion having two degree freedom, namely, vehicle yaw and vehicle side slip. Rolling motions of the spring mass are included by being superimposed on the steady-state analysis in order to enable calculation of the change in vertical loading on the tires resulting from vehicle roll.

Equations of Motion

The following assumptions were made: a) parallel tracks for both wheels; b) side force resulting from wheel camber insignificant; c) no lateral tire deformation; d) the steering wheel is held fixed at a particular setting, and the steering linkage is rigid. Vehicle roll was not included as a motion coordinate, but weight transfer resulting from

the roll about the longitudinal axis of a turning vehicle will be discussed in the next section.

Let (x,y) be a set of Cartesian axes whose origin in fixed at the vehicle's center of gravity (c.g.). The x-axis is along the longitudinal axis of the vehicle with a positive sense toward forward motion. The y-axis runs laterally from the vehicle c.g. with a positive direction toward the center of the radius of curvature along which the vehicle travels. The positive sense of the axes along with symbols of pertinent variables are shown in Figure 5.1.

The steady state response of the vehicle is the final condition of motion of the vehicle which occurs at some finite time after the start of maneuver. Here it is supposed that a specific steer angle δ is applied to the steered wheels and held. For this assessment it is sufficient to assume that the angle γ between the constantly applied drawbar pull Z and the direction of the longitudinal axis of the vehicle is constant.

Suppose that the c.g. of the vehicle is moving with a constant forward speed V as shown in Figure 5.1. If the side slip angle of the vehicle is β, with positive convention as shown in Figure 5.1, then for small values of β the component of velocity along the x-axis is $V \cdot \cos \beta$ or approximately V; in the y-axis direction, the side slip velocity is $V \cdot \sin \beta$ or approximately $V \cdot \beta$.

The equilibrium of moments in terms of the moving (x,y) axes read:

$$I \dot{\psi} = S_{11} (a \cdot \cos \delta + c \cdot \sin \delta) + S_{12} (a \cdot \cos \delta - d \cdot \sin \delta) - b (S_{21} + S_{22})$$

$$\pm T_{11} (c \cdot \cos \delta - a \cdot \sin \delta) \overline{+} T_{12} (d \cdot \cos \delta + a \cdot \sin \delta) + d \, T_{22} - c \, T_{21}$$

$$- Z_y \, \ell_b \tag{5.1}$$

With the instantaneous yawing velocity notated as ψ and positive
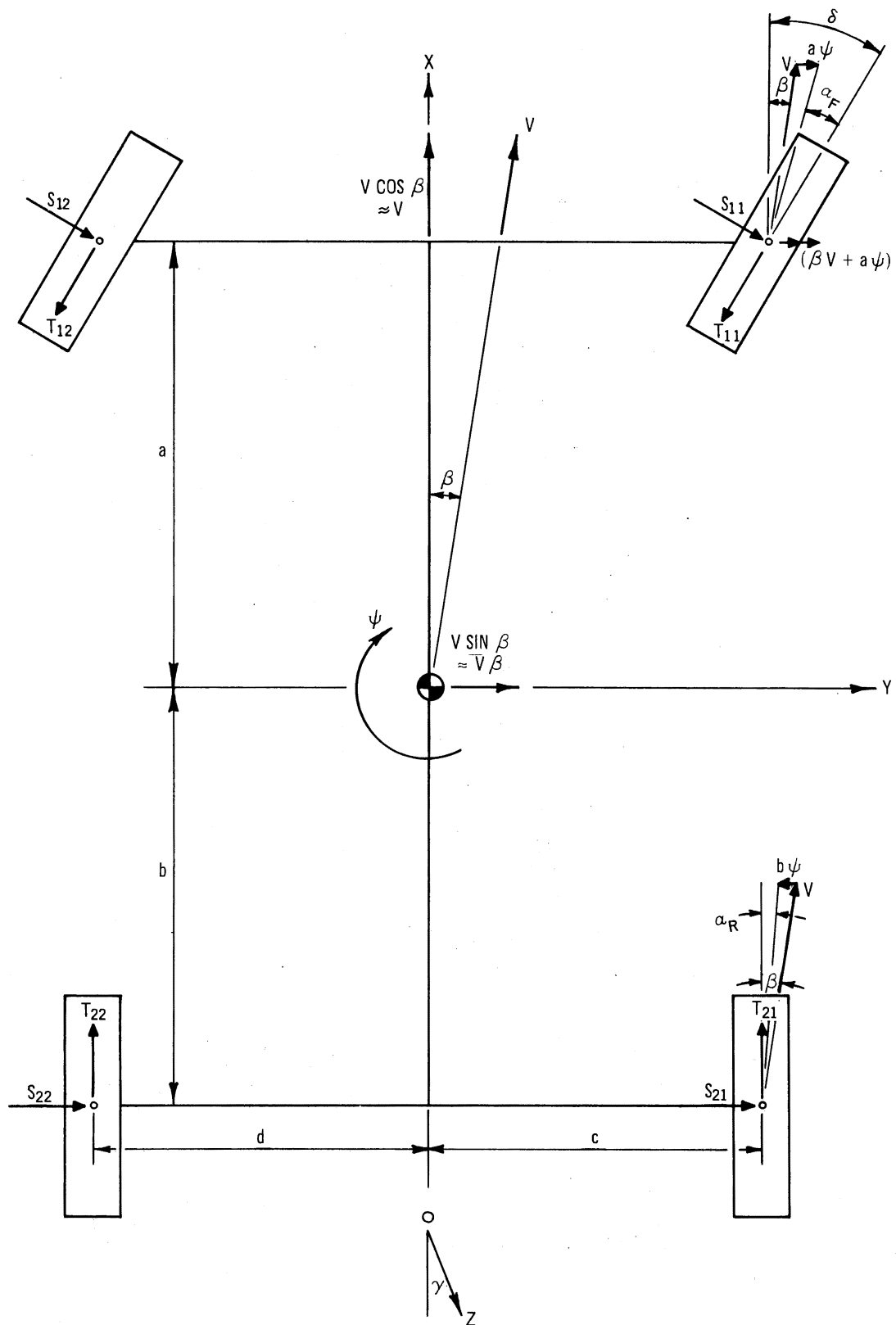
Figure 5.1. Equilibrium of Forces on a Vehicle Describing a Circular Curve with Illustration of the Side Slip Angle.

as shown in Figure 5.1. For realistic maneuvering of vehicles in off-road terrains steering angle δ is sufficiently small that $\cos \delta \approx 1$ and $\sin \delta \approx \delta$. Equation 5.1 is then rewritten

$$I \, \dot{\psi} = S_{11} \, (a + c\delta) + S_{12} \, (a - d\delta) - b \, (S_{21} + S_{22})$$

$$\pm T_{11} \, (c - a\delta) \mp T_{12} \, (d + a\delta) \, Z_y + dT_{22} - cT_{21} - Z_y \cdot \ell_b \quad (5.2)$$

The equilibrium of forces in the traverse (y axis) and longitudinal (x axis) directions with respect to the vehicle yield:

$$M \cdot V \, (\dot{\beta} + \psi) = S_{11} \, \cos \, \delta + S_{12} \cdot \cos \, \delta + S_{21} + S_{22}$$

$$\mp (T_{11} \cdot \sin \, \delta + T_{12} \cdot \sin \, \delta) + Z_y \quad (5.3)$$

$$M \cdot V \, (\dot{\beta} + \psi) = S_{11} + S_{12} + S_{21} + S_{22} \mp (T_{11} \cdot \delta + T_{11} \cdot \delta) + Z_y \quad (5.4)$$

and

$$T_{21} + T_{22} \mp (T_{11} \, \cos \, \delta + T_{12} \, \cos \, \delta) - Z_x = 0 \quad (5.5)$$

$$T_{21} + T_{22} \mp (T_{11} + T_{12}) - Z_x = 0$$

Also note from Figure 5.1 that

$$Z_x = Z \, \cos \, \gamma \quad (5.6)$$

and

$$Z_y = Z \, \sin \, \gamma \quad (5.7)$$

Those terms with double signs the upper sign signifies a negative driving force (rear wheel drive) at the front wheels and the lower sign for a positive driving force (four wheel drive).

In a steady-state turn the yawing and side slip accelerations become zero and the yawing velocity is the rate of turning or

$$\dot{\beta} = 0$$

$$\dot{\psi} = 0$$

$$\psi = \frac{V \cos \beta}{R} \approx \frac{V}{R}$$

for small values of β .

Effective Side Slip Angle

The forward velocity in the x-direction at the center of each wheel hub is equal to

$$V_{i1} = V \cos \beta - c\psi$$
$$V_{i2} = V \cos \beta - d\psi$$

$$(5.8)$$

Recalling the assumption that β is small and $V \cos \beta \approx V$. Also for steady state analysis $V = R\psi$ where R is the radius of curvature and $R \gg c$ or d . Compared to V , $c \cdot \psi$ or $d \cdot \psi$ are small and neglected. On this basis, the forward velocity in the x direction at each wheel is simply V to a sufficiently close approximation.

The lateral or side slip velocity of the right side tires are schematically represented in Figure 5.1, and equal to $\beta V + a\psi$ for the steered tires and $\beta V - b\psi$ for the rear tires. These velocity vectors form an angle with the longitudinal axis of the front and rear wheels $\beta + \frac{a\psi}{V}$ and $\beta - \frac{b\psi}{V}$, respectively.

The positive sense for the steer angle δ is shown in Figure 5.1 and from inspection the angle between the steered wheel hub and the direction of travel, designated as the effective side slip angle α_F , is

$$\alpha_F = \delta - \beta - \frac{a\psi}{V} \qquad (5.9)$$

The side forces given in the equations of motion (5.2 and 5.4) have their lines of action normal to the wheel hub; however the magnitude of these forces depend primarily upon the angle formed by the side slip velocity vector and the plane of the wheel hub. Similarly the effective side slip angle for the rear wheels can be similarly shown to be

$$\alpha_R = \frac{b\psi}{V} - \beta \qquad (5.10)$$

Vertical Wheel Loading

To maintain the vehicle in an ideal, steady-state, flat turn, the spring mass must roll toward the outside of the curve by a certain amount and a subsequent weight transfer will occur.

To compute the roll angle ε for a four wheel vehicle describing a circular curve let the spring mass be connected to wheels with springs having elastic constants of k_F and k_R corresponding to front and rear springs respectively.

Figure 5.2a shows the representative forces and sign convention of a four wheeled vehicle undergoing a steady-state turn of radius R at a constant velocity V . Figure 5.2b is a dynamical equivalent representation of the vehicle with the roll angle having been developed and the wheels and suspension replaced with idealized springs.

Summary moment about the e.g., about which roll will occur and referring to Figure 5.2b for definition of terms:

$$\sum M_o = I\ddot{\varepsilon} = 0 \text{ for steady state conditions}$$

$$c \cdot \Delta_1 (k_F + k_R) + d \Delta_2 (k_F + k_R) = h \cdot \frac{mv^2}{R} \qquad (5.11)$$
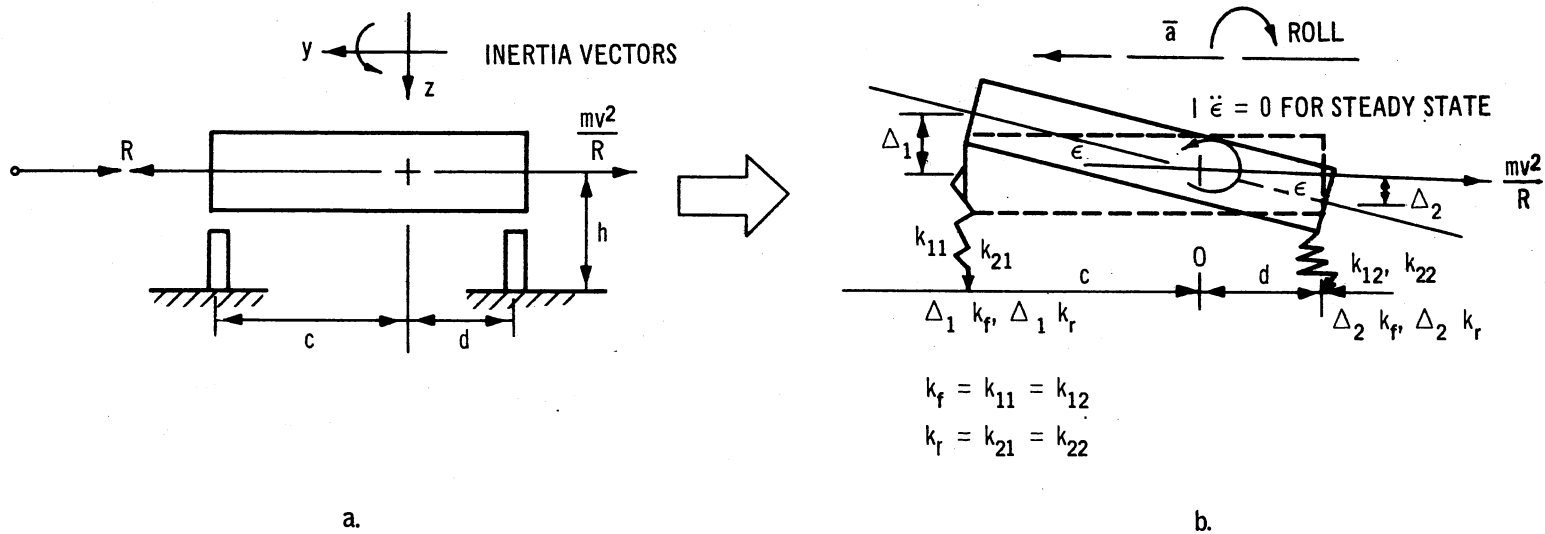
Figure 5.2. Roll Angle of a Vehicle in a Steady-State Turn.

where h is the vertical distance of the vehicle c.g. above the ground. Note that roll angle ε is equal approximately (again using small angle descriptions)

$$\varepsilon \approx \frac{\Delta_1}{c} \approx \frac{\Delta_2}{d} \qquad (5.12)$$

or

$$\Delta_1 = c\varepsilon \qquad (5.13)$$

$$\Delta_2 = d\varepsilon \qquad (5.14)$$

Substituting equation 5.13 and 5.14 into equation 5.11 yields

$$\varepsilon = \frac{W}{(k_F + k_R)} \quad \frac{h}{c^2 + d^2} \quad \frac{v^2}{gR} \qquad (5.15)$$

Returning to Figure 5.1 the vertical weight acting through the c.g. is

$$W_{cg} = W_{11} + W_{12} + W_{21} + W_{22} \qquad (5.16)$$

The static weight of each wheel is proportional to the location from the c.g.

$$W_{11} = \frac{d}{c} W_{12} \quad \text{(a)} \qquad W_{12} = \frac{b}{a} W_{22} \quad \text{(c)}$$

$$\qquad\qquad\qquad\qquad\qquad\qquad\qquad\qquad (5.17)$$

$$W_{21} = \frac{d}{c} W_{22} \quad \text{(b)} \qquad W_{22} = \frac{a}{b} W_{11} \quad \text{(d)}$$

Repeated substitution of equation 5.17 into equation 5.16 yields the static weight at each wheel

$$W_{11} = \frac{bd}{(a + b)(c + d)} \, W_{cg} \qquad \text{(a)}$$

$$\qquad\qquad\qquad\qquad\qquad\qquad\qquad (5.18)$$

$$W_{12} = \frac{bd}{(a + b)(c + d)} \, W_{cg} \qquad \text{(b)}$$

$$W_{21} = \frac{bd}{(a + b)(c + d)} \ W_{cg} \qquad \text{(c)}$$

$$W_{22} = \frac{bd}{(a + b)(c + d)} \ W_{cg} \qquad \text{(d)}$$

Next the vertical force at each wheel during steady-state turning of the vehicle is computed by assuming the forces to be composed of the static component weight acting when the vehicle is at rest on a level horizontal plane plus the component arising as a result of dynamic body roll. The weight at each wheel will then be

$$W_{ij} = W_{ij} \pm k_j \ \varepsilon x \qquad (5.19)$$

where x is the left or right vehicle dimension. The upper sign designates the outside wheels and the lower sign for the inside wheels. As previously subscript i refers to front (i = 1) and rear (i = 2) axle and j designates whether the wheel is nearest the inside of curvature (j = 1).

$$W_{11} = \frac{bd}{(a + b)(c + d)} \ W - k_F \ c\varepsilon \qquad (5.19a)$$

$$W_{12} = \frac{bc}{(a + b)(c + d)} \ W + k_F \ d\varepsilon \qquad (5.19b)$$

$$W_{21} = \frac{ad}{(a + b)(c + d)} \ W - k_R \ c\varepsilon \qquad (5.19c)$$

$$W_{22} = \frac{ac}{(a + b)(c + d)} \ W + k_R \ d\varepsilon \qquad (5.19d)$$

Tire Deflection Dependency Upon
Wheel Load and Tire Inflation Pressure

For a four wheel vehicle undergoing a steady-state turn the load for each wheel and the corresponding tire deflection probably differs. The clay and sand numerics introduced and discussed in Chapter II and

utilized in Chapter IV vary inversely with changes in load W , and either directly or proportionately as the deflection ratio δ/h fluctuates. If a change in these variables occur a procedure is required to ensure that the numeric property reflect existing parameters. Numerous tires have undergone static dynometer testing at the Mobility Testing Facility at the WES in establishing interrelated data on wheel load, tire deflection, and inflation pressure. Figures 5.3 and 5.4 illustrate the seemingly linear dependency of the ratio of wheel load W to tire deflection ratio δ/h on inflation pressure IP . Figure 5.3 contains W/(δ/h) versus IP data for the 6.00-9, 4-PR tire used in the test program and discussed in Chapter IV. Figure 5.4 illustrates W/(δ/h) versus IP data for four times common to U. S. Army tactical wheeled vehicles.

A linear equation based on least-squares-fit has been developed for each set of W/(δ/h) versus IP data. Having tire deflection expressed as equations continuous across possible range of tire inflation pressures is important because as roll and subsequent weight transfer occur a change of the tire deflection results. Hence if inflation pressure is considered constant[1] and the load per wheel is computed from the roll equation of the last section then the resulting deflection can be computed from the corresponding equation provided on Figures 5.3 and 5.4.

---

[1]Constant inflation pressure of military tires is a meaningful assumption since the pressures for either on-road or off-road operations is generally designated on the vehicle and strictly enforced.
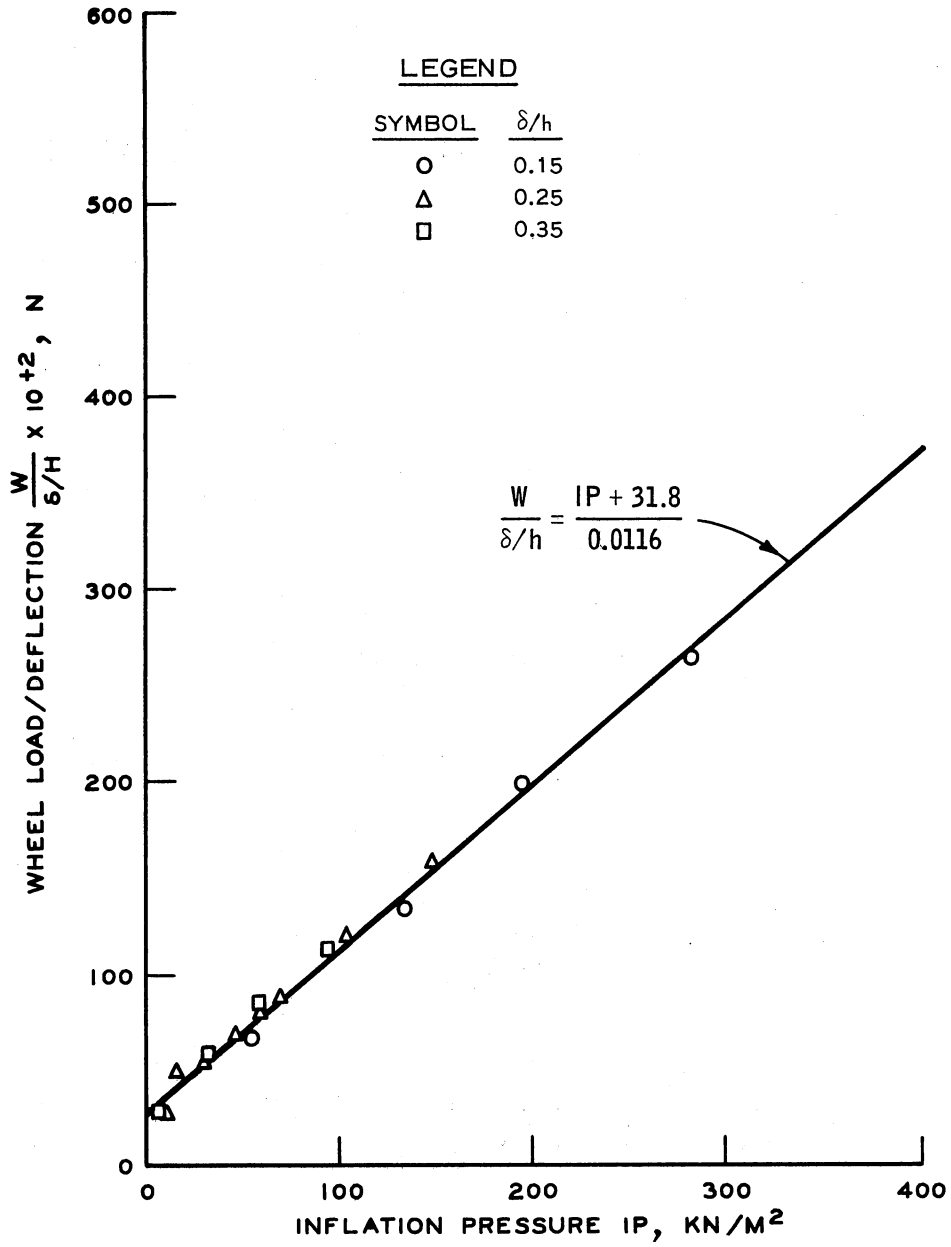
Figure 5.3. Dependency of Load/Deflection Ratio on Tire
Pressure.
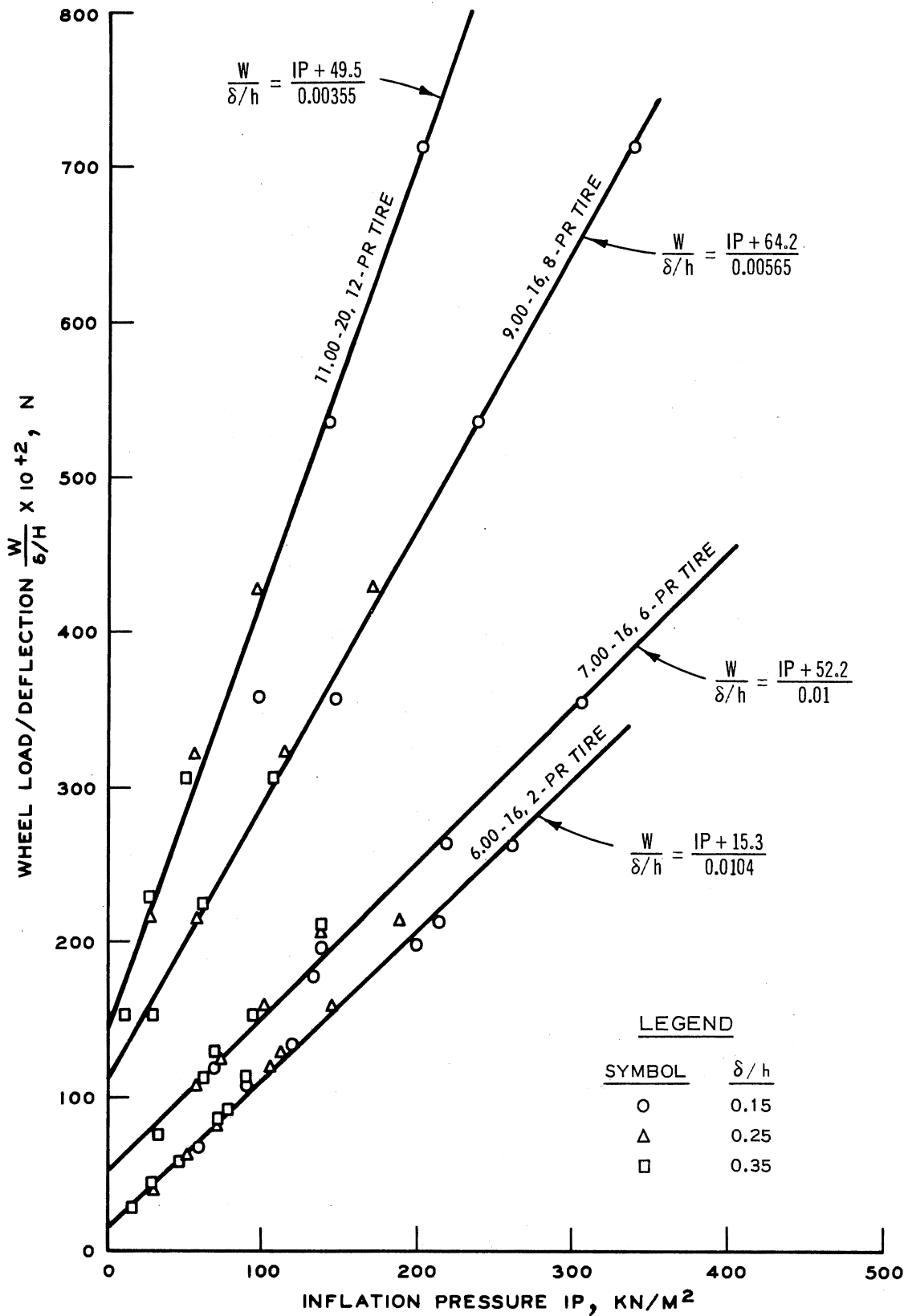
Figure 5.4. Dependency of Load/Deflection Ratio on Tire Pressure and Size.

Turned Tire/Soil Interaction Application

Digital Model

The dynamical degrees of freedom chosen for analysis consist of
vehicle yaw and vehicle side slip. Vehicle roll is not considered as a
dynamical coordinate but as a quasi-static factor dependent upon the
yaw velocity. With the axes fixed in the body of the vehicle the two
degree of freedom model may be expressed by

$$MV \, (\dot{\beta} + \psi) = F_y$$

and

$$I\dot{\psi} = M_z$$

which are notational forms of Equations 5.5 and 5.2, respectively.
Solving the above set of equations require that tractive and side
forces be determined, which, in turn, are dependent upon vehicle para-
meters and soil conditions in addition to nonlinear functions of wheel
side slip. A alogrithm developed by Brown (1967) was adopted to solve
the two simultaneous nonlinear equations having unknowns of vehicle
yaw ψ and vehicle slip β .

Brown's alogrithm is a modification of Newton's method for solving
simultaneous nonlinear equations, requiring no derivative evaluations.
As with most iterative numerical techniques, the closer the initial
guess is to the true solution the fewer iterations that will be neces-
sary for a closed solution; also the accuracy or even the ability of
the alogrithm to converg toward the solution often depends upon the
initial guess of the variables. To aid in selecting a close approxima-
tion of ψ and β for initial input values to the Brown's alogrithm, a

method was adopted that is used for finding complex zeros of functions (Hamming, 1973).

The previous equations can be rewritten as

$$MV \dot{\beta} = F_y - MV\psi$$

and

$$I\dot{\psi} = M_z$$

In a steady state turn the yawing and side slip accelerations, $\dot{\psi}$ and $\dot{\beta}$, respectively, are zero making the right side of the above equations equal zero when compatible values of β and ψ are known. Finding real zeros of the above equations can be very easy and yet very robust. The approach is to assume a set of values for β and ψ and solve Equations 5.2 and 5.5 arranged to the above form. Yaw velocity and vehicle side slip values are varied about a m × n matrix in which m represent the number of ψ values under consideration and n represents the number of β values. Generally ψ is varied from 0 to 0.6 radians per second and β is varied from minus to plus 1.5 times the wheel steer angle δ at each location of the matrix, values of β and δ are used in Equations 5.2 and 5.5 and a value of 1, 2, 3, or 4 is recorded at each point in the matrix depending upon the sign convention of $I\dot{\psi}$ and MV $\dot{\beta}$ as illustrated in Figure 5.5. Obviously when the values are printed for the m × n matrix, where the four quadrants meet at a point is the general region of zero. The solution could be made more refined by enlarging the zero region with a finer and finer grid spacing. However, the system requires too much interaction with the operator and after an approximate determination of ψ and β are known then the Brown's alogrithm can be effectively used to refine the

solution. Generally a matrix size of 60 × 60 is used since this size
is readily adaptable to a computer time sharing teletype terminal.
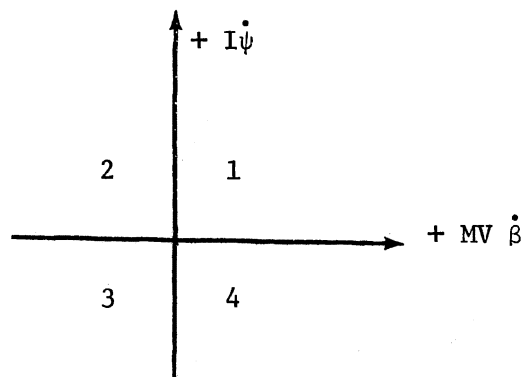
Figure 5.5. Scheme for Finding Real Zeros.

The flow diagram for determining approximate values of ψ and β
is shown in Figure 5.6. The input data are read in by data statements.
Required input data, designation of variable names, and engineering
units are listed in Table V.

TABLE V

LISTING OF INPUT DATA FOR COMPUTER MODEL

Name	Description	Dimension
	Vehicle	
WIG	Gross vehicle weight	Newtons
ADMIN	Distance between front axial and vehicle CG	Metre
BDIM	Distance between rear axial and vehicle CG	Metre
CDIM	Horizontal distance between inside wheels and vehicle CG	Metre
DDIM	Horizontal distance between outside wheels and vehicle CG	Metre
HDIM	Vertical distance from ground surface to vehicle CG	Metre

TABLE V (Continued)

Name	Description	Dimension
Vehicle		
LDIM	Distance point of application of drawbar pull to CG	Metre
GAMMA	Angle between drawbar pull and longitudinal axis of vehicle	Degrees
CTR	Ratio of centrifugal acceleration (V^2/R) to gravity acceleration (G)	--
SPKE	Spring constant for front axle	Newtons/Metre
SPKR	Spring constant for rear axle	Newtons/Metre
Tire		
SLIP	Powered wheel slip	--
TIRED	Cross section width of unloaded-inflated tire	Metre
TIRED	Diameter of unloaded-inflated tire	Metre
DEFI	Tire deflection	--
ITIR	Tire code - from MSD tire book	--
TRIP	Tire inflation pressure	kPa
Soil		
KSOIL	0 = clay; 1 = sand	--
CPR	Cone penetration resistance, clay	kPa
CPR	Cone penetration resistance, sand	MPa/m
Parametric Variation for Specific Vehicle		
KDRIVE	+1 = rear wheel drive; -1 = four wheel drive	--
VEL	Vehicle speed	Metre/Second
DELTA	Steering angle of steered wheels	Degrees
IEND	0 = more data; 1 = last data	--

Approximate values of ψ and β are then placed as input to a driver computer program which has a subroutine utilizing Brown's alogrithm and another subroutine to solve Equations 5.2 and 5.5. The
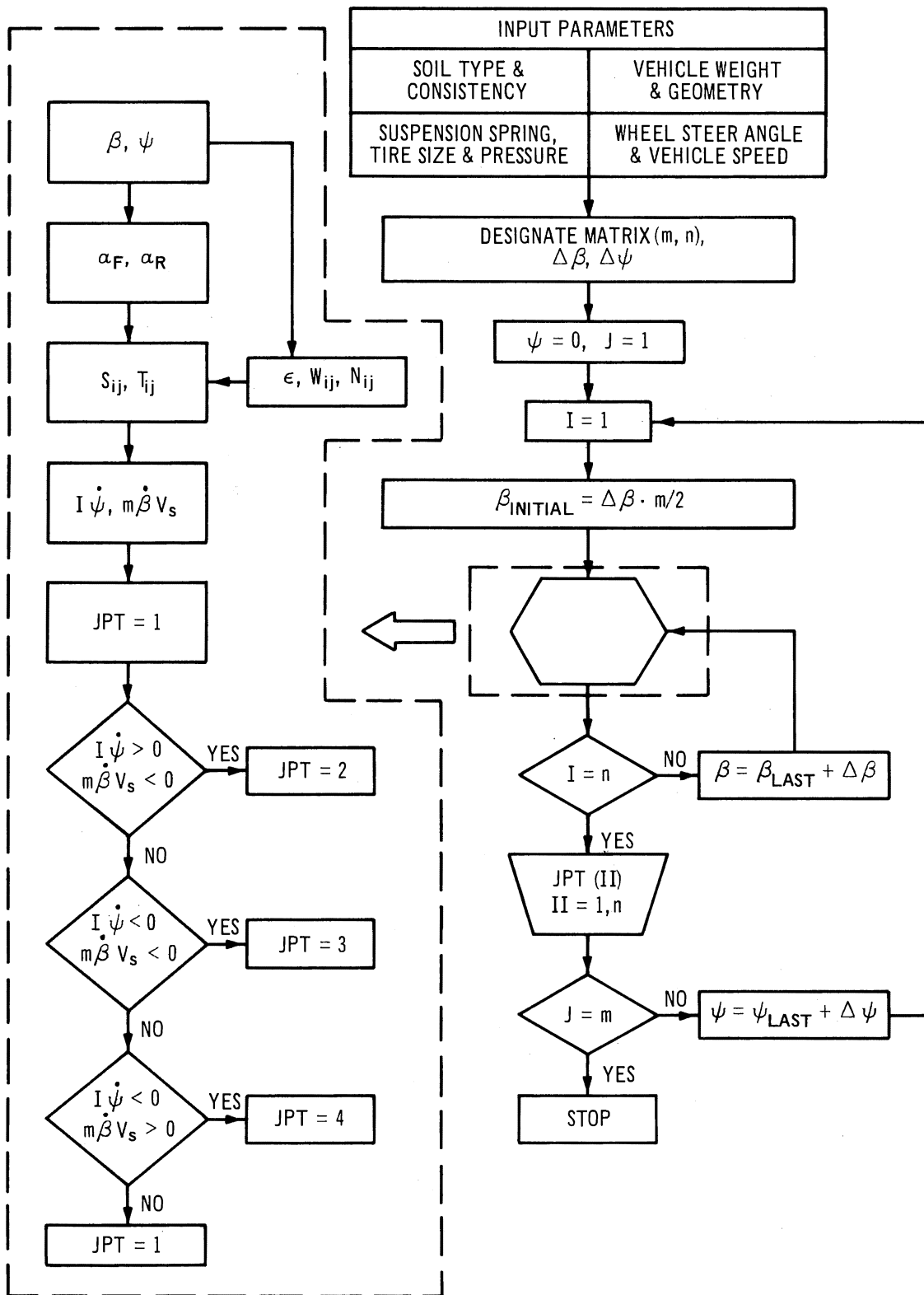
Figure 5.6. Flow Diagram for Finding Real Zeros.

flow diagram is illustrated in Figure 5.7 and the complete computer

program listed in Appendix C.

The computation of thrust and side forces is the same irrespective of whether the program for finding real zeros[2] or the general turning program utilizing the Brown's alogrithm is used. Significant computations begin by determining front and rear wheel slip angles from Equations 5.9 and 5.10, respectively, from input values of forward velocity, fore and aft displacement of the axles from the vehicles center of gravity, and assumed values of vehicle yaw and side slip angle. Next the program computes the vehicle roll about the x-axis and respective wheel loads per Equations 5.19a through 5.19d. A mobility number is computed for each wheel using Equation 2.2 if the surface soil is sand and Equation 2.3 for a soft clay medium. If either of the clay mobility numbers is less than 7 or else either of the sand mobility numbers is less than 2; then immobility of the vehicle is said to exist. Examination of dependent performance parameters illustrated in Figure 2.4 for clay and Figure 2.5 for sand indicates that for $N_c = 2.5$ (approximately equivalent to $N_c' = 7$) and $N_s = 2$ that sinkage and resistance to pull and tow become excessive whereas forward movement would cease. The program branches depending upon whether the soil is sand or clay and upon whether rear drive or four wheel drive is employed for computing tractive and side forces acting at each wheel. Finally

---

[2]A listing of the computer program for finding real zeros is not given since, except for the DO loops used to step through the $m \times n$ matrix and output print statements signifying the sign of $I\dot\psi$ and $MV_s \dot\beta$ both amply illustrated in Figure 5.6, it is identical to the subroutine TURN used in the computer program listing in Appendix C.
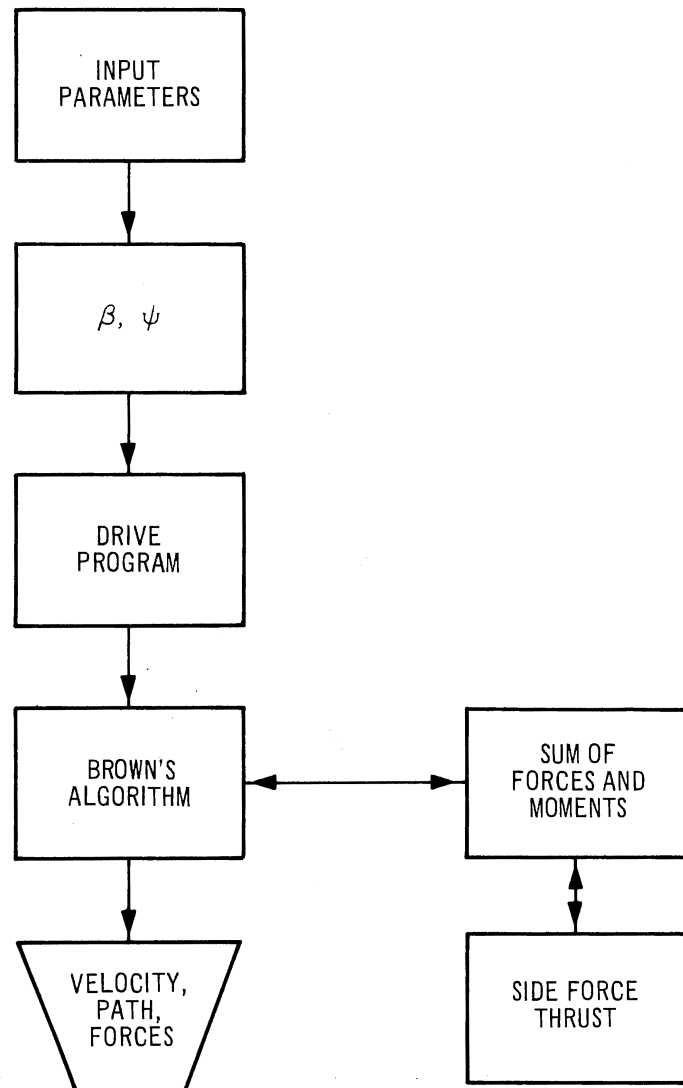
Figure 5.7. Turning Program Block Diagram

these forces and their respective moments are summed according to
Equations 5.2 and 5.5, and if the solution of the system has sufficient-
ly converged, output of pertinent forces, velocities, and turning
configuration are displayed to the user.

All of the horizontal components of force acting on a powered
wheel and in the direction of travel can be summed, and their sum de-
fined as thrust T . The sum of the horizontal forces acting parallel
with the wheel hub and opposite to the direction of travel can be
defined as rolling resistance. From equilibrium conditions, thrust is
equal to rolling resistance plus pull. Because both thrust and rolling
resistance occur in the same physical area, they are difficult to
separate; however their difference, pull, can be measured. The input
torque M to the powered wheel can also be measured and it represents
the thrust times the lever arm (the distance below the axle where the
horizontal thrust acts). Also the difference between the torque and pull
coefficient at any positive slip (see Figure 2.2) represents resistance
losses. Besides rolling resistance there are also mechanical (mainly
frictional) losses of the wheel and forces expended in deforming the
pneumatic tire. However, the tires used to develop all relations pre-
sented thus far have side walls which flex rather easily; hence that
force required for deforming the pneumatic tire is small for relations
developed herein. Also the laboratory wheel bearing has been well
designed and maintained to reduce friction to a minimum. Therefore for
purposes of this study the torque coefficient was taken as the thrust
coefficient.

Sample Calculations

To illustrate the nature of the results which follow from the analysis, numerical calculations have been carried out and the changes of predicted forces and yawing vehicles described when steady-state flat turns are traversed over a sand of uniform consistency at various speeds and curvatures. In the following numerical example the steady-state condition for a rear-wheel-drive and a four-wheel-drive vehicle was calculated corresponding to the previously derived expressions and limiting assumptions. The vehicle data presented in Table VI corresponds closely to a M-151, 1/4-ton capacity military jeep.

TABLE VI

VEHICLE DATA USED IN NUMERICAL EXAMPLE

Item	Symbol	Units
Gross vehicle weight	W	14,240 N
Drawbar pull	Z	0 N
Tire size	--	7.00-16, 6 PR
Tire pressure	IP	103.5 kN/M^2
Wheel slip	S	20%
Front axle spring constant	k_F	25,228 N/M
Rear axle spring constant	k_R	25,228 N/M
Vehicle dimensions (see Figure 5.1)		
a	--	1.143 M
b	--	1.016 M
c	--	0.890 M
d	--	0.890 M
h	--	0.629 M
ℓ	--	1.758 M
γ	--	0°
Steer angle	δ	7°
Sand penetration resistance	G	2.5 MPa/m

The steer angle was kept constant and the forward speed of the vehicle was the variable parameter. Figure 5.8 provides a comparison of path curvature $1/R = \dot{\psi}/V$, yaw velocity $\dot{\psi}$, vehicle side slip angle β, and vehicle body roll ε versus speed. The advantage of four-wheel-drive over rear-wheel drive when pulling on a curve is seen to become more apparent with increases of forward velocity from the $1/R$ versus V plot of Figure 5.8. As V approaches zero R approaches Ackermann neutral steer which can be closely approximated by

$$R_{neutral} = \frac{a + b}{\delta} = 17.7 \text{ m}$$

or for path curvature, $1/R = 0.057 \text{ m}^{-1}$. The smaller turning radius at equal speeds exhibited by the example vehicle in the four-wheel drive mode is also reflected in higher yaw velocity and greater vehicle body roll as compared to the rear-wheel-drive configuration. The vehicle side slip angle begins at an angle equal to the steer angle as the velocity approaches zero and has a positive sense the same as that of the steered front wheels. As speed increases β reduces such that the velocity vector approaches the longitudinal axis of the vehicle and with further increases in forward speed β again increases in magnitude but in the opposite angular direction from that of the steered wheels. Over the range of speeds investigated, the vehicle side slip angle changes considerably faster for the four-wheel-drive vehicle.

A pictoral comparison is presented in Figure 5.9 of the equilibrium configuration that are established in a right turn for the rear-driven and all-wheel-drive at 4-m/sec and steer angle of 7 degrees. Included on each diagram are the three components of force on each tire,
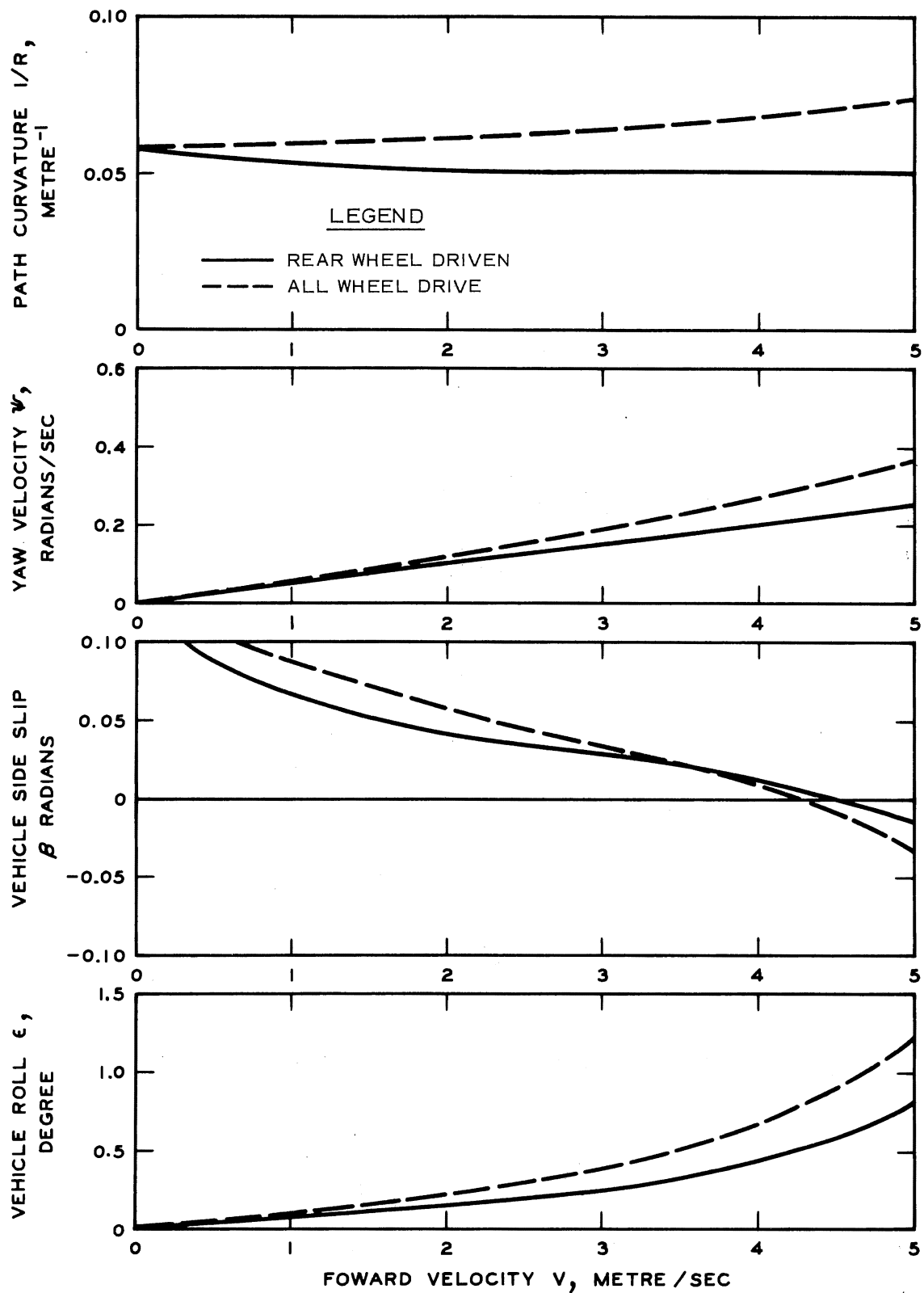
Figure 5.8. Comparison of Motion Inducted Parameters Versus Velocity
for Rear Wheel and Four Wheel Driven Vehicle. Steer
Angle δ = 7 Degrees .
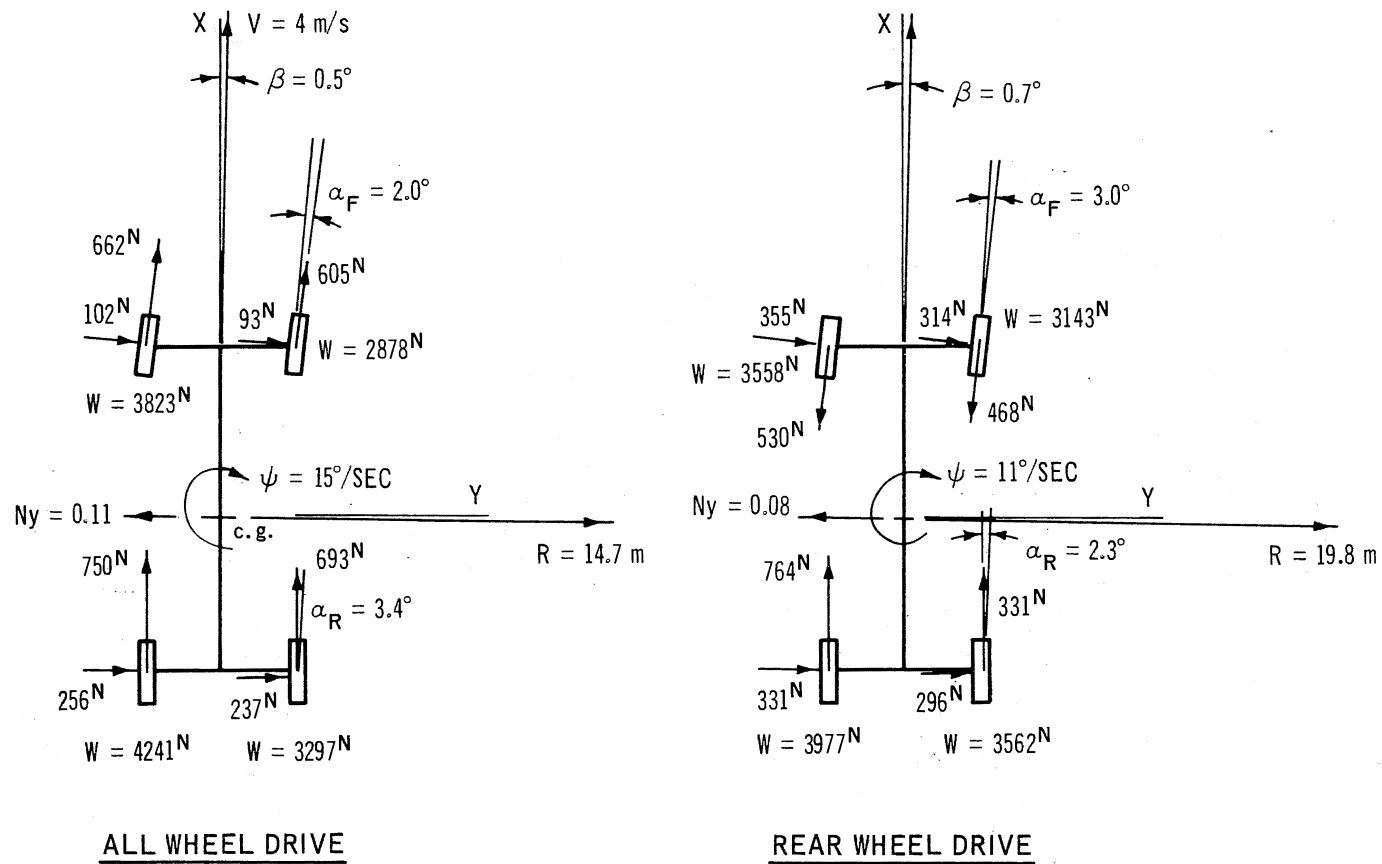
Figure 5.9. Plan View of Vehicle Showing Responses and Tire Forces (δ = 7 Degrees).

and the vehicle responses V , ψ , β , N_y (centrifugal acceleration force), and R . The proper angular orientation and magnitudes of the horizontal forces and velocity vectors are shown. Note that for the rear-drive vehicle $\alpha_F > \alpha_R$ and $R > R_{neutral}$, whereas for the all-wheel driven $\alpha_F < \alpha_R$ and $R < R_{neutral}$. This would indicate by definition that at $V = 4$ m/s and $\delta = 7$ degrees the vehicle is in an oversteer condition when all-wheel-drive is utilized and in an understeer condition when only rear-drive pervails. These conditions of oversteer and understeer over the full velocity range considered are evident from the $1/R$ versus V relation of Figure 5.8 in that $1/R$ increases with increases of V for the rear driven version.

CHAPTER VI

CONCLUSIONS AND RECOMMENDATIONS

Conclusions

Based on the analysis of the data obtained during this research the following conclusions can be drawn with regard to the performance of single powered wheels equipped with pneumatic tires and operating in the turn mode on soft yielding soils.

1) For the test variables considered in this study, the WES systems for predicting the performance of powered wheels operating at zero turn angle on saturated clay and air-dried sand can be extended and modified to treat turn angles larger than zero and wheel slips other than 20 percent such that the principal performance parameters of pull and torque can be effectively predicted.

2) Performance expressed in terms of pull coefficient, side force coefficient, input torque coefficient, and sinkage coefficient was found to be influenced by the same independent variables identified in previous studies plus that of wheel turn angle. From the test results the following generalities can be made concerning the individual relations of the performance parameters:

a) At specific values of wheel slip and mobility number, increasing the wheel turn angle reduces the pull coefficient. For a given clay mobility number, the reduction in pull

coefficient from that associated with a zero turn angle
for the powered turned wheel operating with a constant
turn angle is nearly constant over the wheel slip range
tested; however, for tests performed on sand the amount of
decrease of the pull coefficient lessens with increases in
wheel slip.

b) It was shown that by increasing the driving force at con-
stant wheel turn angle and mobility number the side force
was considerably reduced. For a specified wheel turn angle
and mobility number the relation between side force coef-
ficient and pull coefficient can be approximated with a
straight line over the wheel slip range tested. This
observation was found to be true for both clay and sand
tests.

c) If the independent variables expressed in terms of mobil-
ity number and the wheel slip is kept constant, the side
force coefficient increases as the wheel turn angle becomes
greater. Further, if the wheel turn angle and slip is held
constant, the side force coefficient increases with in-
creases in the mobility number. Finally, if the wheel turn
angle and mobility number has specific values, the side
force coefficient decreases with increases of wheel slip.

d) Sinkage coefficients for clay and sand decreases at a power
decay rate as the mobility number increases for a given
wheel turn angle. For a given sand mobility number, the
sinkage coefficient increases with increasing wheel turn

angle. Over the range tested, wheel slip does not

appreciably effect sinkage in either clay or sand.

Experimental results on single tires running at various turn

angles were applied via equations of motion to the analysis of four-

wheel vehicles executing a turn on flat, level, soft soil. The steady-

state turning behavior of four-wheeled vehicles at different values

of steer angle and speed was studied to illustrate how the interaction

of the side force and the driving force affects the motion of the

vehicle.

Recommendations

In order to develop a better understanding of wheeled vehicle

agility in off-road operations, the following recommendations for fur-

ther research may prove useful:

1) Research reported in this thesis is limited to application

of wheeled vehicles in soft soil. A study would be beneficial that

investigated the turned tire-soil interaction when operating in soils

of medium to stiff consistency. These results could be combined with

the results reported herein concerned with soft soil and from the

numerous published results of turned tires operating on rigid or flexi-

ble pavements toward developing generalized relations for tire-surface

interaction.

2) The example used in Chapter V to illustrate steady state

turning behavior indicates that effective side slip at the wheels are

small in magnitude. Hence, laboratory tests should be extended to

examine the side forces developed with wheel turn angles of less than

5 degrees.

3) Formulate rationals for bridging steered tire-soil inter-action relations developed from laboratory experiments using cohesion-less sands and a saturated cohesive clay to wheeled-vehicles operating in intermediate soils having both cohesive and frictional properties.

4) Determine the influence of a thin, slippery surface layer of soil on the performance of off-road wheeled vehicles while turning.

5) Conduct laboratory testing program to determine the influence that braking has on the development of side forces on a turned tire.

6) Incorporate the effects on vehicle performance produced by terrain side slope and braking into the computer model developed during this study for predicting the time history of a wheeled vehicle travers-ing a prescribed path. This path following model should be developed to exploit as much of the existing (straight line travel) AMC Mobility Model philosophy, modeling technique, and terrain representation as possible.

SELECTED REFERENCES

American Society of Testing and Materials. "Moisture-Density Relations of Soils Using 5.5-lb Rammer and 12-in. Drop." ASTM Test D 698-70, Part 19, ASTM 1975 Annual Standards, Philadelphia, Pa.

Bridgman, P. W. Dimensional Analysis. New Haven, Connecticut: Yale University Press, 1931.

Broulhiet, G. "The Suspension of the Automobile Steering Mechanism: Shimmy and Trump." Bull. Soc. Ing. Civ. Fr., Bulletin 78 (Jul 1925), pp. 540-554.

Brown, K. M. "Solutions of Simultaneous Non-Linear Equations." Communications of the ACM, Vol. 10, No. 11 (Nov 1967), p. 728.

Duncan, W. J. Physical Similarity and Dimensional Analysis. London: Edward Arnold and Co., 1953.

Ellis, J. R. Vehicle Dynamics, London: Business Books Limited, 1969.

Fiala, E. "Lateral Forces on Rolling Pneumatic Tires." Zeitschvift V. D. I, Vol. 96, No. 29 (11th Oct 1954), pp. 973-979.

Freitag, D. R. "A Dimensional Analysis of the Performance of Pneumatic Tires on Soft Soils." Technical Report No. 3-688, Aug 1965, U. S. Army Engineer Waterways Experiment Station, CE, Vicksburg, Miss.

Green, A. J., J. L. Smith, and N. R. Murphy. "Measuring Soil Properties in Vehicle Mobility Research; Strength-Density Relations of an Air-Dry Sand." Technical Report 3-652, Report No. 1, Aug 1964, U. S. Army Engineer Waterways Experiment Station, CE, Vicksburg, Miss.

Green, A. J. "Effect of Yaw Angle on Steering Forces for the Lunar Roving Vehicle Wheel." Technical Report M-71-7, Oct 1971, U. S. Army Engineer Waterways Experiment Station, CE, Vicksburg, Miss.

Hamming, R. W. Numerical Methods for Scientists and Engineers. New York: McGraw-Hill Co., 1973.

Honeywell Time-Sharing Applications Library Guide Volume I - Mathematics. Manual DA 44, Wellesley Hills, Mass., 1971.

Jurkat, M. P., C. J. Nuttall, Jr., and P. Haley. "AMC-74 Mobility Model." Technical Report No. 11921 (LL-149), May 1975, U. S. Army Tank-Automotive Command, Warren, Mich.

Kraft, D. C. and N. S. Phillips. "Turning Forces Developed by a Pneumatic Tire Operating in Soils, with Application to Vehicle Design Criteria." Proceedings, Fifth International Conference of the International Society for Terrain-Vehicle Systems, Vol. 2, Detroit, Mich. (1975), pp. 473-492.

Krick, G. "Behavior of Tyres Driven in Soft Ground with Side Slip." Journal of Terramechanics, Vol. 9, No. 4 (1973), pp. 9-30.

Langhaar, H. L. Dimensional Analysis and Theory of Models. New York, New York: John Wiley and Sons, Inc., 1951.

McRae, J. L., C. J. Powell, R. D. Wismer. "Performance of Soils Under Tire Loads; Test Facilities and Techniques." Technical Report No. 3-666, No. 1, Jan 1963, U. S. Army Engineer Waterways Experiment Station, CE, Vicksburg, Miss.

Melzer, J.-J. "Power Requirements for Wheels Operating in Sand." Proceedings of the International Conference on Prospectives of Agricultural Tractor Development, Vol. 1, Warsaw (Sep 1973), pp. 197-207.

Melzer, K.-J. "Performance of Towed Wheels Operating in Turned Mode on Soft Soil-A Pilot Study." (Unpublished Technical Report, U. S. Army Engineer Waterways Experiment Station, CE, Vicksburg, Miss. 1976).

Office of the Director of Defense Research and Engineering. "Part 1 - Land Mobility Technology Coordinating Proper." Washington, D. C.: Department of Defense, July 1974.

Rula, A. A. and C. J. Nuttall, Jr. "An Analysis of Ground Mobility Models (ANAMOB)." Technical Report M-71-4, Jul 1971, U. S. Army Engineer Waterways Experiment Station, CE, Vicksburg, Miss.

Schuring, D. "The Energy Loss of a Wheel." Proceedings of the Second International Conference of the International Society for Terrain-Vehicle Systems, Vol. 1, Quebec City, Quebec (1966), pp. 391-424.

Schwanghart, H. "Lateral Forces on Steered Tyres in Loose Soil." Journal of Terramechanics, Vol. 5, No. 1 (1968), pp. 9-29.

Segel, L. "Theoretical Prediction and Experimental Substantiation of the Response of the Automobile to Steering Control." Proceeding, The Institution of Mechanical Engineers, (Automobile Division), London (1956), pp. 26-46.

Segel, L. "A Review of the State of Knowledge of the Directional Behavior of Automotive Vehicles." Proceedings of the Second International Conference of the International Society for Terrain-Vehicle Systems, Vol. 1, Quebec City, Quebec (1966), pp. 172-179.

Smith, J. L. "Strength-Moisture-Density Relations of Fine-Grained Soils in Vehicle Mobility Research." Technical Report No. 3-639, Jan 1964, U. S. Army Engineer Waterways Experiment Station, CE, Vicksburg, Miss.

Smith, M. E. "Performance of Soils Under Tire Loads; An Extended System for Predicting Tire Performance in Fine-Grained Soils." Technical Report No. 3-666, Report 9 (to be published in 1976), U. S. Army Engineer Waterways Experiment Station, CE, Vicksburg, Miss.

Steeds, W. Mechanics of Road Vehicles. London: Iliffe and Sons, Ltd., 1960.

Taylor, P. A. and R. Birthwistle. "Experimental Studies of Force Systems on Steered Agricultural Tyres." Proceedings of the Institute of Mechanical Engineers, Vol. 181, Part 2A, London (1966).

Turnage, G. W. "Tire Selection and Performance Prediction for Off-Road Wheeled-Vehicle Operations." Fourth International Conference of the International Society for Terrain-Vehicle Systems, Vol. 1, Stockholm (Apr 1972), pp. 61-82.

Turnage, G. W. "Performance of Soils Under Tire Loads; Application of Test Results of Tire Selection for Off-Road Vehicles." Technical Report No. 3-666, Report 8, Sep 1972, U. S. Army Engineer Waterways Experiment Station, CE, Vicksburg, Miss.

U. S. Army Engineer Waterways Experiment Station and U. S. Army Tank-Automotive Command. "The AMC '71 Mobility Model." Technical Report No. 11789 (LL 143), Jul 1973, Warren, Mich.

APPENDIX A

TABULATION OF RESULTS FROM

SINGLE WHEEL TIRE TESTS

SIGN CONVENTION

PULL
$$P = P'\cos\alpha + S'\sin\alpha$$

SIDE FORCE
$$S = S'\cos\alpha - P'\sin\alpha$$
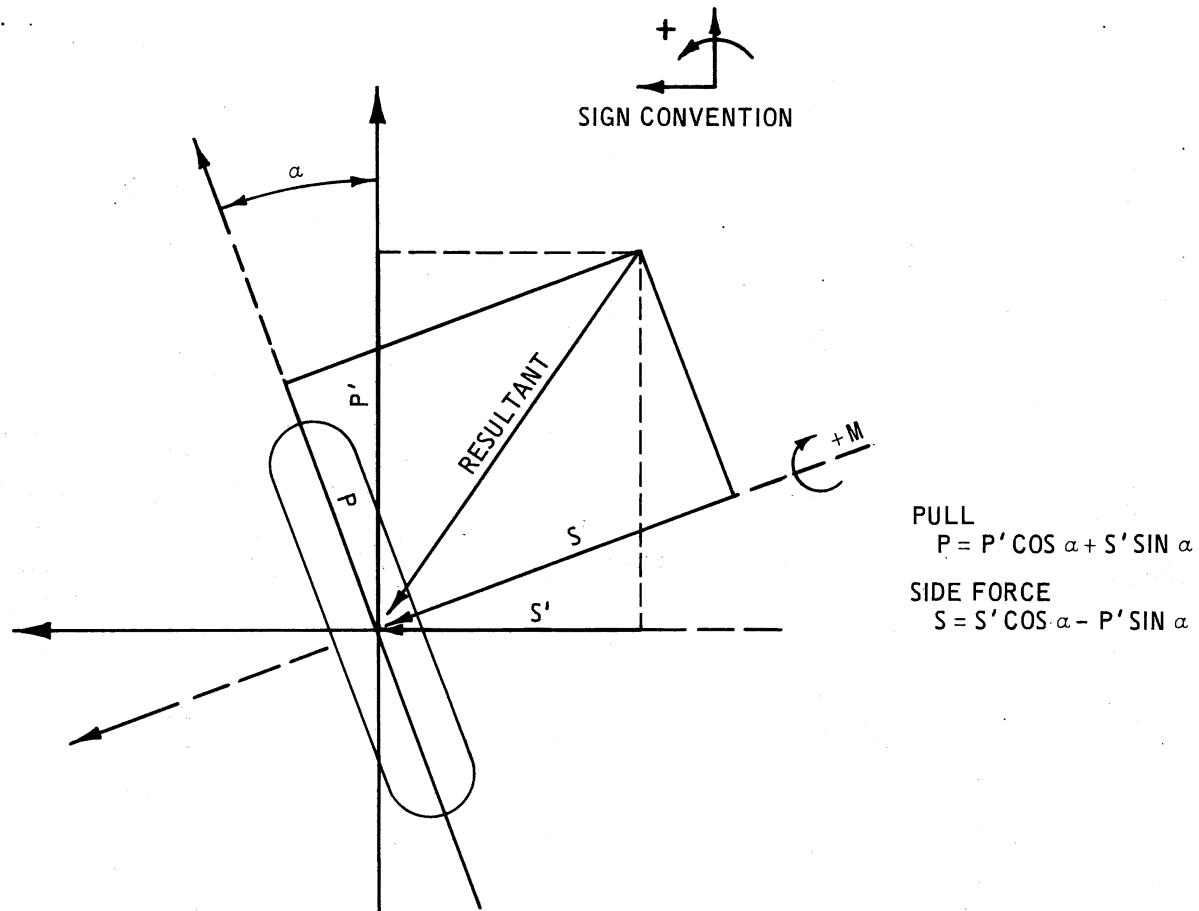
Figure A.1. Forces and moments acting on the powered turned tire (effect of trail moment neglected)

TABLE A.1

RESULTS OF POWERED TURNED TIRE TESTS ON VICKSBURG CLAY

| | Test Conditions | | | | | | | | Measured Test Values | | | | Forces Acting on Wheel | | Performance Coefficients | | |
| | | | | | | | | | Forces Acting on Carriage | | | Vertical | | | | | |
Test No.	Penetration Resistance C, Pr Pa	Wheel Speed V_W, m/sec	Carriage Speed V_a, m/sec	Turn Angle α, deg.	Deflection Coefficient δ/h	Wheel Load W, N	Wheel Slip s, %	Clay Mobility Number N'_c	Pull P', N	Lateral Force S', N	Torque M, M-N	Hub Movement z, cm	Pull P, N	Side Force S, N	Torque M/Wr_a	Pull P/W	Side Force S/W
A-73-0048-3	294	1.57	1.35	0	35	2002	14.3	18.8	671	0	199	0.43	671	0	0.42	0.34	0.00
A-73-0049-3	313	1.50	1.33	0	35	2007	10.9	20.0	760	0	223	0.30	760	0	0.47	0.38	0.00
A-73-0050-3	282	1.49	1.32	0	35	2024	11.4	17.9	817	0	232	0.67	817	0	0.49	0.40	0.00
A-73-0051-3	273	1.43	1.38	10	35	2019	5.0	17.3	199	892	132	0.77	351	844	0.28	0.17	0.42
A-73-0052-3	300	1.44	1.29	10	35	2028	11.4	19.0	411	834	183	0.84	549	750	0.38	0.27	0.37
A-73-0053-3	286	1.45	1.21	10	35	2028	17.8	18.1	716	832	252	0.40	850	695	0.53	0.42	0.34
A-73-0054-3	309	1.55	1.49	20	35	2006	9.4	19.8	-215	1152	58	0.32	191	1156	0.12	0.10	0.58
A-73-0055-3	305	1.53	1.30	20	35	2005	20.2	19.5	31	1136	144	0.43	418	1057	0.30	0.21	0.53
A-73-0056-3	300	1.53	1.42	20	35	2016	12.8	19.1	- 75	1200	97	0.42	339	1153	0.20	0.17	0.57
A-73-0057-3	293	1.45	1.11	5	35	2018	23.7	18.6	924	475	277	0.28	962	392	0.58	0.48	0.19
A-73-0058-3	290	1.48	1.35	5	15	1976	9.1	12.6	186	455	116	0.81	225	438	0.24	0.11	0.22
A-73-0059-3	293	1.53	1.35	5	15	1989	12.1	12.6	234	451	128	0.70	272	429	0.26	0.14	0.22
A-73-0060-3	296	1.46	1.14	5	15	1953	22.2	13.0	381	315	177	1.31	407	281	0.37	0.21	0.14
A-73-0061-3	275	1.49	1.49	15	15	1971	3.4	12.0	-358	829	13	1.35	-131	894	0.03	-.07	0.45
A-73-0062-3	282	1.48	1.20	15	15	2006	21.7	12.1	68	934	150	0.81	308	885	0.30	0.15	0.44
A-73-0063-3	301	1.48	1.32	15	15	1996	13.8	12.9	- 55	855	88	0.78	168	840	0.18	0.08	0.42
A-73-0064-3	297	1.49	1.42	10	25	1990	6.1	15.4	9	829	67	0.84	153	815	0.14	0.08	0.41
A-73-0065-3	284	1.47	1.35	10	25	2007	9.6	14.6	221	922	135	0.49	378	869	0.28	0.19	0.43
A-73-0066-3	275	1.48	1.21	10	25	1999	19.5	14.2	457	723	196	0.47	576	633	0.41	0.29	0.32
A-73-0067-3	292	1.46	1.15	10	25	4008	22.4	7.5	- 79	1053	215	2.50	104	1050	0.22	0.03	0.26
A-73-0068-3	290	1.47	1.22	10	25	989	18.3	30.3	492	668	177	0.12	601	573	0.74	0.61	0.58
A-73-0069-3	285	1.45	1.11	5	35	2900	23.7	12.6	817	431	290	0.80	851	359	0.42	0.29	0.12
A-73-0070-3	293	1.48	1.44	0	35	1980	2.7	19.0	382	0	118	0.32	382	0	0.25	0.19	0.00

TABLE A.2

RESULTS OF POWERED TURNED TIRE TESTS ON YUMA SAND

| | Test Conditions | | | | | | | | Measured Test Values | | | | Forces Acting on Wheel | | Performance Coefficients | | |
| | Penetration Resistance G MPa/m | Wheel Speed V_w, m/sec | Carriage Speed V_a, m/sec | Turn Angle α, deg. | Deflection Coefficient δ/h | Wheel Load W, N | Wheel Slip s, % | Sand Mobility Number N_s | Forces Acting on Carriage | | Torque M M-N | Vertical Hub Movement z, cm | | | | | |
Test No.									Pull P', N	Lateral Force S', N			Pull P, N	Side Force S, N	Torque M/Wr_a	Pull P/W	Side Force S/W
A-73-0011-1	1.95	1.50	1.43	0	35	2000	4.7	8.0	284	0	146	1.51	284	0	0.31	0.14	0.00
A-73-0012-1	1.91	1.50	1.37	0	35	2000	8.8	7.9	370	0	163	1.30	370	0	0.35	0.19	0.00
A-73-0013-1	1.83	1.49	1.25	0	35	1975	16.1	7.6	462	0	193	1.92	462	0	0.41	0.23	0.00
A-75-0011-1	2.13	1.50	1.53	5	35	2044	-2.1	8.6	-106	292	64	1.04	-80	300	0.13	-0.04	0.15
A-75-0012-1	2.00	1.49	1.41	5	35	2032	5.4	8.1	186	301	133	0.98	211	283	0.28	0.10	0.14
A-75-0013-1	2.11	1.49	1.33	5	35	2009	11.1	8.6	371	288	173	1.06	394	254	0.37	0.20	0.13
A-73-0014-1	2.01	1.49	1.22	5	35	1995	18.4	8.3	390	302	200	1.97	414	266	0.43	0.21	0.13
A-74-0005-1	1.85	1.49	1.46	10	35	1980	3.7	7.7	-76	645	112	2.07	37	648	0.24	0.02	0.33
A-74-0001-1	2.06	1.48	1.41	10	35	1948	6.1	8.7	0	653	122	2.00	113	643	0.27	0.06	0.33
A-74-0003-1	2.04	1.47	1.38	10	35	1965	7.5	8.5	24	636	134	1.95	134	622	0.29	0.07	0.32
A-74-0004-1	2.07	1.46	1.24	10	35	1985	16.3	8.6	315	602	193	2.00	414	538	0.41	0.21	0.27
A-74-0002-1	2.08	1.48	1.23	10	35	1992	17.9	8.6	233	623	185	2.07	337	573	0.39	0.17	0.29
A-73-0015-1	1.86	1.48	1.22	10	35	2011	19.0	7.6	242	594	203	2.90	341	542	0.43	0.17	0.27
A-74-0006-1	2.00	1.49	1.47	20	35	2012	7.4	8.2	-528	893	88	2.78	-190	1019	0.19	-0.09	0.51
A-74-0007-1	2.03	1.49	1.30	20	35	1996	17.7	8.4	-244	949	140	3.02	95	975	0.30	0.05	0.49
A-74-0024-1	2.20	1.52	1.21	15	35	1032	23.3	17.5	184	441	119	1.36	291	378	0.49	0.28	0.37
A-75-0015-1	2.10	1.54	1.55	20	35	1005	5.5	17.2	-177	487	63	1.02	0	518	0.27	0.00	0.52
A-75-0014-1	1.98	1.52	1.40	20	35	1013	13.5	16.1	-88	488	85	1.02	84	488	0.36	0.08	0.48
A-75-0016-1	2.14	1.52	1.28	20	35	1010	20.9	17.4	8	464	104	1.47	166	433	0.44	0.16	0.43
A-74-0023-1	1.85	1.49	1.20	15	35	3018	22.2	5.0	-155	1138	260	4.69	144	1139	0.37	0.05	0.38
A-75-0001-1	2.24	1.54	1.53	10	15	1968	2.0	4.0	-288	453	116	3.79	-204	496	0.24	-0.10	0.25
A-75-0002-1	2.12	1.54	1.40	10	15	1987	10.6	3.8	-141	466	158	4.59	-57	483	0.32	-0.03	0.24
A-75-0003-1	1.96	1.56	1.20	10	15	1978	24.0	3.5	-19	421	104	5.09	54	417	0.21	0.03	0.21
A-74-0008-1	1.90	1.52	1.45	20	15	1920	10.2	3.5	-167	250	130	3.93	-71	292	0.27	-0.04	0.15
A-74-0025-1	1.99	1.50	1.20	10	25	2000	21.2	5.8	184	561	191	2.99	278	520	0.39	0.14	0.26
A-74-0022-1	2.08	1.48	1.19	15	25	2025	22.2	6.0	43	833	184	3.59	257	793	0.38	0.13	0.39
A-74-0009-1	3.18	1.49	1.45	5	35	2037	2.7	12.8	147	446	100	0.75	185	431	0.21	0.09	0.21
A-74-0010-1	3.10	1.48	1.34	5	35	2045	9.7	12.5	475	462	177	0.58	513	418	0.37	0.25	0.20
A-74-0011-1	3.22	1.48	1.24	5	35	1980	16.4	13.4	580	402	206	0.55	612	349	0.44	0.31	0.18
A-74-0012-1	3.57	1.46	1.41	15	35	2047	6.1	14.3	-133	957	106	1.43	119	958	0.22	0.06	0.47
A-74-0014-1	3.13	1.48	1.39	15	35	2013	9.3	12.8	-163	1015	103	1.52	105	1022	0.22	0.05	0.51
A-74-0020-1	3.11	1.47	1.34	15	35	2045	11.6	12.5	-30	950	139	1.48	216	925	0.29	0.11	0.45
A-74-0013-1	3.45	1.47	1.23	15	35	2045	19.2	13.9	314	849	199	1.16	523	738	0.41	0.26	0.36
A-75-0006-1	3.26	1.57	1.50	10	35	1066	5.5	25.2	56	397	74	0.41	124	381	0.29	0.12	0.36
A-75-0005-1	3.26	1.55	1.42	10	35	1042	9.9	25.7	173	386	106	0.17	237	350	0.43	0.23	0.34
A-75-0004-1	3.11	1.57	1.41	10	35	1081	11.5	23.7	193	392	107	0.16	258	352	0.42	0.24	0.33
A-75-0007-1	3.28	1.55	1.27	10	35	1070	19.3	25.2	390	233	150	0.64	424	161	0.60	0.40	0.15
A-75-0010-1	3.16	1.56	1.57	15	35	1015	2.7	25.6	-158	521	45	0.41	-17	544	0.19	-0.02	0.54
A-75-0009-1	3.31	1.56	1.43	15	35	1044	11.3	26.1	30	506	95	0.68	159	480	0.39	0.15	0.46
A-75-0008-1	3.01	1.57	1.39	15	35	1067	14.3	23.2	87	502	108	0.56	213	462	0.43	0.20	0.43
A-74-0021-1	2.98	1.51	1.18	15	35	1000	24.6	24.5	228	404	123	0.78	324	331	0.52	0.32	0.33
A-75-0019-1	3.32	1.51	1.52	20	35	1068	5.6	25.6	-185	513	63	1.26	1	545	0.25	0.00	0.51
A-75-0018-1	3.47	1.56	1.39	20	35	1066	15.8	26.8	-47	540	91	0.51	140	523	0.36	0.13	0.49
A-75-0017-1	3.68	1.55	1.28	20	35	1038	22.3	29.2	48	516	118	0.63	221	468	0.48	0.21	0.45
A-74-0018-1	3.21	1.47	1.21	15	35	3004	20.6	8.8	45	1263	250	2.58	370	1208	0.35	0.12	0.40
A-74-0015-1	3.36	1.46	1.19	15	15	2063	21.0	5.7	-10	767	164	2.45	188	743	0.32	0.09	0.36
A-74-0019-1	3.36	1.54	1.45	15	25	2000	8.8	9.9	-264	957	83	1.52	-7	992	0.17	-0.00	0.50
A-74-0017-1	3.26	1.50	1.30	15	25	2045	16.2	9.4	36	930	156	1.88	275	888	0.32	0.13	0.43
A-74-0016-1	3.24	1.49	1.22	15	25	2005	20.9	9.5	186	928	182	1.90	419	848	0.38	0.21	0.42

APPENDIX B

MOBILITY NUMBER COMPUTED FROM

MEASURED TEST VALUES

Clay Tests

The dependent parameters of pull, input torque, and wheel slip measured in each clay test can be substituted into Equations 2.4 through 2.7 and the clay mobility number computed which in turn can be compared with the clay mobility number determined by test conditions for assessing the influence of wheel turn angle on performance parameters. Three combinations of the above mentioned measured dependent parameters can be used for computing the clay mobility number: (1) pull and wheel slip, (2) input torque and pull, and (3) input torque and wheel slip.

Pull and Wheel Slip

Beginning with Equation 2.5

$$S_{sp} = \frac{21}{\left(N_c'\right)^{5/2}} + 0.005 \tag{2.5}$$

and substituting into Equation 2.7

$$\frac{P}{W} = \frac{1}{2}\log \frac{S}{S_{sp}} = \frac{1}{2}\log \left[\frac{5}{\frac{21}{\left(N_c'\right)^{5/2}} + 0.005} \right]$$

and finally solving for N_c'

$$N_c' = \left[\frac{21}{\frac{5}{\log^{-1}\left(\frac{2P}{W}\right)} - 0.005} \right]^{2/5} \tag{B.1}$$

Input Torque and Pull

Solving for $\dfrac{M_{sp}}{Wr_a}$ from Equation 2.4 yields

$$\frac{M_{sp}}{Wr_a} = \frac{M}{Wr_a} - \frac{P}{W} (1 + \frac{b}{d})^{1/4} \qquad (2.4)$$

Equation 2.6 states

$$\frac{M_{sp}}{Wr_a} = \frac{2}{N'_c{}^2} + 0.007 \qquad (2.6)$$

Equating the right side of the two previous relations and solving for N'_c yields

$$N'_c = \left[\frac{12}{\frac{M}{Wr_a} - \frac{P}{W} (1 + \frac{b}{d})^{1/4} - 0.007} \right]^{1/2} \qquad (B.2)$$

Input Torque and Wheel Slip

Smith (1976) found that the torque coefficient and the slip at the self-propelled point are related to the clay mobility number by

$$\frac{M_{sp}}{Wr_a} = \frac{12}{\left(N'_c\right)^2} + 0.007 \qquad (2.6)$$

and

$$S_{sp} = \frac{21}{N^{5/2}} + 0.005 \qquad (2.5)$$

Substituting the above into Equation 2.7.

$$\frac{M - M_{sp}}{Wr_a} \cdot K_T = \frac{1}{2} \log \frac{S}{S_{sp}} \qquad (2.7)$$

creates an expression having terms or input torque, wheel slip, and the clay mobility number, i.e.

$$\frac{2M}{Wr_a} \cdot K_T - \log S = \frac{24}{N_c'^2} \cdot K_T + 0.014\ K_T - \log\ \frac{21}{N_c'^{5/2}} + 0.005 \qquad (B.3)$$

N_c' can be calculated for specific values of input torque and wheel slip from the above relation by a simple interaction algorithm programmed into a computer.

Table B.1 provides a comparison of the clay mobility number N_c' as computed from Equations B.1, B.2, and B.3. These values did not differ significantly however, N_c' as computed from the pull and wheel slip test values were used in further developments since they represent system outputs of the powered wheel.

TABLE B.1

CLAY MOBILITY NUMBER COMPUTED
FROM PERFORMANCE PARAMETERS

Test No.	Angle α, deg.	Computed Clay Mobility Number				N_c'
		Pull & Slip	Torque & Pull	Torque & Slip	Avg.	
A-73-0048-3	0	14.65	14.52	14.58	14.58	18.84
A-73-0049-3	0	18.63	13.99	17.35	16.66	20.00
A-73-0050-3	0	19.35	15.59	17.55	17.50	17.87
A-73-0051-3	10	13.96	11.92	12.94	12.94	17.34
A-73-0052-3	10	14.16	11.74	13.19	13.03	18.97
A-73-0053-3	10	15.89	12.86	14.77	14.51	18.88
A-73-0054-3	20	10.73	29.94	16.41	19.03	19.75
A-73-0055-3	20	9.67	12.67	9.65	10.67	19.50
A-73-0056-3	20	10.87	26.10	14.57	17.18	19.88
A-73-0057-3	5	15.72	13.40	14.56	14.56	18.61

TABLE B.1 (Continued)

| Test No. | Angle α, deg. | Computed Clay Mobility Number | | | | N'_c |
		Pull & Slip	Torque & Pull	Torque & Slip	Avg.	
A-73-0058-3	5	11.29	10.55	10.92	10.92	12.59
A-73-0059-3	5	10.46	10.64	10.55	10.55	12.63
A-73-0060-3	5	9.29	9.44	9.36	9.36	13.00
A-73-0061-3	15	12.08	11.40	11.74	11.74	11.96
A-73-0062-3	15	8.43	9.60	8.93	8.98	12.06
A-73-0063-3	15	8.90	12.13	8.20	9.74	12.93
A-73-0064-3	10	12.49	15.55	13.38	13.81	15.44
A-73-0065-3	10	12.90	13.13	13.02	13.02	14.64
A-73-0066-3	10	11.52	11.50	11.51	11.51	14.23
A-73-0067-3	10	6.51	8.01	3.34	5.96	7.54
A-73-0068-3	10	25.92	11.81	22.78	20.17	30.32
A-73-0069-3	5	10.68	10.76	10.72	10.72	12.60
A-73-0070-3	0	25.99	17.21	23.52	22.24	18.97

Sand Tests

Equations 2.9 and 2.10 were used to calculate the sand mobility number from test values of wheel slip, input torque, and pull. At this time an equation derived from test data of input torque and wheel slip at the self-propelled has not been developed; hence, there is one less set of relations for the sand tests from which to compute the sand mobility number from dependent test parameters. Table B.2 provides a comparison of the sand mobility number as computed by substituting combinations of dependent performance parameters pull-wheel slip and torque-wheel slip into Equations 2.9 and 2.10, respectively. Also shown

are N_S values computed from independent test conditions. As seen in Table B.2 the computed sand mobility number was highly dependent upon the method and equation selected. Further, when compared with the respective N_S determined by test conditions, the computed values did not follow any well defined trend as values occurred almost equally above and below the base line N_S value.

TABLE B.2

SAND MOBILITY NUMBER COMPUTED
FROM PERFORMANCE PARAMETERS

Test No.	Wheel Turn Angle α, deg.	N_s	Computed Sand Mobility Number	
			Pull & Slip	Torque & Slip
A-73-0011-1	0	8.02	15.27	29.02
A-73-0012-1	0	7.85	11.35	20.44
A-73-0013-1	0	7.62	10.31	17.66
A-75-0011-1	5	8.57	*	*
A-75-0012-1	5	8.10	11.82	18.56
A-75-0013-1	5	8.64	10.44	17.98
A-73-0014-1	5	8.29	8.78	16.10
A-74-0005-1	10	7.68	12.62	18.78
A-74-0001-1	10	8.70	9.16	13.87
A-74-0003-1	10	8.54	8.18	13.59
A-74-0004-1	10	8.58	9.24	16.81
A-74-0002-1	10	8.59	7.57	11.45
A-73-0015-1	10	7.61	7.41	15.84
A-74-0006-1	20	8.18	4.85	3.17
A-74-0007-1	20	8.37	4.60	2.88
A-74-0024-1	15	17.53	11.22	23.81
A-75-0015-1	20	17.19	8.28	16.07
A-75-0014-1	20	16.08	6.12	11.72

* Not computed because wheel slip was negative.

TABLE B.2 (Continued)

Test No.	Wheel Turn Angle α, deg.	N_s	Computed Sand Mobility Number	
			Pull & Slip	Torque & Slip
A-75-0016-1	20	17.43	6.99	15.05
A-74-0023-1	15	5.04	4.11	5.11
A-75-0001-1	10	4.01	19.55	27.68
A-75-0002-1	10	3.76	4.64	11.41
A-75-0003-1	10	3.49	3.58	0.19
A-74-0008-1	20	3.49	4.61	6.47
A-74-0025-1	10	5.85	6.24	8.46
A-74-0022-1	15	6.03	5.81	5.88
A-74-0009-1	5	12.84	25.53	17.75
A-74-0010-1	5	12.47	14.02	22.36
A-74-0011-1	5	13.38	14.24	23.11
A-74-0012-1	15	14.34	9.15	7.68
A-74-0014-1	15	12.79	6.77	3.34
A-74-0020-1	15	12.51	7.22	6.32
A-74-0013-1	15	13.88	10.59	12.88
A-75-0006-1	10	25.15	12.20	21.70
A-75-0005-1	10	25.73	12.54	40.10
A-75-0004-1	10	23.66	12.19	30.29
A-75-0007-1	10	25.21	20.81	84.82
A-75-0010-1	15	25.61	16.84	14.54
A-75-0009-1	15	26.08	8.74	21.82
A-75-0008-1	15	23.20	9.43	24.73
A-74-0021-1	15	24.51	13.41	31.97
A-75-0019-1	20	25.57	8.17	13.07
A-75-0018-1	20	26.77	6.87	9.63
A-75-0017-1	20	29.16	8.40	23.39
A-74-0018-1	15	8.79	5.91	4.97
A-74-0015-1	15	5.74	5.12	2.80
A-74-0019-1	15	9.87	5.76	1.58
A-74-0017-1	15	9.37	6.86	4.68
A-74-0016-1	15	9.49	8.45	6.66

APPENDIX C

COMPUTER PROGRAM LISTING

```
1C*******************************
2C
3C   TTTTT   U   U   RRRR    N    N
4C     T     U   U   R   R   NN   N
5C     T     U   U   RRRR    N N  N
6C     T     U   U   R   R   N   NN
7C     T      UUU    R   RR  N    N
8C
9C*******************************
10C    DRIVE PROGRAM TO SOLVE SIMULTANEOUS NONLINEAR MOTION EQUATIONS
11        DIMENSION X(2)
20        EXTERNAL FUNCT
25C   ESTIMATED YAW VELOCITY (PSI)
30        X(1)=.04
35C   ESTIMATED VEHICLE SIDE SLIP (BETA)
40        X(2)=.115
50        MAXIT=50
60        CALL BROWN(2,MAXIT,1E-4,ISING,X,FUNCT,L)
70        PRINT:"ISING=",ISING,"MAXIT=",MAXIT
80        PRINT:"SOLUTION",X(1),X(2)
85        CALL TURN(K,X,FK,1)
90        STOP;END
91C
92C    *********
93C
94C       S U B R O U T I N E   F U N C T
95C
96C    *********
97C
100       SUBROUTINE FUNCT (X,FK,K)
110       DIMENSION X(2)
120       GO TO (1,2),K
130     1 CONTINUE
140       CALL TURN (K,X,FK,0)
150       RETURN
160     2 CONTINUE
170       CALL TURN (K,X,FK,0)
180       RETURN
190       END
1011C
1012C    **********
1013C
1014C       S U B R O U T I N E   B R O W N
1015C
1016C    **********
1017C
1019       SUBROUTINE BROWN(N,MAXIT,EPS,SING,X,FUNCT)
1020C   BROWNS SUBROUTINE FOR NON-LINEAR SYSTEMS
1022C   N:NUMBER OF EQUATIONS
1024C   MAXIT: UPPER BOUND ON THE NUMBER OF ITERATIONS
1025C   SING=0 IF A JOCOBIAN RELATED MATRIX WAS SINGULAR
1026C   SING=1 IF NO SUCH DIFFICULTY WAS FOUND
1027C   ESP:SMALL NUMBER TO TEST FOR CONVERGENCE
```

```
1028C    X: VECTOR OR INITIAL GUESSES TO THE SOLUTION
1040        EXTERNAL FUNCT
1050        INTEGER SING,CONV,TALLY,POINT(20,20)
1060        DIMENSION ISUB(20),TEMP(20),PART(20),COE(20,20)
1070        DIMENSION X(20)
1080        CONV=1
1090        SING=1
1095        NN=N
1100        DO 12 M=1,MAXIT
1110        DO 1 J=1,N
1120      1 POINT(1,J)=J
1130        DO 9 K=1,N
1135        KK=K
1140        IF(KK .GT. 1) CALL BCKSBS(KK,NN,X,ISUB,COE,POINT)
1150        CALL FUNCT(X,F,KK)
1160        FACTOR=.001
1170      2 TALLY=0
1180        DO 3 I=K,N
1190        ITEMP=POINT(K,I)
1200        HOLD=X(ITEMP)
1210        H=FACTOR*HOLD
1220        IF(ABS(H) .LT. 1E-7) H=.001
1230        X(ITEMP)=HOLD+H
1240        IF(KK .GT. 1)CALL BCKSBS(KK,NN,X,ISUB,COE,POINT)
1250        CALL FUNCT(X,FPLUS,KK)
1260        PART(ITEMP)=(FPLUS-F)/H
1270        X(ITEMP)=HOLD
1280        IF(ABS(PART(ITEMP))-1E-7)26,26,24
1290     24 IF(ABS(F/PART(ITEMP))-1E20)3,3,26
1300     26 TALLY=TALLY+1
1310      3 CONTINUE
1320        IF(TALLY .LE. N-K) GO TO 4
1330        FACTOR=FACTOR*10.0
1340        IF(FACTOR .GT. 0.5) GO TO 14
1350        GO TO 2
1360      4 IF(K .LT. N) GO TO 5
1370        IF(ABS(PART(ITEMP)) .LT. 1E-7) GO TO 14
1380        COE(K,N+1)=0
1390        KMAX=ITEMP
1400        GO TO 9
1410      5 KMAX=POINT(K,K)
1420        DERMAX=ABS(PART(KMAX))
1430        KPLUS=K+1
1440        DO 7 I=KPLUS,N
1450        JSUB=POINT(K,I)
1460        TEST=ABS(PART(JSUB))
1470        IF(TEST .LT. DERMAX) GO TO 6
1480        DERMAX=TEST
1490        POINT(KPLUS,I)=KMAX
1500        KMAX=JSUB
1510        GO TO 7
1520      6 POINT(KPLUS,I)=JSUB
1530      7 CONTINUE
```

```
1540        IF(ABS(PART(KMAX)) .LT. 1E-7) GO TO 14
1550        ISUB(K)=KMAX
1560        COE(K,N+1)=0
1570        DO 8 J=KPLUS,N
1580        JSUB=POINT(KPLUS,J)
1590        COE(K,JSUB)=-PART(JSUB)/PART(KMAX)
1600      8 COE(K,N+1)=COE(K,N+1)+PART(JSUB)*X(JSUB)
1610      9 COE(K,N+1)=(COE(K,N+1)-F)/PART(KMAX)+X(KMAX)
1620        X(KMAX)=COE(N,N+1)
1630        IF(N .GT. 1)CALL BCKSBS(N,N,X,ISUB,COE,POINT)
1640        IF(M.EQ.1)GO TO 11
1650        DO 91 I=1,N
1660     91 IF(ABS((TEMP(I)-X(I))/X(I)) .GT. EPS)GO TO 10
1670        CONV=CONV+1
1680        IF(CONV-3)11,13,13
1690     10 CONV=1
1700     11 DO 12 I=1,N
1710     12 TEMP(I)=X(I)
1720     13 MAXIT=M
1730        RETURN
1740     14 SING=0
1750        RETURN
1760        END
1770        SUBROUTINE BCKSBS(K,N,X,ISUB,COE,POINT)
1780        INTEGER POINT(20,20)
1790        DIMENSION ISUB(20),X(20),COE(20,20)
1800        DO 1 KMM=2,K
1810        KM=K-KMM+2
1820        KMAX=ISUB(KM-1)
1830        X(KMAX)=0
1840        DO 2 J=KM,N
1850        JSUB=POINT(KM,J)
1860      2 X(KMAX)=X(KMAX)+COE(KM-1,JSUB)*X(JSUB)
1870      1 X(KMAX)=X(KMAX)+COE(KM-1,N+1)
1880        RETURN
1890        END
1891C
1892C    **********
1893C
1894C       S U B R O U T I N E    T U R N
1895C
1896C    **********
2000        SUBROUTINE TURN (K,X,FK,L)
2020C
2030C
2040C
2050C    INPUT DATA
2060C
2070C       VEHICLE
2080C          WTG     GROSS VEHICLE WEIGHT, NEWTONS
2090C          ADIM    DISTANCE BETWEEN FRONT AXIAL AND VEHICLE CG,METERS
2100C          BDIM    DISTANCE BETWEEN REAL AXIAL AND VEHICLE CG,METERS
2110C          CDIM    HORIZONTAL DISTANCE BETWEEN INSIDE        METER
```

```
2120C              WHEELS AND VEHICLE  CG
2130C     DDIM     HORIZONTAL DISTANCE BETWEEN OUTSIDE       METER
2140C              WHEELS AND VEHICLE CG
2150C     HDIM     VERTICAL DISTANCE FROM GROUND             METER
2155C              SURFACE TO VEHICLE CG
2160C     LDIM     DISTANCE POINT OF APPLICATION OF DRAWBAR PULL TO CG,METERS
2170C     GAMMA    ANGLE BETWEEN DRAWBAR PULL AND LONG. AXIS OF VEHICLE,DEGREES
2190C     CTR      RATIO OF CENTRIFUGAL ACCELERATION         -
2200C              (V**2/R) TO GRAVITY ACCELERATION(G)
2210C     SPKF     SPRING CONSTANT FOR FRONT AXLE            NEWTONS/METER
2220C     SPKR     SPRING CONSTANT FOR REAR AXLE            NEWTONS/METER
2230C
2240C     TIRE
2250C
2260C     SLIP     POWERED WHEEL SLIP,DECIMAL
2270C     TIREB    CROSS SECTION WIDTH OF UNLOADED-INFLATED TIRE,METER
2280C     TIRED    DIAMETER OF UNLOADED-INFLATED TIRE,METER
2290C     DEFL     TIRE DEFLECTION,DECIMAL
2300C     ITIR     TIRE CODE - FROM MSD TIRE BOOK            -
2310C     TRIP     TIRE INFLATION PRESSURE                   KPA
2330C
2340C
2350C     SOIL
2360C
2370C     KSOIL    0=CLAY  1=SAND
2380C     CPR      CONE PENETRATION RESISTANCE,CLAY-KPA;SAND-MPA/M
2390C
2400C     PARAMETRIC VARIATION FOR SPECIFIC VEHICLE
2410C     KDRIVE   +1=REAR WHEEL DRIVE- -1=FOUR WHEEL DRIVE
2420C     VEL      VEHICLE SPEED, METERS/SECOND
2430C     DELTA    STEERING ANGLE OF STEERED WHEELS,DEGREES
2440C     IEND     0=MORE DATA   1=LAST DATA
2450C
2460C
2470      DIMENSION SF(2,2),TF(2,2)
2480      DIMENSION X(2)
2481      DIMENSION PULL(2,2)
2490      DIMENSION WT(2,2),DEFL(2,2),XNUM(2,2),ITIRGO(5)
2500      DIMENSION TC(2,2),SC(2,2)
2510      REAL LDIM
2515      DATA ITIRGO/20,29,48,62,66/
2520      DATA WTG,ADIM,BDIM,CDIM,DDIM,HDIM,LDIM,GAMMA,SPKF,
2530     &       SPKR,SLIP,ITIR,TRIP,KSOIL,CPR
2540     &         ,XITER
2550     &        /14240.,1.143,1.016,.89,.89,.629,1.758,0.,25228.,25228.,
2551     &.2,48,
2560     &       103.5,1,
2570     & 2.5,13292./
2580      DATA KDRIVE,VEL,DELTA,IEND
2590     &       /-1,2.,7.,1/
2600    5 CONTINUE
2620      GAMMR=(3.14159*GAMMA)/180.
2630      DELTR=(DELTA*3.14159)/180.
```

```
2640      XMASS=WTG/9.81
2650      BETA=X(1)
2660      PSI=X(2)
2665C   COMPUTE FRONT WHEEL SIDE SLIP ANGLE
2670      ALPF=DELTR-BETA-(ADIM*PSI)/VEL
2675C   COMPUTE REAR WHEEL SIDE SLIP ANGLE
2680      ALPR=((BDIM*PSI)/VEL)-BETA
2690      CTR=VEL*PSI/9.81
2700C
2710C PROGRAM SEGMENT "ROLL"
2720C PROGRAM SEGMENT TO COMPUTE THE ROLL ANGLE, SUBSEQUENT WEIGHT TRANSFER,
2730C AND RESULTING NUMERIC FOR A 4-WHEEL VEHICLE NEGOTIATING A FLAT
2740C HORIZONTAL TURN UNDER IDEAL STEADY STATE MOTION
2750C
2760      ROLL=(WTG/(SPKF+SPKR))*(HDIM/(CDIM**2+DDIM**2))*CTR
2770      ROLDEG=ROLL*180.0/3.14159
2780      DEM=(ADIM+BDIM)*(CDIM+DDIM)
2790      WT(1,1)=(BDIM*DDIM*WTG/DEM)-SPKF*CDIM*ROLL
2800      WT(1,2)=(BDIM*CDIM*WTG/DEM)+SPKF*DDIM*ROLL
2810      WT(2,1)=(ADIM*DDIM*WTG/DEM)-SPKR*CDIM*ROLL
2820      WT(2,2)=(ADIM*CDIM*WTG/DEM)+SPKR*DDIM*ROLL
2830      DO 82 I=1,5
2840      IF(ITIRGO(I)-ITIR)82,81,82
2850   82 CONTINUE
2860      STOP "NO MATCH ON ITIR"
2870   81 GO TO (20,29,48,62,66),I
2880C TIRE 6.00-16,2PR;TREAD BUFFED SMOOTH
2890   20 A=15.272
2900      B=1.04
2910      TIREB=0.168
2920      TIRED=0.719
2930      GO TO 400
2940C TIRE 6.00-9,4PR;TREAD BUFFED SMOOTH
2950   29 A=31.8
2960      B=1.16
2970      TIREB=0.159
2980      TIRED=0.516
2990      GO TO 400
3000C TIRE 7.00-16,6PR;NDCC TREAD
3010   48 A=52.2
3020      B=1.0
3030      TIREB=0.189
3040      TIRED=0.750
3050      GO TO 400
3060C TIRE 11.00-20,12PR;TREAD BUFFED SMOOTH
3070   62 A=49.5
3080      B=0.355
3090      TIREB=0.2854
3100      TIRED=1.05
3110      GO TO 400
3120C TIRE 9.00-16,8PR;TREAD BUFFED SMOOTH
3130   66 A=64.2
3140      B=0.565
```

```
3150        TIREB=0.250
3160        TIRED=0.865
3170    400 CONTINUE
3180        DO 500 I=1,2
3190        DO 500 J=1,2
3195C    COMPUTE TIRE DEFLECTION
3200        DEFL(I,J)=(B*WT(I,J)/(TRIP+A))/100.
3210        IF(KSOIL-1)410,420,
3220    410 DEF=(1.-DEFL(I,J))**1.5
3230        TIRE=(1.+(TIREB/TIRED))**0.75
3235C    CLAY MOBILITY NUMBER FOR EACH WHEEL
3240        XNUM(I,J)=(1000.*CPR*TIREB*TIRED)/(WT(I,J)*DEF*TIRE)
3250        GO TO 500
3255C    SAND MOBILITY NUMBER FOR EACH WHEEL
3260    420 XNUM(I,J)=(CPR*(10.**6)*(TIREB*TIRED)**1.5*DEFL(I,J))/WT(I,J)
3270    500 CONTINUE
3280        IF(KSOIL-1),50,50
3290C
3300C       SOIL TIRE FORCES FOR VEHICLE IN CLAY
3310C
3340        TRSL=(1.+(TIREB/TIRED))**.25
3350        IF(KDRIVE-1)21,10,10
3360     10 CONTINUE
3365C    FRONT TIRE FORCES FOR REAR DRIVEN VEHICLE IN CLAY
3390        DO 15 J=1,2
3392        XNEQW=XNUM(1,J)*(1-2.26*ABS(ALPF)**1.5)
3395C    TRACTIVE FORCE
3400        TF(1,J)=(12./(XNEQW**2)+.007)*WT(1,J)
3415C    SIDE FORCE
3420        DTAR=ABS(ALPF)
3422        IF(DTAR.LT.0.0873)GO TO 12
3424C    SIDE FORCE IF ALPF > 5 DEG
3426        BCON=4./DTAR**.5
3428        SF(1,J)=(15.4-15.4*BCON/(XNEQW-7.+BCON))*TF(1,J)
3430        GO TO 15
3432C    SIDE FORCE IF ALPF < 5 DEG
3434     12 RATIO =DTAR/0.0873
3435        SF(1,J)=(15.4-208.5/(XNEQW+6.5))*RATIO*TF(1,J)
3440     15 CONTINUE
3450     16 CONTINUE
3475C    REAR TIRE FORCES IN CLAY
3480        DO 17 J=1,2
3490        XNEQW=XNUM(2,J)*(1.-2.26*ABS(ALPR)**1.5)
3500        IF(XNEQW.LE.4.)XNEQW=4.
3510        CALL POWSF(TRSL,XNEQW,XNUM(2,J),SLIP,ALPR,PR,SF(2,J),PULLC)
3515C    TRACTIVE FORCE
3520        TF(2,J)=PR*WT(2,J)
3525C    SIDE FORCE
3530        SF(2,J)=SF(2,J)*WT(2,J)
3535        PULL(2,J)=PULLC*WT(2,J)
3540     17 CONTINUE
3550        GO TO 300
3560     21 CONTINUE
```

```
3975        PULL(1,J)=PULLC*WT(1,J)
3980    240 CONTINUE
3990        GO TO 220
4000    300 CONTINUE
4005C   COMPUTE DRAWBAR PULL
4010        ZDBX=PULL(2,1)+PULL(2,2)-KDRIVE*(PULL(1,1)+PULL(1,2))
4020        ZDB=ZDBX/COS(GAMMR)
4030        ZDBY=ZDB*SIN(GAMMR)
4035C   SUM OF HORIZONTAL FORCES
4040        BETDOT=SF(1,1)+SF(1,2)+SF(2,1)+SF(2,2)
4050      &      -KDRIVE*DELTR*(TF(1,1)+TF(1,2))-PSI*XMASS*VEL+ZDBY
4055C   SUM OF MOMENTS ABOUT CG
4060        PSIDOT=SF(1,1)*(ADIM+CDIM*DELTR)+SF(1,2)*(ADIM-DDIM*DELTR)
4070      &      -BDIM*(SF(2,1)+SF(2,2))+KDRIVE*(CDIM-ADIM*DELTR)*TF(1,1)
4080      &      -KDRIVE*TF(1,2)*(DDIM+ADIM*DELTR)-CDIM*TF(2,1)+DDIM*TF(2
4081      &,2)
4090      &      -ZDRY*LDIM
4100        IF(L)90,90,
4110    777 RAD=VEL/PSI
4120        WRITE(6,678) DELTA,VEL,PSI,ROLDEG,RAD,CTR,BETA,ALPF,
4125      &      ALPR
4130    678 FORMAT(1X,"STEERING ANGLE, DEGREES =",F5.1,/,
4140      &        "VEHICLE SPEED, METRE/SEC =",F5.1,/,
4150      &        "YAW VELOCITY, RAD/SEC =", G12.4,/,
4155      &        "VEHICLE ROLL, DEGREES =",F5.1,/,
4160      &        "CURVATURE RADIUS,METRE =",F6.1,/,
4170      &        "CENTRIFUGAL ACC./G. =",G12.4,/,
4180      &        "VEHICLE SIDE SLIP ANGLE, RADIAN =", G12.4,/,
4190      &        "FRONT WHEEL SIDE SLIP ANGLE, RADIAN =", G12.4,/,
4200      &        "REAR WHEEL SIDE SLIP ANGLE, RADIAN =", G12.4,///)
4210        WRITE(6,679)
4220    679 FORMAT(8X,"WHEEL",7X,"MOBILITY",4X,"TRACTIVE",4X,
4230      & "SIDE",/,8X,"LOAD,N",6X,"NUMBER",6X,"FORCE,N",5X,
4240      &        "FORCE,N")
4250        PRINT 1000,((II,JJ,WT(II,JJ),XNUM(II,JJ),TF(II,JJ),
4260      &        SF(II,JJ),JJ=1,2),II=1,2)
4270   1000 FORMAT(2H (,I1,1H,,I1,1H),4G12.5)
4280        IF(K.NE.1.OR.K.NE.2)RETURN
4290     90 GO TO (1,2),K
4300      1 FK=BETDOT
4310        RETURN
4320      2 FK=PSIDOT
4330        RETURN
4340        END
4350C
4360C   **********
4370C
4380C      S U B R O U T I N E    P O W S F
4390C
4400C   **********
4410C
4415C   POWSF SUBROUTINE TO COMPUTE SIDE FORCE COEFFICIENT
4416C      (S/W) FOR POWERED WHEELS OPERATING IN CLAY
```

```
3575C    FRONT TIRE FORCES FOR ALL WHEEL DRIVE VEHICLE IN CLAY
3590         DO 22 J=1,2
3600         XNEQW=XNUM(1,J)*(1.-2.26*ABS(ALPF)**1.5)
3610         IF(XNEQW.LE.4.)XNEQW=4.
3620         CALL POWSF(TRSL,XNEQW,XNUM(1,J),SLIP,ALPF,PF,SF(1,J),PULLC)
3625C     TRACTIVE FORCE
3630         TF(1,J)=PF*WT(1,J)
3635C     SIDE FORCE
3640         SF(1,J)=SF(1,J)*WT(1,J)
3645         PULL(1,J)=PULLC*WT(1,J)
3650      22 CONTINUE
3660         GO TO 16
3670      50 CONTINUE
3680C
3690C     SOIL TIRE FORCES FOR VEHICLE IN SAND
3700C
3740         IF(KDRIVE-1)250,200,
3750     200 CONTINUE
3755C     FRONT DRIVE FORCES FOR REAR DRIVEN VEHICLE IN SAND
3760         DO 210 J=1,2
3765C     TRACTIVE FORCE
3770         TF(1,J)=(.015+.83/(XNUM(1,J)-2.))*WT(1,J)
3775         DTAR=ABS(ALPF)
3777         IF(DTAR.LT.0.0873)GO TO 195
3779C     SIDE FORCE IF ALPF > 5 DEG
3780         SF(1,J)=(1.275*DTAR**1.23+.83-46./(XNUM(1,J)+55.4))*WT(1,J)
3782         GO TO 198
3783C     SIDE FORCE IF ALPF < 5 DEG
3784     195 RATIO=DTAR/0.0873
3786         SF(1,J)=RATIO*(.89-46./(XNUM(1,J)+55.4))*WT(1,J)
3788     198 CONTINUE
3790     210 CONTINUE
3800     220 CONTINUE
3815C     REAR TIRE FORCES IN SAND
3830         DO 230 J=1,2
3840         DUMALP=ABS(ALPR)
3850         CALL PWSAN(XNUM(2,J),SLIP,DUMALP,TC(2,J),SC(2,J),PULLC)
3855C     TRACTIVE FORCE
3860         TF(2,J)=TC(2,J)*WT(2,J)
3865C     SIDE FORCE
3870         SF(2,J)=SC(2,J)*WT(2,J)
3875         PULL(2,J)=PULLC*WT(2,J)
3880     230 CONTINUE
3890         GO TO 300
3900     250 CONTINUE
3915C     FRONT TIRE FORCES FOR ALL WHEEL DRIVE IN SAND
3930         DO 240 J=1,2
3940         DUMAR=ABS(ALPF)
3950         CALL PWSAN(XNUM(1,J),SLIP,DUMAR,TC(1,J),SC(1,J),PULLC)
3955C     TRACTIVE FORCE
3960         TF(1,J)=TC(1,J)*WT(1,J)
3965C     SIDE FORCE
3970         SF(1,J)=SC(1,J)*WT(1,J)
```

```
4420        SUBROUTINE POWSF(TRSL,XNEQN,XNUM,SLIP,ALP,TPOW,SFP,PULLC)
4430        SSP=(21./(XNEQN**2.5))+.005
4440        SLF=SLIP/SSP
4450        PULLC=.5*ALOG10(SLF)
4452        QSP=(12./XNEQN**2.)+.007
4453        Q=TRSL*PULLC+QSP
4454        IF(PULLC.GT.Q)GO TO 10
4455        TPOW=Q
4456        GO TO 20
4457     10 TPOW=PULLC
4458     20 CONTINUE
4460        SI=((XNUM+4.)**2/16.*0.0081)**0.5*(3.37*ABS(ALP)
4470     &          -4.24*ABS(ALP)**2)*(1./.46)
4480        SLOPE=1.7189*ABS(ALP)
4490        SFP=SI-TPOW*SLOPE
4500        RETURN
4510        END
4520C     **********
4530C
4540C.    S U B R O U T I N E   P W S A N
4550C
4560C     **********
4570C
4575C     PWSAN SUBROUTINE TO COMPUTE SIDE FORCE COEFFICIENT(S/W)
4576C        AND TRACTIVE FORCE COEFFICIENT FOR POWERED WHEELS
4577C        OPERATION IN SAND
4580        SUBROUTINE PWSAN(XNUM,SLIP,ALP,TCS,SCS,PULLC)
4590        A=.69-.01/SLIP-1.42*ALP**(.6+3.1*SLIP)
4600        B=10.8-16.*ALP**.8
4610        C=2.23/SLIP**(1./3.)+(15./SLIP)*ALP**3.
4620        PULLC=(A-A*B/(XNUM-C+B))
4621        BM=4.71+1.72/SLIP
4622        Q=.66-.66*BM/(XNUM+10.+BM)
4623        IF(PULLC.GT.Q)GO TO 10
4624        TCS=Q
4625        GO TO 20
4626     10 TCS=PULLC
4627     20 CONTINUE
4630        E=2.3+.03*XNUM
4640        F=2.4+.065*XNUM
4650        SZPU=E*ALP-F*ALP**2.
4660        SCS=SZPU-(1.65*ALP)*TCS
4670        RETURN
4680        END
```

VITA

Gary Neil Durham

Candidate for the Degree of

Doctor of Philosophy

Thesis: POWERED WHEELS IN THE TURNED MODE OPERATING ON YIELDING SOILS

Major Field: Civil Engineering

Biographical:

Personal Data: Born in Bessemer, Alabama, June 20, 1942, the son
of Mr. and Mrs. Thurman L. Durham.

Education: Graduated from Bessemer High School, Bessemer, Alabama,
in May, 1960; received the Bachelor of Science in Civil
Engineering degree from the University of Alabama, University,
Alabama, in August, 1967, with a major in Civil Engineering;
received the Master of Science degree from Mississippi State
University, Mississippi State, Mississippi, in August, 1971,
with a major in Civil Engineering; completed the requirements
for the Doctor of Philosophy degree at Oklahoma State
University in July, 1976.

Professional Experience: Served as assistant to the Chief, Soils
Testing Branch, U. S. Army Engineer Waterways Experiment
Station, Vicksburg, Mississippi, September, 1967, to March
1974. Immediate responsibility for conduct of soils labora-
tory operations on routine and special projects and activi-
ties for development and confirmation of new or improved
equipment, processes, and test techniques. Served as Research
Civil Engineer, Mobility Research and Methodology Branch,
U. S. Army Engineer Waterways Experiment Station, Vicksburg,
Mississippi, March, 1974 to present. Served as a research
manager and technical advisor on soil mechanics in the area
of off-road mobility.

Professional and Honorary Societies: Member, American Society of
Civil Engineers; Member, American Society for Testing and
Materials, Chi Epsilon, Phi Kappa Phi, Professional Engineer,
Mississippi.